博士論文

Computational Modeling of Mechanical Sensors Using Ionic Electroactive Polymers

(イオン性電気活性ポリマーを用いた力学センサの計算モデリング)

柳誠元

Doctoral Thesis

Computational Modeling of Mechanical Sensors Using Ionic Electroactive Polymers

Thesis submitted to Department of System Innovation,
School of Engineering, University of Tokyo
in fulfillment of requirement for degree of doctor of philosophy (Engineering)

December 2014

SeongwonYoo

Supervisor: Yutaka Toi

Contents

Contents

Contents

Notations

w	water uptake
ϕ	porosity
p^t or p	(total) pressure
p^s	stress-induced pressure
p^h	hydration-induced pressure
m^t or m	(total) mass of porous polymer (on a hydrated condition)
m^{dry}	mass of porous polymer on dry condition
m^f	mass of absorbed water
m^s	mass of polymer matrix (on dry condition)
ε_{ij}^t or ε_{ij}	(total) strains
ε_{ij}^s	stress-induced strains
e^t or e	(total) volumetric strain
e^h	hydration-induced strain
σ_{ij}^t or σ_{ij}	(total) stress
E^t or E	(total) elastic modulus
E^u	undrained elastic modulus
E^d	drained (static) elastic modulus
E_{dry}	elastic modulus on dry condition
v^t or v	(total) Poisson's ratio
v^u	undrained Poisson's ratio
v^B or v^b	beam undrained Poisson's ratio
v^d	drained (static) Poisson's ratio
K^t or K	(total) bulk modulus
K^s	bulk modulus of solid matrix
K^f	bulk modulus of absorbed fluid
K^u	undrained bulk modulus

Notations

K^d	drained (static) bulk modulus
K_{dry}	bulk modulus on dry condition
G^t or G	(total) shear modulus
G^d	drained (static) shear modulus
b	Biot coefficient
B	Skempton coefficient
α	correction factor of shear stiffness
β	correction factor of Poisson's ratio
Φ	hydration potential
H	hydration coefficient
κ_h	hydraulic permeability
V or ψ	electric potential
k_e	electric permittivity
η_w	water dynamic viscosity
a_w	water activity
C_I	I-ion concentration referring to bulk material
c_I	I-ion concentration referring to absorbed water
z_I	I-ion valence
D_I	diffusivity of I-component
T	absolute temperature
R	gas constant
F	Faraday constant

Chapter 1

Introduction

1.1 Ionic Electroactive Polymers

1.1.1 Polymers and Mechanical Properties

Polymers are defined as macromolecules which are made up of repeated structural units. The structure units, as shown in Fig. 1.1, are covalently attached each other and repeated. Nowadays the term, 'Polymer,' became familiar to us. Much long before the origin of the terminology in polymer science, polymers had been a part of our lives such as a natural resource. With the historical development of chemistry, polymers have been made by human since two hundred years ago. Eventually, the synthetic polymers have changed our lives profoundly. The synthetic polymers are produced by 'Polymerization.' The polymerization makes monomers (structural units) form linked chains (polymers) with electrochemical reactions. The synthetic polymers consist of thousands or ten thousands of monomers linked together (Rudin and Choi, 2012).

Polymers have very useful properties, e.g. they are easy to form any shape, saves manufacturing cost, light with low density, and have good resistance to corrosion, electricity and heat. Owing to the useful properties, such polymers became an indispensable part of our lives.

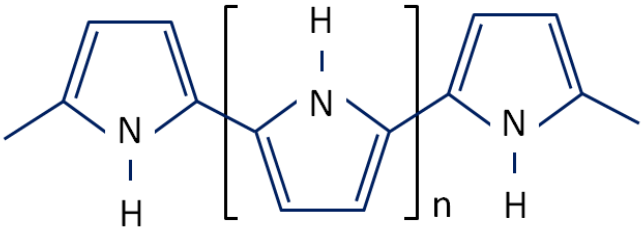

Fig. 1.1 Structure units of a conducting polymer, Polypyrrole

In the applications of polymers, one of important factors is mechanical properties. Actually, polymers are distinguished as elastomer (rubber), plastics and fibers. The distinction is based on mechanical properties.

Mechanical properties are conventionally characterized from the tensile stress-strain relations of representative samples. The tensile stress-strain relations are obtained from

standard tensile tests measuring uniaxial load and elongation as shown in Fig. 1.2. In conventional, mechanical properties, which are independent on specimen dimensions, are expressed with nominal stress and nominal strain. The nominal stress and nominal strain are defined as follows.

$$\sigma_{nominal} = \frac{P}{A_0}$$

$$\varepsilon_{nominal} = \frac{\Delta L}{L}$$

where, $\sigma_{nominal}$ is nominal stress, P is uniaxial load, A_0 is initial section, $\varepsilon_{nominal}$ is nominal strain, ΔL is uniaxial elongation, L is initial length.

Using the above nominal stress and nominal strain, many mechanical properties of polymers can be explained. In the description of the mechanical properties, key points are stiffness, recovery and ductility. The stiffness can be explained with elastic modulus. The elastic modulus is defined as follows.

$$E = \frac{\sigma_{nominal}}{\varepsilon_{nominal}}$$

The recovery can be explained with elastic strain. The elastic strain is a part of total strain returns to its original shape when external force is removed. Ductility can be explained with fracture strain. The fracture strain is quantified as total strain at breaking point.

Using the above quantities, elastomer, fibers and plastics are characterized as follows.

Elastomer has extraordinary elasticity. Elastomer is elongated up to 1000% or more and is fully recovered. That is, the portion of elastic strain to total strain is usually 100%. The elastic modulus of elastomer is low in the range of a certain strain, after that elastic modulus is suddenly increased. Under a high temperature, the stiffness of elastomer is increased as temperature is increased. Below a low temperature, elastomer becomes brittle and loses recovery (Rudin and Choi, 2012).

Fibers have high elastic modulus, but low ductility (brittle). Fibers are usually fractured around 20 % elongation. When fibers are deformed, some part of deformation is remained. Fibers are relatively unaffected by temperature change (Rudin and Choi, 2012).

Plastics have an intermediate stiffness between elastomer and fibers. Plastics are usually fractured around 400% elongation. The portion of elastic strain to total strain is not constant (Rudin and Choi, 2012).

Mechanical properties are elementally related to the advantages of polymers, so have been essential specifications in the applications of polymers. Especially for the polymers of actuators and mechanical sensors, mechanical properties are directly related to their performance, so the present study has paid attention to mechanical standpoints.

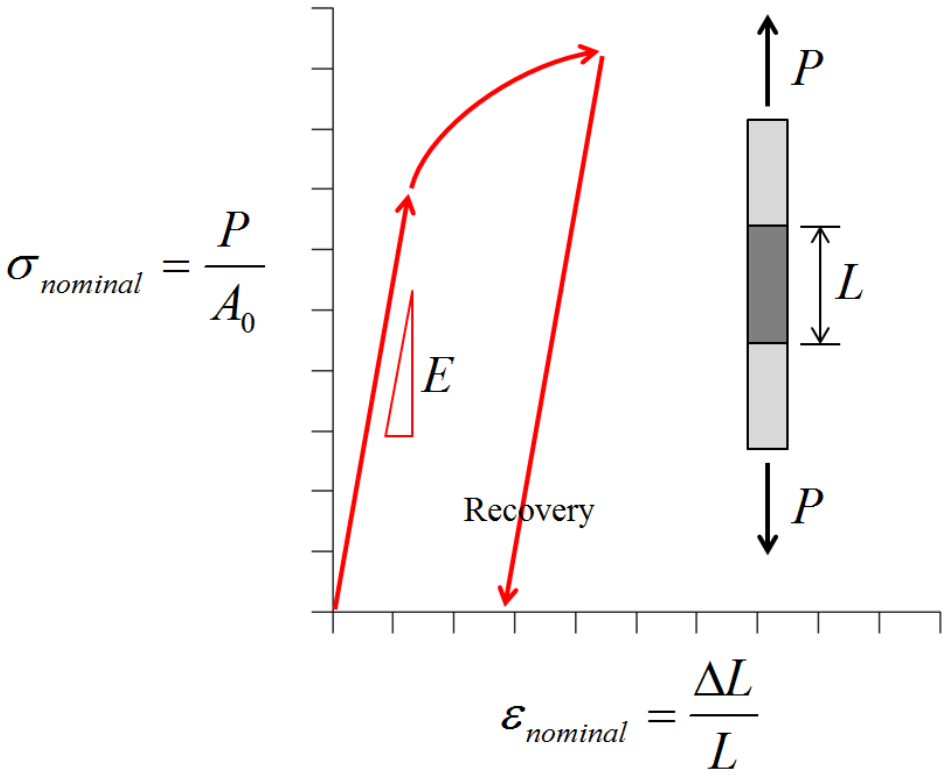

Fig. 1.2 Tensile stress-strain relation from standard tests

1.1.2 Conducting Polymers

Conducting polymers are extraordinary polymers that conduct electricity. Maintaining the advantages of ordinary polymers, conducting polymers shows key advantages in electronic properties. In the late 1970s, conducting polymers were firstly discovered by Shirakawa et al. (2003), who won the 2000 Nobel Prize. The discovery derived great innovations in various fields of science and engineering, especially in electronics with wide ranges of electrical conductivity. Eventually, conducting polymers have made remarkable changes in our lives, e.g. thin film transistors, polymer light emitting diodes (LEDs), electromagnetic shielding, sensor technology, molecular electronics, supercapacitors, and electrochromic devices (Ates, M. et al., 2012). Since the 1990s, conducting polymers have received attentions as ionic electroactive polymers in robotics, MEMS (micro-electro-mechanical systems), energy harvesting, artificial muscles and bioengineering fields.

Conducting polymers show extraordinary properties with various electric conductivities. There are many advantages such as electronic, magnetic, water uptake, optical, mechanical, and microwave-absorbing properties. Among many advantages, mechanical properties, electrical conductivity and water uptake are related to the electroactive performances of actuators and mechanical sensors. Conducting polymers have the mechanical properties of plastics as mentioned in the previous section. Electrical conductivity of conducting polymers can reach the metallic conducting regime by doping process. Furthermore, the electrical conductivity of conducting polymers can be enhanced by incorporating nano-component with high electrical conductivity. For example, CNT (Carbon Nano-Tube) can be served as electrical bridge to improve electrical conductivity. On the other hand, the electrical conductivity of conducting polymers can be controlled as semiconductor. What is incorporated with conducting polymers, the electrical conductivity of conducting polymers can be controlled in a certain wide range or wider ranges. Next, the water uptake of conducting polymers is important for applications such as self-cleaning surfaces, microfluidics, controlled drug delivery and bio-separation. The superhydrophobic properties of conducting polymers can be enhanced by doping hydrophobic acids. A reversibly switch between superhydrophobic and superhydrophilic conducting polymers can be realized by controlling the chemical compositions (Das and Prusty, 2012).

Mechanical properties, electric conductivity and water uptake are important factors on the performance of actuators and mechanical sensors using ionic electroactive polymers. The contributions of the interesting properties on the performance can be estimated in numerical simulation.

1.1.3 Ionic Electroactive Polymers for Actuators and Mechanical Sensors

'Electroactive polymers' are polymers that show mechanical deformation when electrical simulation is applied. Since the 1990s, electroactive polymers have shown potentials as a novel material in robotics, MEMS and medical fields. The potentials can be realized as actuating and mechanical sensing functions. The actuating and mechanical sensing functions are based on the measurements of electrical and mechanical behaviors. The electromechanical behaviors of electroactive polymers have been investigated for actuators since the 1990s and for mechanical sensors recently.

'Electroactive polymers' is a technical term in the field of actuator engineering. Bar-Cohen and Zhang (2008) classified the electroactive polymers as shown in Fig. 1.3. The classification is based on the material type of actuators. There are different materials with different mechanisms in actuation. In Fig. 1.3, EAP means electroactive polymer. EAP is deformed when electric field is applied. Within EAP, there are dielectric EAP and ionic EAP. Dielectric EAP is actuated by dielectric polarization when electric field is applied, and ionic EAP is actuated by ion transport process when electric field is applied. Ionic EAP is classified as conducting polymer and IPMC. The conducting polymer is actuated by reaction and oxidation when electric field is applied. Polypyrrole is one of conducting polymers for actuators. IPMC means ionic polymer metal composite. IPMC is actuated by ion migration when electric field is applied. Flemion and Nafion belong to IPMC.

The advantages and disadvantages between dielectric and ionic electroactive polymers are shown in table 1.1. The large deformations of ionic electroactive polymers with low electricity come from low mechanical stiffness, so the actuation forces of ionic electroactive polymers are naturally low. Even though ionic electroactive polymers are known as show relatively slow responses, some ionic electroactive polymers such as a Nafion with a certain ion form show fast response (Nemat-Nasser and Wu, 2003). Ionic

electroactive polymers inducing conducting polymers and IPMCs have a strong advantage. That is, ionic electroactive polymers can operate with low electric voltage ranges around 2 V. In contrast, dielectric electroactive polymers need high electric voltage range around 200V which is dangerous for human. Therefore, ionic electroactive polymers have particularly attracted attention in medical and bioengineering fields.

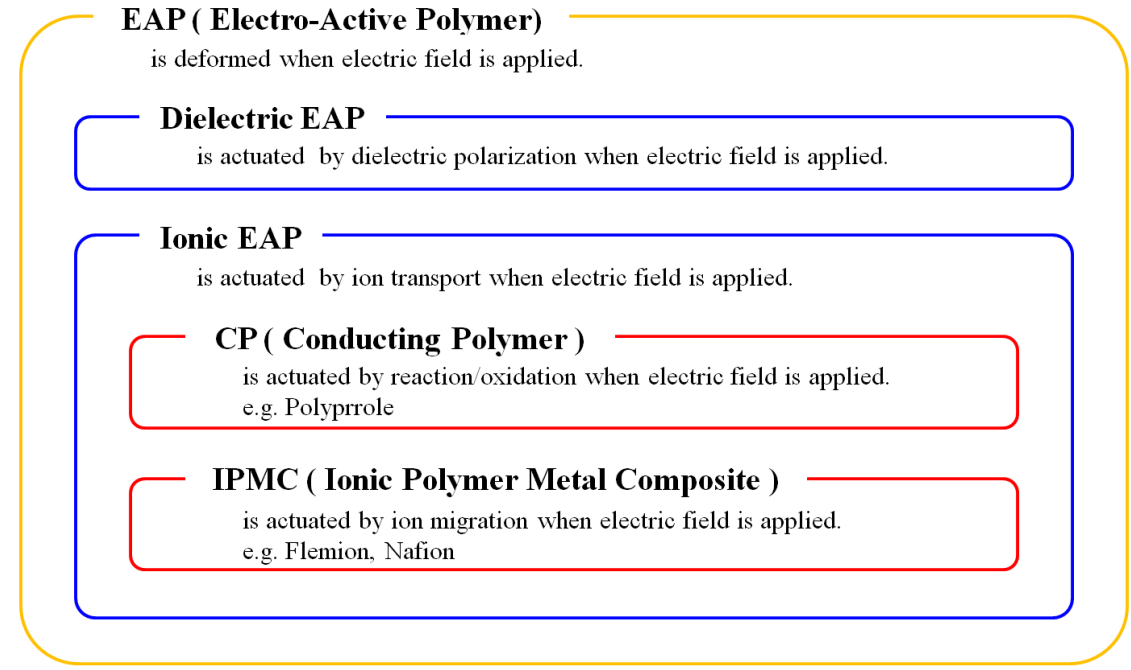

Fig. 1.3 Classification of electroactive polymers (Bar-Cohen and Zhang, 2008)

Table 1.1 Comparison between dielectric and ionic electroactive polymers (Bar-Cohen and Zhang, 2008)

Group	Advantages	Disadvantages
Ionic EAPs	Low voltage operation, e.g. 2 V	Relatively slow response Low actuation force Possibility of hydrolysis
Dielectric EAPs	Rapid response Large actuation force	High voltage operation, e.g. 200 V

Ionic electroactive polymers can be said as electroactive polymers actuating with the mechanism of ion transport. As explained before, ionic electroactive polymers are divided into conducting polymers and IPMCs.

'Conducting polymer' in the present study means the conducting polymer of actuators. The electroactive properties of conducting polymers have been observed since the 1990s. The application of conducting polymers with various electric conductivities has been expanded into actuator engineering. Furthermore, conducting polymers have recently attracted interest in sensor application (Gerard et al., 2002). One of prospective possibilities is mechanical sensors which generate electricity when mechanical stimulation is enforced.

'IPMCs' are ion polymer-metal composites which have the electroactive property for actuators. Ionic polymers such as Nafion and Flemion have been originally applied as polyelectrolyte. After the discovery of their electroactive properties, IPMCs have attracted attention as a novel material for actuators. IPMCs are composed of ion exchange membranes and metal deposits. In detail, the ion exchange membrane is ionic polymers as polyelectrolyte with ionizable groups on molecular backbone. The polyelectrolyte is filled with liquid containing ions, and the ionizable groups dissociate and attain net charges in a variety of solvent. When electric field is applied, ions inside the polyelectrolyte migrate and cause mechanical deformation (Shahinpoor et al., 1998). Bio-inspired dome structure using IPMCs is one of the applications of mechanical sensors (Wang et al, 2009).

The present study focuses on the computational modeling of mechanical sensors using ionic electroactive polymers. The numerical simulation of mechanical sensors using conducting polymers is introduced in Chapter 2 and 3, and the numerical simulation of mechanical sensors using IPMCs is introduced in Chapter 4.

1.2 Actuators and Mechanical Sensors Using Ionic Electroactive Polymers

Actuator can be said as a device for moving or controlling a mechanism or system. Sensor can be defined as a device for detecting changes in quantities and provides information corresponding to the changes. Mechanical sensors are sensors detecting changes mechanical force and displacement.

Both of actuator and sensor response to external actions as input, and then generates their own output. Generally, actuators convert from a certain type of energies to mechanical motions. The supplied energy and generated motion can be thought as the input and output of the actuators. The inverse of the input and output of the actuators becomes mechanical sensors. The actuators and mechanical sensors are similar with human muscles like we control our body and feel our motion.

As mentioned in the previous section, ionic electroactive polymers exhibit electromechanical behaviors that change shapes responding to electrical stimulations. In addition, ionic electroactive polymers inherently possess superior properties like other polymers, e.g. mechanical flexibility and chemical stability. Such ionic electroactive polymers are prospective materials for actuators and mechanical sensors.

Actuators using ionic electroactive polymers have started to be applied into practical engineering. For example, fish robot using ionic electroactive polymers have commercially been developed and globally announced. The application of ionic electroactive polymers have gradually been expanded (http://eamex.co.jp/). Furthermore, the key advantage of ionic electroactive polymers is that can operate in low electric voltage around 2 V. The capability with low voltage shows a prospective potential for artificial muscles.

With the development of the actuators, ionic electroactive polymers have shown mechanical sensing function (Shahinpoor et al., 1998). The present study focuses on mechanical sensors using ionic electroactive polymers. The schematics of actuators and mechanical sensors using ionic electroactive polymers are shown in Fig. 1.4. The left figure shows an actuator using an ionic electroactive polymer. When electric potential is applied across electrodes, the actuator shows large deformation. The right figure shows a mechanical sensor using the same ionic electroactive polymer. When a deformation is enforced, the

mechanical sensor generates electricity. We can know that ionic electroactive polymers can be applied into both of actuators and mechanical sensors.

The above applications are based on the measurements of electric potential and mechanical deformation as shown in Fig. 1.5. For mechanical sensors, deformation is input and electricity is output. For actuators, electricity is input and deformation is output. For practical application, the input-output relations for actuators and mechanical sensors have to be investigated.

The ionic electroactive polymers of actuators and mechanical sensors show very different magnitude in input-output relations as shown in Fig. 1.5. Even though actuators and mechanical sensors are made up of the same material and structure, the generated electric voltage of the mechanical sensors is very much small compared to the generated electric voltage of the actuators. The previous researches had focused on only one between actuators and mechanical sensors. Therefore, they could employ black box models like a linear relation between electric voltage and mechanical deformation. The black box models are empirical relations on well-controlled condition like experiments. If ionic electroactive polymers are exposed to various conditions, the black box models are not reasonable any more, so white box models with detailed considerations are needed. White box models have recently been reported, but they are only for actuators. Furthermore, the existing white box models of actuators are insufficient for the simulation of the mechanical sensors. In addition, ionic electroactive polymers have received expectation as a novel material for artificial muscle, so the models of actuating and mechanical sensing behaviors of the same ionic electroactive polymer have to be integrated.

For both of actuators and mechanical sensors, the integrated relation between mechanical stress and electric potential seems difficult to be determined by using just mechanical stress and electric potential. Like white box model for actuators, the simulation of the mechanical sensors needs more considerations upon understanding the mechanism of the mechanical sensors. The mechanism is qualitatively explained with the transport phenomena of ion and solvent which are absorbed into porous ionic electroactive polymers. Based on the qualitative mechanism, the black box of the mechanical sensors can be decomposed with numerical simulation considering other physical parameters such as fluid pressure of porous conducting polymers, ion and water concentrations as shown in Fig. 1.6. The black box of the mechanical sensors has so far not been revealed with the numerical simulation.

The present study newly attempts to solve the black box of mechanical sensors using ionic electroactive polymers.

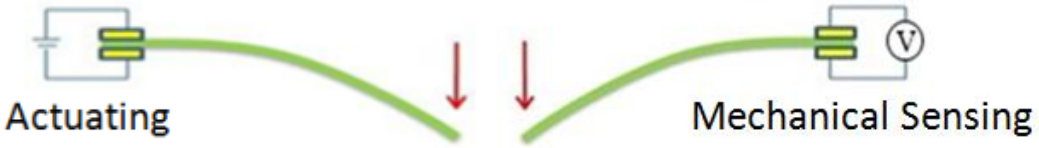

Fig. 1.4 Schematics of an actuators and mechanical sensors using ionic electroactive polymers

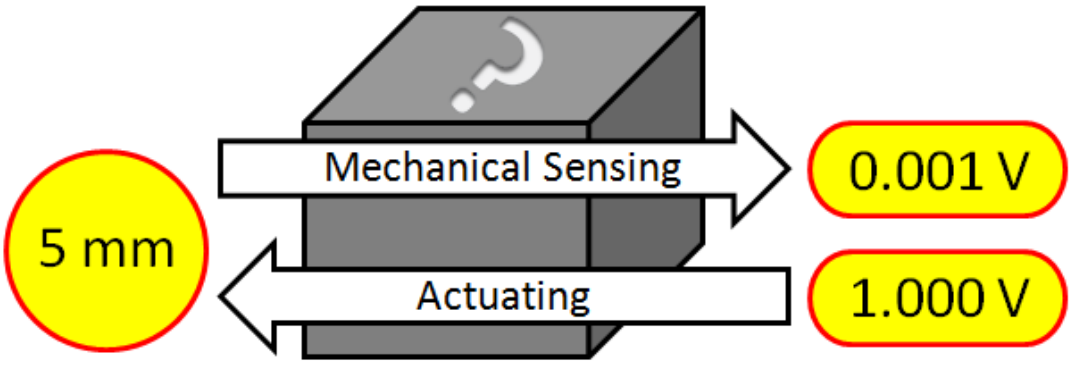

Fig. 1.5 Black box model of actuators and mechanical sensors

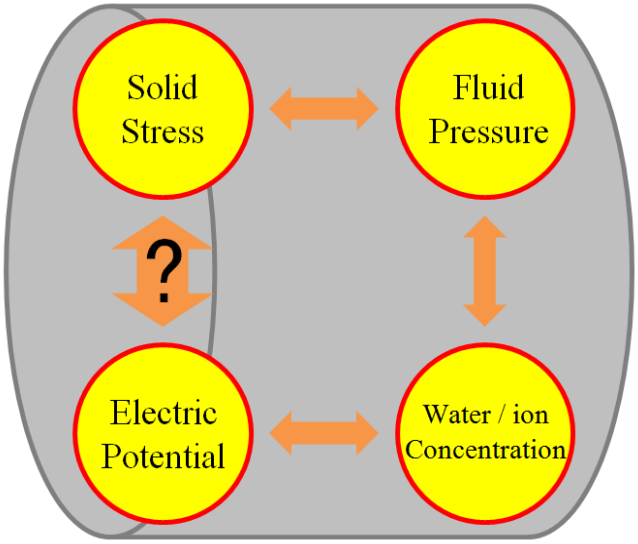

Fig. 1.6 Black box model of input-output of IPMCs

1.3 Backgrounds and Objectives

1.3.1 Previous Experiments for Actuators and Mechanical Sensors Using Ionic Electroactive Polymers

Since the late 1990s, ionic electroactive polymers have been received attentions as a novel material for mechanical sensors. Shahinpoor et al. (1998) introduced the application of IPMCs as biomimetic sensors and actuators. Conducting polymers have been issued as biosensors (Gerard, M. et al., 2002). Spinks et al. (2002) investigated the mechanical properties of polypyrrole for actuators. Nemat-Nasser and Wu (2003) conducted the comparative experiments of IPMCs with different backbone ionomers and in various cation forms. They investigated the interesting properties of IPMCs with water uptake. Guilly et al. (2003) investigated Flemion-based actuators for mechanically controlled microwave switch. Mauritz (2004) introduced the mechanical sensing behavior of IPMCs, which generates electricity by deformation. Wu et al. (2007) investigated the mechanism of mechanical sensors and actuator using polypyrrole. Wang et al. (2009) introduced the bio-inspired design of tactile sensors based on an IPMC, Flemion. Zhao et al. (2011) investigated the transport phenomena of water in an IPMC, Nafion. Until now, conducting polymers have continuously been received attention as prospective materials (Ates et al., 2012, Das and Prusty, 2012).

1.3.2 Previous Simulations for Actuators and Mechanical Sensors Using Ionic Electroactive Polymers

Since the late 1990s, the actuators using ionic electroactive polymers have been investigated with simulation methods. Della Santa et al. (1997) employed poroelastic theory into the analysis of an actuator using polypyrrole. They introduced a performance analysis of a conducting polymer film actuator made of polypyrrole. Shahinpoor et al. (1998) introduced mathematical modeling for artificial muscle using IPMCs. Tadokoro et al. (2001) modeled the actuation mechanisms of IPMCs. They modeled forces acting on molecules

in the solvent. Nemat-Nasser and Zamani (2006) modeled the electrochemomechanical response of IPMC-based actuators with various solvents. They estimated the pressure of cluster with microscopic model and the pressure leads actuating strain as eigen-strain. Alici et al. (2006) introduced a methodology towards geometry optimization of high performance polypyrrole actuators. They employed finite element method, and the actuating strain is considered like thermal strain. Alici, G. et al. (2008) investigated the response of electroactive polymers as mechanical sensors. They proposed empirical relations between electric potential and mechanical stress. Otero and his coworker (2012) attempted the integration of actuating and sensing models. The simulation of actuators using IPMCs has been continuously investigated for their real applications (Jo et al., 2013).

In the field of numerical simulation, there are many papers for actuators using ionic electroactive polymers, but only black box models have been found for mechanical sensors using ionic electroactive polymers.

1.3.3 Previous Researches for Actuators Using Ionic Electroactive Polymers in Toi Lab

Toi laboratory aims at developing computational methods in solid mechanics and applying them to various structural and material problems including academic as well as industrial aspects (http://as1200.iis.u-tokyo.ac.jp/).

For IPMCs, the precious researches of Toi Lab. have collaborated with the experiments of Taya Lab. in Univ. of Washington. Taya and his coworkers (Guilly et al., 2003) have experimentally investigated for actuators using Flemion-based IPMCs. Kang and Toi (2005) modeled the forward and backward motions of IPMCs and developed finite element formulation. Jung et al. (2010) modeled electro-osmosis and electrolysis, and developed computational modeling of electrochemical–mechanical behaviors of Flemion-based actuators

For conducting polymers, Toi and Jung (2007) attempted the finite element modeling of actuators using conducting polymers (Toi and Jung, 2007 and 2008).

The previous researches in Toi Lab. have focused on numerical simulation with finite element method, but their targets were only actuators.

1.3.4 Present Researches for Mechanical Sensors Using Ionic Electroactive Polymers

Most researches have been focused on actuators, and a few researches have been reported for mechanical sensors. The previous researches in Toi Lab. have focused on actuators using ionic electroactive polymers. Regarding to mechanical sensors using ionic electroactive polymers, only black box models, which are empirical relations between input and output, have been reported. Therefore, Yoo and Toi (2013) newly attempted the numerical simulation of mechanical sensors using conducting polymers.

Recently, Taya and his coworkers, who are Toi's collaborators, have conducted experimental investigations for mechanical sensors using Flemion-based IPMCs (Wang et al. 2009). Based on the experimental investigations of Taya Lab., Yoo and Toi (2014) modeled hydration effects on volume and mechanical stiffness, and introduced the numerical simulation of mechanical sensors using hydrated IPMCs.

1.3.5 Present Simulation for Mechanical Sensors Using Ionic Electroactive Polymers

Ionic electroactive polymers have been investigated as a novel material for actuators since the 1990s. Like other approaches, numerical simulation has been added into the investigations. Since the late 1990s, the numerical simulation of ionic electroactive polymers has been reported. However, the numerical simulations have focused only on actuating behaviors.

Recently, the mechanical sensing behaviors of ionic electroactive polymers, which are converse to the actuating behaviors, have been investigated. Following the investigation, numerical simulation can be added. This is the starting point of the present study. Mechanical sensors using ionic electroactive polymers have experimentally investigated based on linear relations between mechanical stress and electric voltage. Since mechanical stress has to be obtained, structural analysis becomes important here. In general, the structure analysis of the mechanical sensors has simply been conducted with ordinary beam theory in solid mechanics (Alici et al., 2008). The mechanism of the mechanical sensors can be explained by non-linear distribution of interesting parameters over thickness (Alici et al.,

2006), so the present study initially attempted to propose a method of structure analysis for the non-linear distribution, and electric voltage was estimated with the black box model of a linear relation between mechanical stress and electric voltage.

In detailed considerations, the input-output relations between actuator and mechanical sensor using ionic electroactive polymers are quantitatively very different. Furthermore, the mechanical sensors show time dependent responses with relaxation and hysteresis. Recently, white box models for actuators have been reported (Jung et al., 2010). The white box models showed important physical quantities such as the pressure of ion-containing fluid, ion concentration and electric field with time. In addition, they can estimate the contributions of the interesting quantities or material properties such as mechanical and electrochemical properties. Eventually, a more complicated model like the white box models becomes needed for the mechanical sensors.

However, it is found that the white box model of actuating behaviors using ionic electroactive polymers cannot reproduce mechanical sensing behaviors using the same ionic electroactive polymers. The white box model can be understood by dividing into transport process and structural analyses as shown in Fig. 1.7. The white box model solves the transport process of ion and ion-containing fluid, and the transported quantities of the fluid are related to volumetric change. Here, the volumetric change is considered as eigenstrain in structural analysis, and then results in the deformation of actuators. For actuating behaviors, when ion-containing fluid is transported due to electric field, the solid matrix of porous membrane rapidly obtains mechanical equilibrium. For mechanical sensing behaviors, when the solid matrix of the membrane is deformed, the fluid in the porous membrane needs more time relative to solid matrix until mechanical equilibrium. During the unbalance state, electric voltage is peaked. This phenomenon is of the mechanical sensors is modeled in the present study. Next issue is ion convection due to the transport of ion-containing fluid. For actuators, ion convection due to ion-containing fluid is negligible, but for the mechanical sensors, the ion convection is expected to have a significant effect on the electric voltage, because the generated voltage of the mechanical sensors is very much small one-hundredths times. The ion convection term is considered in the present study. In addition, the dependency of water uptake on the performance of the mechanical sensors is modeled in the present study. Details of the computational modeling of mechanical sensors using ionic electroactive polymers are written in Chapter 2~4.

The present study sets the same basic governing equations of the mechanical sensors with the actuators. Based on mechanical and electric properties from conventional test, the mechanism of the mechanical sensors has been modeled, and computational system is totally proposed.

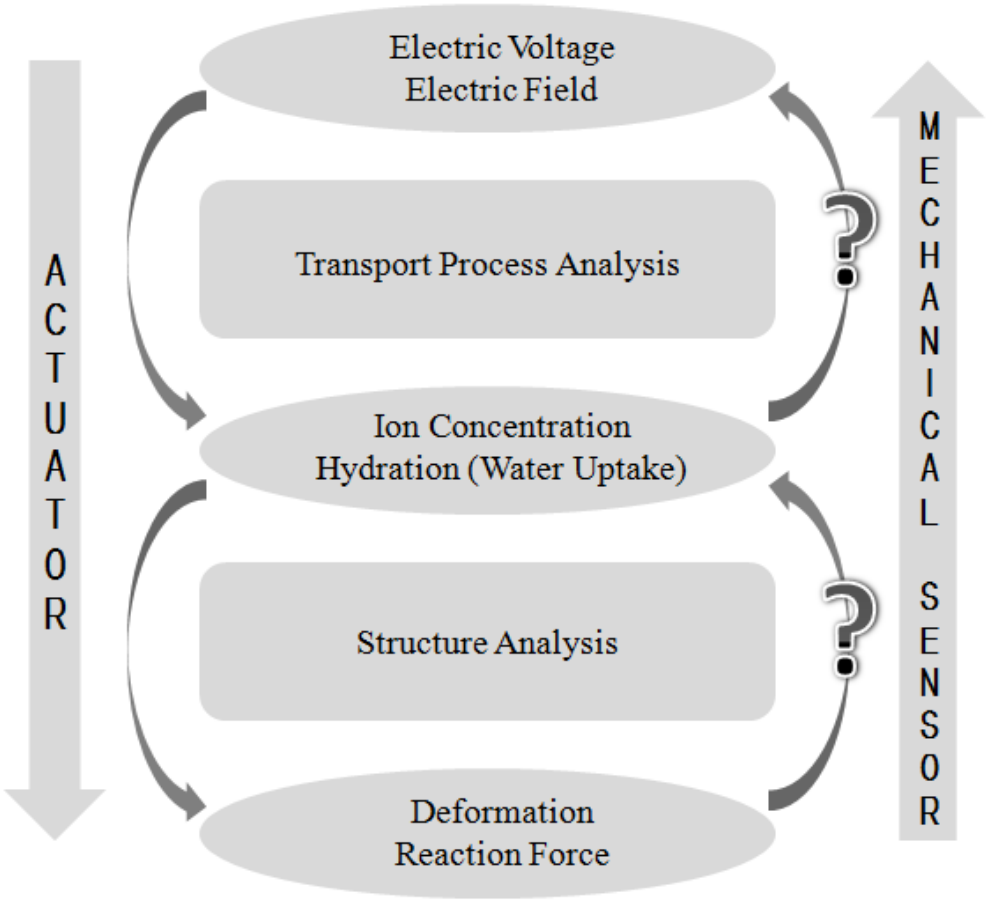

Fig. 1.7 Flowchart of numerical simulations of actuators and mechanical sensors using ionic electroactive polymers

1.4 Overviews

The title of the present study is the computational modeling of mechanical sensors using ionic electroactive polymers. The simulation to reproduce the electromechanical behaviors of ionic electroactive polymers is still difficult even though a lot of researches have been conducted. For the estimation of the electromechanical behaviors, most researches employed simple black box models from experimental observations, e.g. an empirical relation between mechanical stress and electric voltage. Here, structure analysis becomes important to obtain the mechanical stress. In such backgrounds, the present study was started with a black box model and focused on structure analysis. The first attempt for the numerical simulation of the mechanical sensors is introduced in chapter 2. The mechanical sensors show quantitatively different input-output relations even with the same material and structure of actuators. Moreover, the mechanical sensors show time dependent responses such as relaxation and hysteresis. Therefore, as the further research of chapter 2, a more complicated model was developed for the mechanical sensors. The second attempt is introduced in chapter 3. Next, another material of ionic electroactive polymer for mechanical sensors is IPMC. IPMCs show hydration effect that mechanical stiffness and volume are significantly changed as water is absorbed. The hydration effect is modeled, and the proposed model in chapter 3 is employed into IPMCs. The third attempt is introduced in chapter 4.

Chapter 2

Black Box Model of Mechanical Sensors Using Conducting Polymers

Chapter 2 introduces a computational system, using a simple black box model, for mechanical sensors using conducting polymers. The conducting polymers, which belong to ionic electroactive polymers, have attracted attention as a prospective material for mechanical sensing from mechanical stimulation to electricity. When mechanically stimulated by an external force, the mechanical sensors are elastically deformed and then show a large reduction of reaction forces. The elastic deformation of the mechanical sensors, in

response to mechanical stimulation, is analyzed with layered Timoshenko beam theory. The subsequent reduction of the reaction forces, quantitatively idealized with initial strain method, is calculated with finite element method. Therefore, the net reaction force is obtained and employed to estimate a generated potential as the response of the mechanical sensors. As the application of the proposed method, the mechanical sensing behaviors are simulated in cases of prescribed and stepwise loading conditions, and those results are compared with experimental results in order to validate the proposed method.

Chapter 3

Numerical Simulation of Mechanical Sensors Using Conducting Polymers

Chapter 3 introduces a more complicated model for mechanical sensors using conducting polymers which generate electricity in the transient response to mechanical stimulation. The generated electric potential in the mechanical sensors is very much smaller than the supplied electric potential of the actuators with respect to the same deformation and structure. Furthermore, the mechanical sensors show transient responses with relaxation and hysteresis. In order to compensate the complicated behaviors of the mechanical sensors, the present study modifies and integrates the existing theories and the features of the transient behaviors, e.g. the non-invertible relation between electrical potential and deformation, relaxation and hysteresis, are numerically simulated. The governing equations of the physical phenomena of the mechanical sensors coupled by embedding driving forces with physical parameters such as solid stress, fluid pressure, ion concentration and electric potential. The governing equations and the fields of the physical parameters are spatially simplified as one-dimensional in the thickness direction of the sensors, because their variations over thickness dominantly determine the behavior of the sensor. In addition, the numerical procedure is efficiently simplified as possible as the transient behaviors are expressed. Next, the undrained Poisson's ratio is modified with a correction factor, and its significant effect on the transient behavior is investigated. Lastly, the procedure of the present computational system for the mechanical sensors is introduced and fully coupled simulation is conducted. As a result, the present study reports the simulation results of the important physical quantities over the microscale thickness of the mechanical sensors.

Chapter 4

Numerical Simulation of Mechanical Sensors Using Hydrated IPMCs

Chapter 4 introduces the numerical simulation of mechanical sensors using hydrated IPMCs. IPMCs can be applied into both of actuators and mechanical sensors, but the existing models of the actuators cannot be inversely applied to the mechanical sensors. The mechanical sensors generate very much smaller electric potential compared to the supplied electric potential of actuators with respect to the same displacement and structure. The non-invertible response of the mechanical sensors is numerically simulated, and the simulation considers hydration and transient behaviors. IPMCs have hydration effect that volume and mechanical stiffness are significantly changed with water uptake. In order to consider the volume swelling due to hydration, the total strains and pore pressure of IPMCs are respectively decomposed into stress-induced and hydration-induced parts. The hydration-induced strain is considered as eigen-strain, and the stress-induced strain and stress-induced pore pressure are employed into Biot poroelastic constitutive equations. The mechanical stiffness of a hydrated IPMC is expressed as empirical relations with water uptake. Furthermore, mechanical sensors using IPMCs show transient response with the relaxation and time lag of reaction force and electric potential. The transient response is modeled with a set of basic equations, e.g. layered Timoshenko beam model, Biot poroelastic model, Darcy-flow model, Poisson-Nernst-Plank model. The instantaneous peak of reaction force is estimated on undrained condition, the relaxation of reaction force is considered with pore pressure and its Poisson effect, and hydration-induced water migration is modeled with hydration potential. The hydration potential is modeled with an empirical chemical potential at free swelling equilibrium and is expressed as a function of water uptake. Next, discretization and numerical formulation with layered finite beam elements is introduced. Lastly, the transient responses of a Flemion-based mechanical sensor are numerically simulated with different deflections, and the distributions of stress, pore pressure, ion concentration and electric potential are obtained with time. Lastly, the numerical results are compared with experimental results.

1.5 References

Ates, M. et al., 2012, Conducting polymers and their applications, Development (Cambridge), Vol. 51, pp. 52

Alici, G. et al., 2006, A methodology towards geometry optimization of high performance polypyrrole (PPy) actuators, Smart Materials and Structures, Vol. 15, No. 2, pp. 243-252

Alici, G. et al., 2008, Response characterization of electroactive polymers as mechanical sensors, Mechatronics, IEEE/ASME Transactions, Vol. 13, No. 2, pp. 187-196

Bar-Cohen, Y. and Zhang, Q., 2008, Electroactive polymer actuators and sensors, MRS bulletin, Vol. 33, No. 3, pp. 173-181

Das, T. K., and Prusty, S., 2012, Review on conducting polymers and their applications, Polymer-Plastics Technology and Engineering, Vol. 51, No. 14, pp. 1487-1500

Della Santa, A. et al., 1997, Performance and Work Capacity of a Polypyrrole Conducting Polymer Linear Actuator, Synthetic Metals, Vol.90, pp.93-100

Delia Santa, A. et al. 1997, Passive mechanical properties of polypyrrole films: a continuum, poroelastic model, Materials Science and Engineering: C5.2, pp. 101-109

Della Santa, A. et al., 1997, Performance and work capacity of a polypyrrole conducting polymer linear actuator, Synthetic metals, Vol. 90, No. 2, pp. 93-100

Gerard, M. et al., 2002, Application of conducting polymers to biosensors, Biosensors and Bioelectronics, Vol. 17, No. 5, pp. 345-359

Guilly, Marie Le et al., 2003, Flemion based actuator for mechanically controlled microwave switch, Proceeding of SPIE, Vol. 5051, pp. 363

Jo, C. et al., 2013, Recent advances in ionic polymer–metal composite actuators and their modeling and applications, Progress in Polymer Science, Vol. 38, No. 7, pp. 1037-1066

Jung, W. et al., 2010, Computational modeling of electrochemical–mechanical behaviors of Flemion-based actuators considering the effects of electro-osmosis and electrolysis, Computers & structures, Vol. 88, No.15, pp. 938-948

Mauritz, K. A. and Moore, R. B., 2004, State of understanding of Nafion, Chemical reviews, Vol. 104, No, 10, pp. 4535-4586

Nemat-Nasser, S. and Zamani, S., 2006, Modeling of electrochemomechanical response of ionic polymer-metal composites with various solvents, Journal of Applied Physics, Vol. 100, No. 6, pp. 064310.

Nemat-Nasser, S. and Wu, Y., 2003, Comparative experimental study of ionic polymer–metal composites with different backbone ionomers and in various cation forms, Journal of Applied Physics, Vol. 93, No. 9, pp. 5255-5267

Otero, T. F. et al., 2012, Biomimetic dual sensing-actuators based on conducting polymers, Galvanostatic theoretical model for actuators sensing temperature, The Journal of Physical Chemistry B, Vol. 116, No. 17, pp. 5279-5290

Rudin, A. and Choi, P., 2012, The Elements of Polymer Science & Engineering, Academic Press.

Shahinpoor, M. et al., 1998, Ionic polymer-metal composites (IPMCs) as biomimetic sensors, actuators and artificial muscles-a review, Smart materials and structures, Vol. 7, No. 6, R15

Shirakawa, H. et al., 2003, Twenty-five years of conducting polymers, Chemical Communications, Vol. 1, pp. 1-4

Spinks, G. M. et al., 2002, Strain response from polypyrrole actuators under load, Advanced Functional Materials, Vol. 12, pp. 437–440

Tadokoro, S. et al., 2001, Modeling IPMC for design of actuation mechanisms, Electroactive Polymer (EAP) Actuators as Artificial Muscles, Reality, Potential, and Challenges, 331-366

Toi, Y., and Kang, S, 2005, Finite element analysis of two-dimensional electrochemical–mechanical response of ionic conducting polymer–metal composite beams, Computers & structures, Vol. 83, No. 31, pp. 2573-2583

Toi, Y. and Jung, W., 2007, Finite element modeling of electrochemical-poroelastic behaviors of conducting polymers, Computers & Structures, Vol. 85, No. 19, pp. 1453-1460

Toi, Y. and Jung W., 2008, Finite Element Modeling of Electrochemical-Poroelastic Behaviors of Conducting Polymer Films, Journal of Solid Mechanics and Materials Engineering, Vol. 2, No. 7, pp. 865-876

Toi, Y., and Jung, W., 2008, Computational Modeling of Electrochemical-Poroelastic Bending Behaviors of Conducting Polymer (PPy) Membranes, Journal of Computational Science and Technology, Vol. 2, No. 4, pp. 523-534

Wang, J. et al., 2009, Bioinspired design of tactile sensors based on Flemion, Journal of Applied Physics, Vol. 105, No. 8, pp. 083515

Wu, Y. et al., 2007, Soft mechanical sensors through reverse actuation in Polypyrrole, Advanced Functional Materials, Vol. 17, pp. 3216-3222

Yoo, S. and Toi, Y., 2013, Numerical Simulation of Mechanical Sensors Using Conducting Polymers, Journal of Solid Mechanics and Materials Engineering, Vol. 7, No. 6, pp. 585-600

Yoo, S. and Toi, Y., 2014, Numerical Simulation of Mechanical Sensors using Hydrated IPMCs, Mechanics Engineering Journal, submitted (under review)

Zhao, Q., Majsztrik, P., and Benziger, J., Diffusion and interfacial transport of water in Nafion, The Journal of Physical Chemistry B, Vol.115, No. 12 (2011), pp 2717–2727

Chapter 2

Black Box Model of Mechanical Sensors Using Conducting Polymers

2.1 Introduction

Conducting polymers can be briefly said as extraordinary plastics able to conduct electricity. They have already been applied to various fields and very common in our life such as batteries, displays and so on. Moreover, they have still shown endless potentials in a very wide range of applications. Conducting polymers have recently received amplified expectations as a novel material especially in robot-engineering, micro-electro-mechanical systems (MEMS) and medical fields. The attention is thanks to attractive characteristics as follows. They are driven by low voltage (1~3V), micro-miniature, light weight, flexible and silent, durable and stable chemically, and working in water or wet condition. Owing to such advantages, conducting polymers have recently shown a multitude of potentials as a candidate of actuators and sensors, from electricity to motion and from stimulation to electricity, which are the topic of the present study.

Conducting polymers play principal role in mechanical sensing process from mechanical stimulation to electricity. When mechanical sensors using conducting polymers are deformed, they generate electric potential corresponding to the magnitude of mechanical stimulation. Hence, the mechanical sensors estimate the external force and displacement by measuring the generated electric potential. As for the simulation model of mechanical sensors, mechanical displacement or force is input and then electric potential or current is output as shown in Fig. 2.1. In spite of many simulations of the actuators, the simulation results of the mechanical sensors have not been reported. The numerical simulation is needed for the design and control of the mechanical sensors. Therefore, the present study proposes the simulation model for the mechanical sensors.

Along with a variety of applications of conducting polymers, a lot of researches have been conducted. Della Santa et al. (1997) investigated mechanical properties of conducting polymers, and proposed an electroactive actuator model to predict the static and dynamic responses of conducting polymers. Alici et al. (2006) introduced an approach using finite element analysis to estimate the behaviors of conducting polymer actuators. They introduced a computational method for the design of conducting polymer actuators, and their approach was applied for the scantling of the actuators. The approach employed a

prescribed temperature distribution and considered the thermal expansion as volume change. Toi and Jung (2007) also proposed a more detailed model for finite element analysis, in order to simulate the electroactive behaviors of conducting polymers, using ion transportation and poroelastic models. Wu et al. (2007) introduced a relation between the potential and bending stresses of mechanical sensors using conducting polymers that is linear but dependant on dopant ions and electrolytes. Alici et al. (2008) experimentally investigated the responses of mechanical sensors using conducting polymers and proposed an estimation model for the mechanical sensors. Nevertheless, research results for mechanical sensors using conducting polymers are so far scarce, even though many researches for actuators using the same conducting polymers have been conducted. The computational model for mechanical sensors using conducting polymers has not so far been distinctly established, because the generated potential of the mechanical sensor, which is induced by mechanical action, is very different from the supplied potential of the actuator inducing the same mechanical action.

In the present study, the behaviors of mechanical sensors using conducting polymers are investigated, and a computational system for the estimation of their behaviors is proposed. If an enforced displacement or external force is prescribed as the input of the mechanical sensors, the resultant reaction force is estimated by structural analysis. In this stage, finite element method is employed to analyze the mechanical states of the mechanical sensor. Next, electric potential as the output of the mechanical sensors is estimated by an experimental linear relation between mechanical stress and electric potential. Finite element analysis for the behaviors of the mechanical sensors is hardly reported even though finite element method has been well employed to analyze the actuations of conducting polymers.

If a black box model using mechanical input and electrical output is employed, structural analysis becomes important in order to estimate the responses of the mechanical sensors more precisely. In the present study, a structural analysis method for the mechanical sensors, using initial strain method which quantitatively idealizes the reduction of reaction force, is proposed with layered Timoshenko beam theory and finite element method. In addition, the numerical results, in cases of prescribed and stepwise loading conditions, are shown with experimental results.

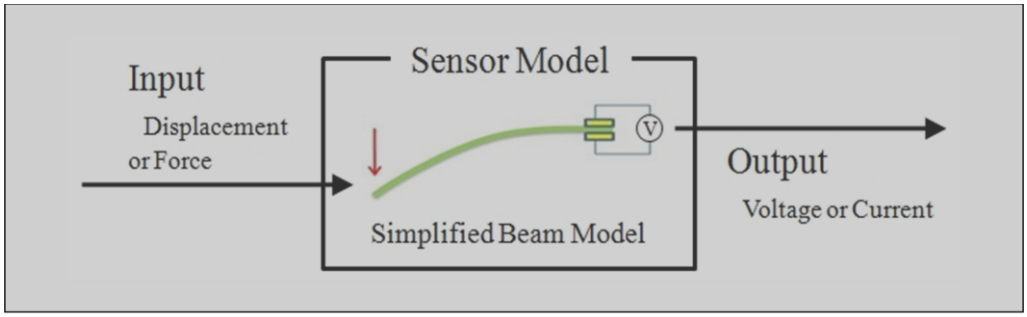

Fig. 2.1 Black box model of mechanical sensors using conducting polymers

2.2 *Theoretical Models*

A structure of mechanical sensors using the conducting polymer is illustrated in Fig. 2.2. This type is efficiently designed by Alici et al. (2006 and 2008). The mechanism of mechanical sensors using conducting polymers is shown in Fig. 2.3. When mechanical stimulation such as an external force or enforced displacement is applied into the mechanical sensors, bending deformation occurs that the gradient of pressure takes place over beam sections. Due to the gradient of pressure, ions and solvent are pushed out from the compressive sides of polypyrrole and enter into the tensile sides of polypyrrole. The movements of ions and solvent cause a gradual reduction of reaction forces. The ion movements also electronically cause the gradient of charge density, so instant electric potential difference occurs. Subsequently, electric potential is decreased with time by gradual neutralization of the electric charges (Wu et al., 2007 and Alici et al., 2008).

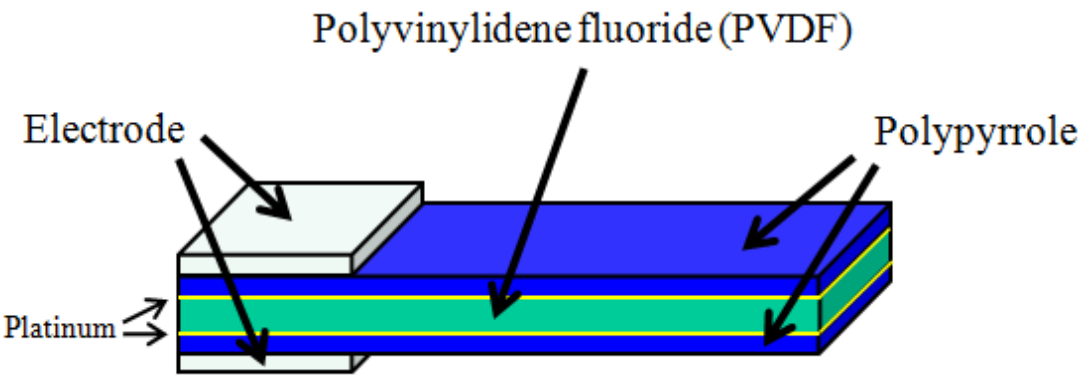

Fig. 2.2 Structure of actuators and mechanical sensors using conducting polymers (Alici et al., 2006 and 2008)

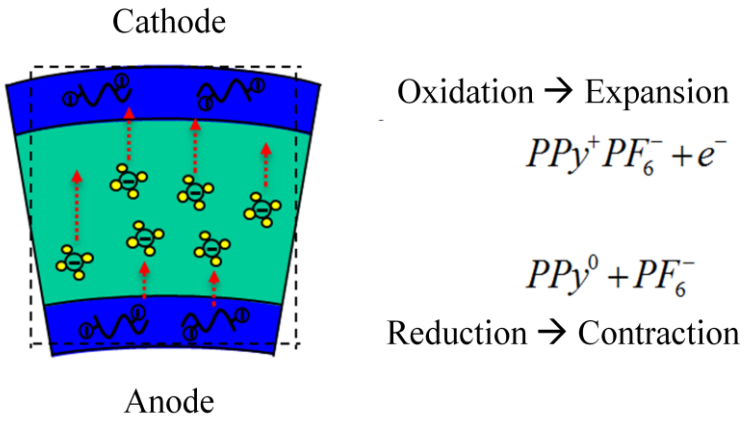

Fig. 2.3 Mechanism of actuators and mechanical sensors using conducting polymers (Wu et al., 2007 Alici et al., 2008)

In the present study, a computational system for mechanical sensors using conducting polymers estimates a generated electric potential as the output of the mechanical sensors when a prescribed displacement or external force is given as shown in Fig. 2.1. The present computational system has to define the input-output relation of the mechanical sensors. Unfortunately, applying the input-output relation of actuators to the mechanical sensors is difficult, because the generated potential of the sensor is quite different from the potential of the actuator with respect to the same mechanical force or prescribed displacement. The mechanical sensors generate microscale potential about one thousandth of the electric potential of the actuator. Wu et al. (2007) concluded that the difference of electric potential between actuator and mechanical sensors with respect to the same deformation is caused by that most external electric energy for electroactive actuation is stored as electrochemical charge in conducting polymers. That is, very small amount of external electric energy is converted to mechanical energy. Alici et al. (2008) measured the reaction forces and induced electric potential when a prescribed or stepwise displacement was applied at the tip of the conducting polymer sensor. As a result, a linear relation between the generated potential and bending stress was introduced. However, the bending stress was calculated from non-layered ordinary beam theory. In their experiments, the reaction force is instantaneously increased and subsequently decreased to static reaction force as shown in Fig. 2.4.

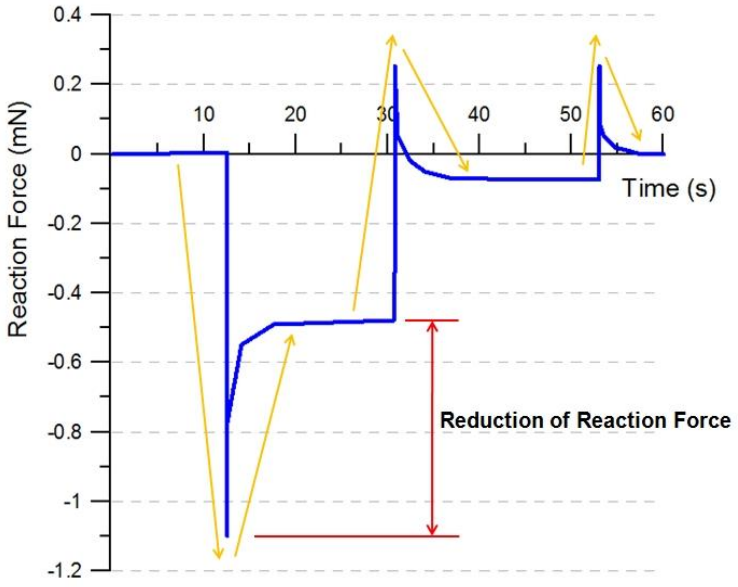

Fig. 2.4 Schematic of behavior of mechanical sensors using conducting polymers

Based on the researches of Alici et al. (2008), the present study attempts more accurate analysis of the mechanical states of mechanical sensors using conducting polymers, and considers the reduction of reaction force. First, when an external force is given, the reaction force of the mechanical sensors is calculated by layered Timoshenko beam theory. Timoshenko beam theory can more accurately analyze the mechanical states of the mechanical sensors. Layered approach is also employed because the stress and property of each layer are non-uniformly distributed over the section of the mechanical sensors. Next, the reduction of reaction force is idealized with initial strain method, using a parameter, C_ε. Finally, the net stress of conducting polymers is obtained, and the generated electric potential of the mechanical sensors is estimated by the linear relation between axial stresses and potential.

In order to predict the response of mechanical sensors using conducting polymers, the present study employs finite element method. Finite element method has been frequently employed in order to analyze the behaviors of actuators using conducting polymers, and it was revealed as a suitable method for the simulation of the conducting polymers. Next, the mechanical behavior of the mechanical sensors is assumed as bending of a beam in solid mechanics. The mechanical deformations of actuators and mechanical sensors using con-

ducting polymers are experimentally observed as the bending of a beam in solid mechanics (Della Santa et al., 1997, Toi and Jung, 2007, Wu et al., 2007, Alici et al., 2008). The estimation model of Alici et al. (2008) was based on Euler–Bernoulli beam theory. In the present study, layered Timoshenko beam model is employed to express the deformation of the mechanical sensor. The layered beam model can express the non-linear distribution of axial stresses, and the Timoshenko beam can consider transverse shear deformation effects. For short or sandwich composite beams, the layered Timoshenko beam model is more accurate than the non-layered ordinary beam. The layered Timoshenko beam in solid mechanics is given as follows (Toi, 2008).

$$u(x,z) = -z\theta(x) \tag{2.1}$$

$$w(x,z) = w(x) \tag{2.2}$$

$$\varepsilon_x(x,z) = \frac{\partial u}{\partial x} = -z\frac{d\theta}{dx} \tag{2.3}$$

$$\gamma_{zx}(x) = \frac{\partial w}{\partial x} + \frac{\partial u}{\partial z} = \frac{dw(x)}{dx} - \theta(x) \tag{2.4}$$

$$\sigma_x(x,z) = E(z)\ \varepsilon_x(x,z) \tag{2.5}$$

$$\tau_{zx}(x,z) = \alpha\ G(z)\ \gamma_{zx}(x) \tag{2.6}$$

In the above equations, the following notations are used: u is axial displacement; z is distance from neutral axis; θ is rotation of the normal section; w is lateral displacement; ε_x is axial strain; γ_{zx} is transverse shear strain; E is elastic modulus; G is shear modulus; α is shear correction factor employed as 5/6 in case of rectangular section. Timoshenko beam theory assumes that axial strains over a beam section are linearly distributed. Thus, we assume that axial strains over the sections of the mechanical sensors are also proportional to the distance from neutral axis as shown in Fig. 2.5 (Toi, 2008).

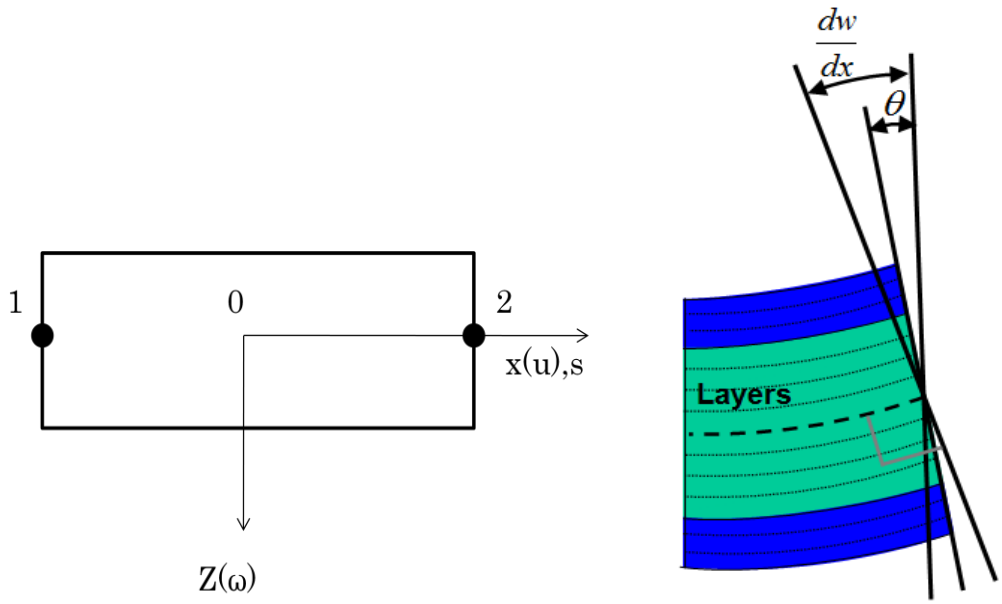

Fig. 2.5 Simplified displacement field of layered Timoshenko beam

Mechanical sensors using conducting polymers are composites having different properties of different layers over their sections, so layered approach is employed. The beam sections of the mechanical sensors are divided into several layers, each of which has different property. As the number of the layers is increased, the present beam model can more accurately represent the separated stiffness and stresses over the section with numerical integration.

The reduction of reaction force is observed that is constant ratio to the total reaction force at instant of loading from the experiment of Alici et al. (2008) as shown in Fig. 2.4. After an enforced displacements are given, its reaction force is immediately generated, which is well-known phenomenon in elastic mechanics. Subsequently, ions and solvent at compressive sides move to tensile sides even when the displacement remains constant, and the reaction force is decreased. The reduction of the reaction force is idealized with initial strain method using parameter, C_ε, in Eq. (2.11) which is determined so as to give the agreement between the calculated reaction force and the experimental value after the movements of ions and solvent. Therefore, the steady reaction force is calculated by subtracting the reduction of reaction force from total reaction force.

As final step, electric voltage as the output of mechanical sensors using conducting polymers is estimated with a relation between electric potential and mechanical stress. Alici

et al. (2008) proposed the linear relation between bending stress and potential as Eq. (2.7). Hence, the potential is estimated with the below.

$$V = C_V \sigma_x \tag{2.7}$$

where, V is potential, and C_V is a coefficient which is the ratio of the bending stress of the conducting polymer layer to the generated potential.

2.3 Numerical Formulations

The layered Timoshenko beam model in the previous section is employed into finite element analysis. The finite element stiffness equation is formulated with the following equations (Toi, 2008).

$$[K]\{d\} = \{f^{ext}\} + \{f^{red}\} \tag{2.8}$$

$$[K] = \int_V [B]^T [D][B] dV \tag{2.9}$$

$$\{f^{red}\} = \int_V [B]^T \{\sigma^{ini}\} dV \tag{2.10}$$

$$\{\varepsilon^{ini}\} = C_\varepsilon \{\varepsilon\} \tag{2.11}$$

$$\{\sigma^{ini}\} = [D]\{\varepsilon^{ini}\} \tag{2.12}$$

In the above equations, the following notations are used: $[K]$ is stiffness matrix; $\{d\}$ is nodal displacement vector; $\{f^{ext}\}$ is external force vector; $\{f^{red}\}$ is reduction of reaction force vector induced by the movements of ions and solvent; $[B]$ is strain-displacement matrix; $[D]$ is stress-strain relation matrix; $\{\varepsilon\}$ is strain vector; C_ε is parameter considering the reduction of axial stresses; $\{\varepsilon^{ini}\}$ is initial strain vector; $\{\sigma^{ini}\}$ is initial stress vector.

Preventing the shear locking by 1-point Gauss-Legendre integration, the element stiffness matrix, $[K]$, is shown as follows (Toi, 2008).

$$[K]=\begin{bmatrix} \left(\frac{G^tA}{L}\right) & \left(\frac{G^tA}{2}\right) & \left(-\frac{G^tA}{L}\right) & \left(\frac{G^tA}{2}\right) \\ & \left(\frac{E^tI}{L}+\frac{G^tAL}{4}\right) & \left(-\frac{G^tA}{2}\right) & \left(-\frac{E^tI}{L}+\frac{G^tAL}{4}\right) \\ & & \left(\frac{G^tA}{L}\right) & \left(-\frac{G^tA}{2}\right) \\ \textit{sym.} & & & \left(\frac{E^tI}{L}+\frac{G^tAL}{4}\right) \end{bmatrix} \tag{2.13}$$

where, L is element length, A is element section area.

2.4 Numerical Results

Alici et al. (2006) optimized a conducting polymer composite for efficient actuations as shown in Fig. 2.6. Its structure is composed of five layers. The material of outmost two layers is polypyrrole (PPy), which is an electroactive polymer, and the middle layer is polyvinylidene fluoride (PVDF). Platinum membrane is positioned between polypyrrole and PVDF. This type is selected for the present simulation as a mechanical sensor using a conducting polymer. The elastic modulus of polypyrrole and PVDF are respectively 80 MPa and 440 MPa. The stiffness of the platinum membrane, in mechanical structure analysis, is negligible because of very small thickness, 10-100Å (Alici et al., 2006, Wu et al., 2007 and Alici et al., 2008).

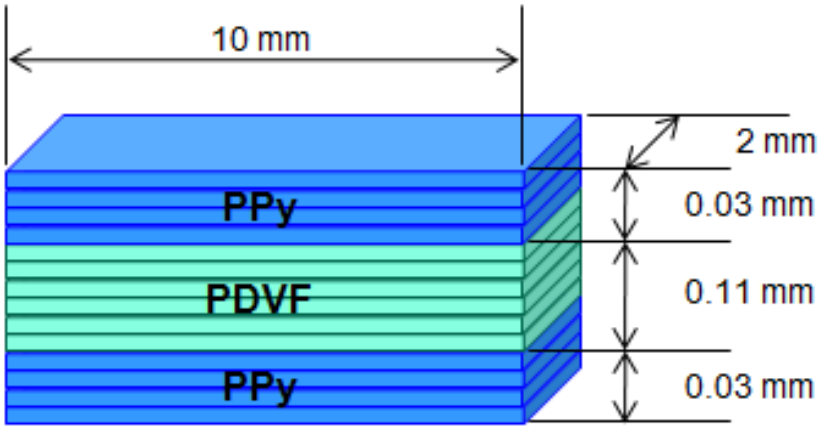

Fig. 2.6 Layered beam model

Timoshenko beam theory needs a sufficient number of beam elements because of C_1 continuity of its assumed deformation field. Thus, 20 elements were used in the finite element analysis of the mechanical sensor.

As shown in Fig 2.6, the beam elements of the mechanical sensor are divided by several layers in order to consider different states of different layers. The number of the layers is up to the property and parameter, C_ε . of each layer.

Depending on the parameter, C_ε , in Eq. (2.11), the reduction of reaction force is quantitatively expressed. Physically, the gradients of concentration and pressure cause the

movements of ions and solvent. We assume that the pressure at instant of rapid loading is ideally proportional to the strains of solid. The parameter, C_ε, is constant over section, then, it is determined as 0.55 concerning the experimental results.

Monotonic case at a prescribed displacement is simulated at first. The prescribed displacement is enforced at the beam tip as shown in Fig. 2.7.

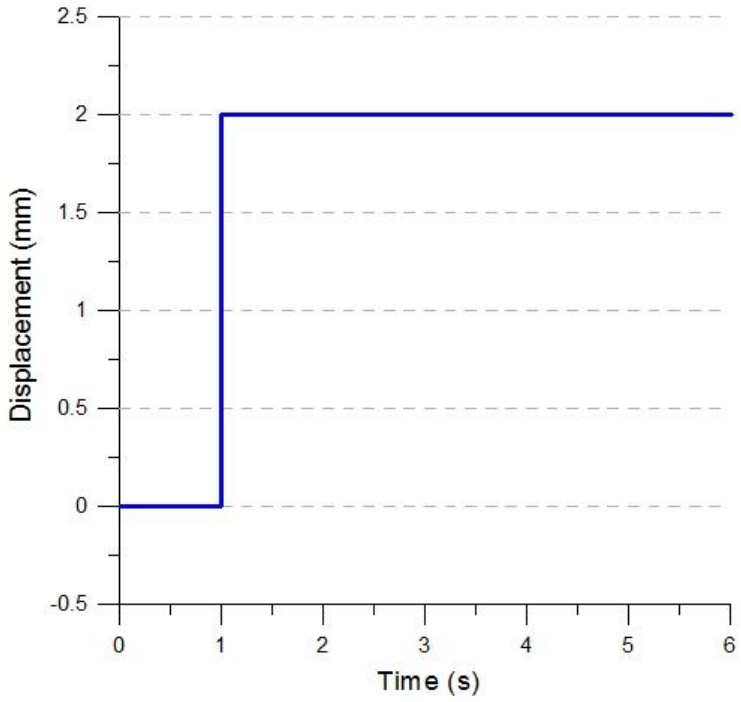

Fig. 2.7 Time history of a prescribed displacement (simulation and experiment)

The comparisons between the non-layered ordinary beam and the layered Timoshenko beam are illustrated in Figs. 2.8 and 2.9 for the referred conducting polymer sensor (Alici et al., 2008) on the same prescribed deflection. As shown in Fig. 2.8, the deflection and axial strain fields are very similar to each other, because shear deformation is negligible in high aspect ratio of length to thickness. On the other hand, there is a large difference in the stress distribution between the non-layered and layered beam models as shown in Fig. 2.9. The non-layered beam model assumes that stiffness is uniform over beam sections so the axial stresses over the thickness become proportional to the distance from the neutral axis. The layered beam model subdivides the section of beams into several layers to consider the different properties of each layer, and the different axial stresses are calculated by the

different stiffness. Since the experiments (Alici et al., 2008) showed that the electric potential generated from mechanical sensors using conducting polymers is largely dependent on the mechanical stress, more accurate analysis of the axial stress distribution over thickness is needed.

In the present study, the layered beam model is selected because conducting polymer sensors have the non-linear distribution of axial stresses over thickness. The beam section of conducting polymer sensor has to be subdivided into several layers, each of which has different physical parameters.

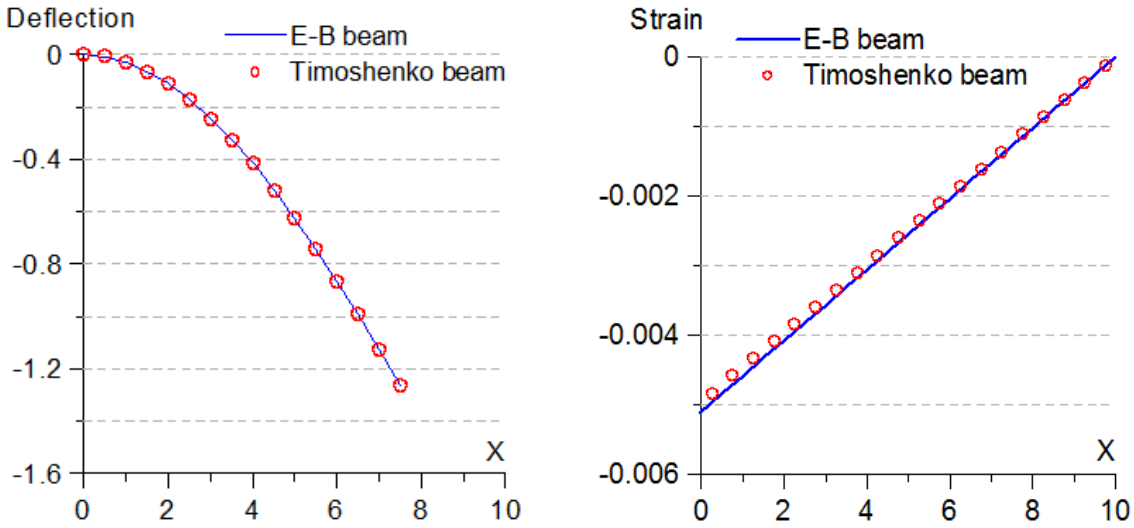

Fig. 2.8 Displacement and axial strain over length (simulation)

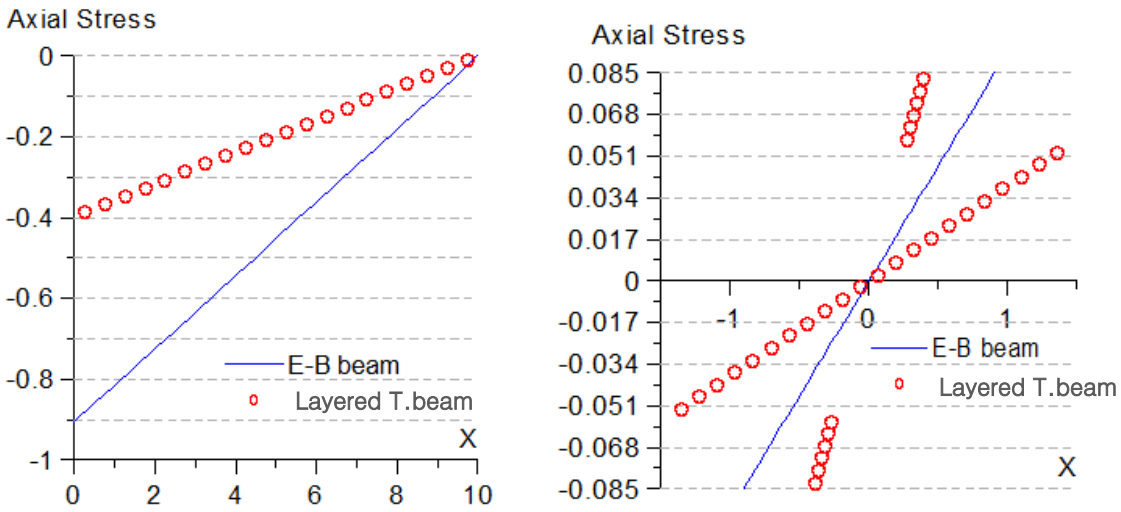

Fig. 2.9 Distributions of axial stresses over length and thickness (simulation)

The simulation result of the monotonic case is shown in Fig. 2.10. The total reaction force is 0.875mN. Considering the reduction of reaction force, the net reaction force is 0.3938mN which is matched with the experimental result. The average stresses at instant of loading and in steady state, of polypyrrole layer, are respectively 0.3277MPa and 0.1475MPa that the former decreased to the later by 55%.

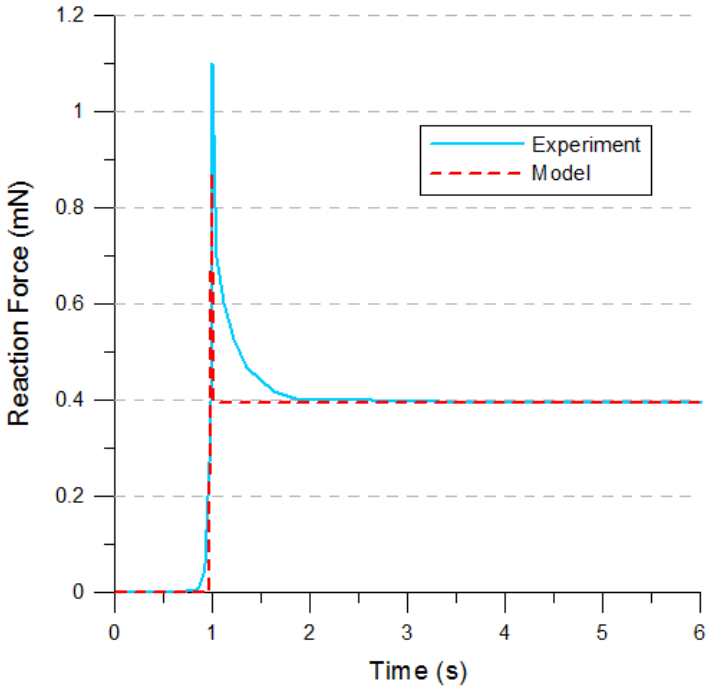

Fig. 2.10 Time history of reaction force (simulation and experiment)

Next, another simulation in case of stepwise displacements is conducted. The time history of stepwise displacements is input into the present computational system as shown in Fig 2.11. As a result, reaction forces are calculated as shown in Fig. 2.12. Each reduction of the reaction forces is constant as proportional to each total reaction force at different prescribed displacements. The calculation results agree with the experiment even if static analysis is employed.

In the experiments of Alici et al. (2008), the linear relation between electric potential and mechanical stress on the steady state shows consistency in both of cases of the monotonic and stepwise loadings. If the black box model were well verified with experiments, the present computational system could be useful for the prediction of the behaviors of mechanical sensors using conducting polymers.

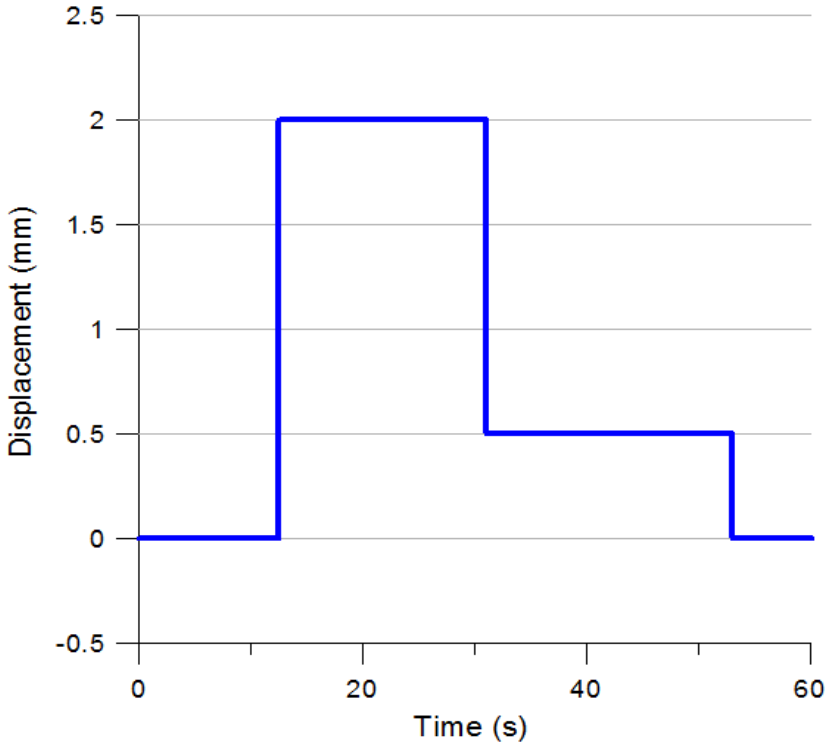

Fig. 2.11 Time history of stepwise displacement (simulation and experiment)

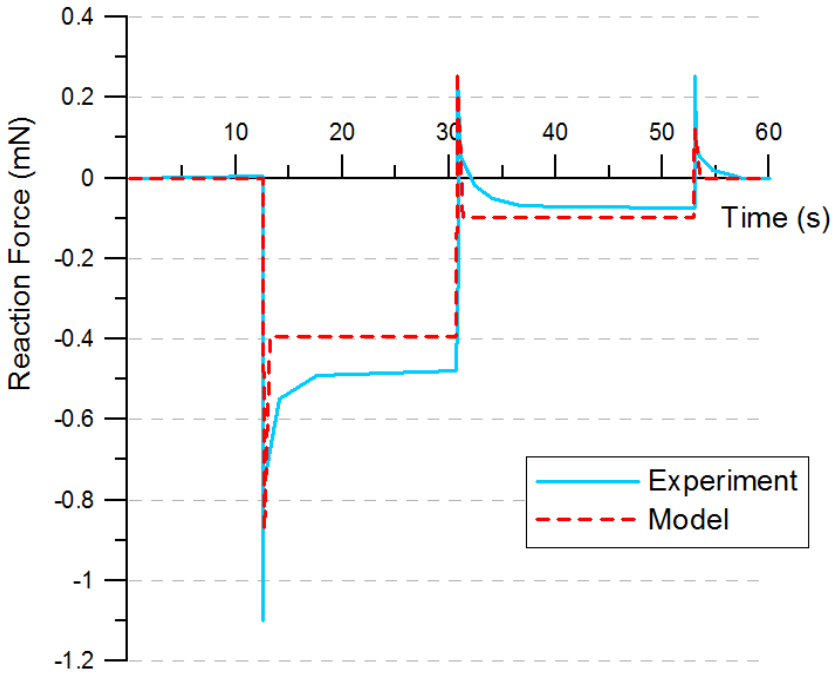

Fig. 2.12 Time history of reaction force (simulation and experiment)

2.5 Conclusion

The present study has attempted to develop the computational system for the design of mechanical sensors using conducting polymers, focusing on structural analysis. The structural analysis of the mechanical sensors was conducted with finite element method, and layered Timoshenko beam model was employed to the structural analysis. In addition, the reduction of reaction force after a prescribed displacement was reproduced with initial strain method. The reduction of reaction force was quantified with a parameter from the observation that the reduction of reaction force is proportional to total reaction force. Therefore, the instantaneous and steady reaction forces were obtainable. Next, the bending stress of conducting polymer layer was employed into the experimental linear relation between electric potential and axial stress. As a result, the electric potential was estimated as the output of the mechanical sensors, and the present computational system could express the behaviors of mechanical sensors using conducting polymers. Lastly, the simulation results in cases of monotonic or stepwise input were validated with the experimental results.

The researches for mechanical sensors using conducting polymers are insufficient in contrast with many researches for the conducting polymer actuator. Further research would be the following. Even though the linearity of the relation is experimentally shown, the electric potential is observed at instant of loading as transient response and the stresses are measured at steady state after a while. Time-dependant model for the mechanical sensors is needed to explain the time gap of the peaks of electric potential and reaction force. The parameters of C_ε and β in the present computational system cannot help being determined by experiments. This simplified model will be basis for a more complicated sensor model.

2.6 References

Alici, G. et al., 2006, A methodology towards geometry optimization of high performance polypyrrole (PPy) actuators, Smart materials and structures, Vol.15, No.2, pp.243-252.

Alici, G.et al., 2008, Response Characterization of Electroactive Polymers as Mechanical Sensors, IEEE/ASME Transactions on Mechatronics, Vol.13, No.2, pp.187-196

Della Santa, A. et al., 1997, Performance and Work Capacity of a Polypyrrole Conducting Polymer Linear Actuator, Synthetic Metals, Vol.90, pp.93-100.

Della Santa, A. et al., 1997, Passive Mechanical Properties of Polypyrrole Films: A Continuum, Poroelastic Model, Material Science and Engineering, C5, pp.101-109.

Toi, Y. and Jung, W.S., 2007, Finite Element Modeling of Electrochemical-Poroelastic Behaviors of Conducting Polymers, Computers and Structures, Vol. 85, pp.1453-1460

Toi, Y., 2008, A Course on Computational Solid Mechanics (Modeling and Simulation of Materials and Structures, Corona Publishing Company, pp.50-52、pp.144-156

Wu, Y. et al., 2007, Soft Mechanical Sensors through Reverse Actuation in Polypyrrole, Advanced Functional Materials, Vol. 17, pp.3216-3222

Chapter 3

Numerical Simulation of Mechanical Sensors Using Conducting Polymers

3.1 Introduction

Conducting polymers have recently received amplified expectations as a novel material especially in robot-engineering, micro-electro-mechanical systems (MEMS). The attention is thanks to attractive characteristics as follows. They are driven by low voltage **(**1~2V), micro-miniature, light weight, flexible and silent, durable and stable chemically, and working in water or wet condition. Owing to such advantages, some conducting polymers, e.g. polypyrrole, have shown a multitude of potentials as a candidate of mechanical actuators and sensors, from electricity to motion and from motion to electricity. The researches of the sensor (Wu et al., 2007, Alici et al., 2008, Toi and Mochizuki, 2010) have recently started in spite of the earlier researches of the actuators (Spinks et al., 2002, Alici et al., 2006, Nemat-Nasser and Zamani, 2006, Toi and Jung, 2007).

Alici et al. (2006 and 2008) shows that one conducting polymer can operate as both of mechanical actuators and sensors like artificial muscle. When the conducting polymer sensors are deformed, they generate electric potential corresponding to the magnitude of the stimulation, conversely to the process of the actuation. The problem is, as shown in Fig. 3.1 (Alici et al., 2006 and 2008), the non-invertible relation that the generated electric potential of the sensation is very much smaller than the electric potential of the actuation with respect to the same displacement and structure.

As the references (Alici et al., 2006, Nemat-Nasser and Zamani, 2006, Toi and Jung, 2007, Wu et al., 2007, Alici et al., 2008) mentioned, the physical quantities over the thin thickness, e.g. stresses and ion concentration, is dominant factors on the behaviors of the conducting polymers. The mechanical sensors of the conducting polymers have very thin thickness comparing length and width, e.g. 0.17mm thickness and 10mm length (Alici et al., 2006, Nemat-Nasser and Zamani, 2006, Wu et al., 2007, Alici et al., 2008). On the length scale of the sensor, the researches (Spinks et al. 2002, Alici et al., 2006, Nemat-Nasser and Zamani, 2006, Wu et al., 2007, Alici et al., 2008) have investigated the macroscopic properties of the conducting polymers, but the quantitative measurements over the microscale thickness, which are the evidences for the validation of hypotheses,

have not been obtained, so the simulation is needed to help the prediction and validation. However, there is no simulation result over the thin thickness of the mechanical sensor.

In the experiments of Wu et al. (2007) and Alici et al. (2008), the electricity of the conducting polymer sensor is induced during transient responses. However, the simulation model for the transient behaviors has not been established until now. Only black box models (Wu et al., 2007, Alici et al., 2008, Toi and Mochizuki, 2010), as shown in Fig. 3.1, have been empirically proposed with experimental results. More detailed models (Nasser and Zamani, 2006, Toi and Jung, 2007), from the simulation of the actuators, cannot induce electricity from deformation, so they cannot be applied into the simulation of the sensor. In addition, Alici et al. (2006) applied numerical simulation to the geometry optimization of the actuators, but the simulation procedure and quantitative results of the sensors has not been reported for the design and control.

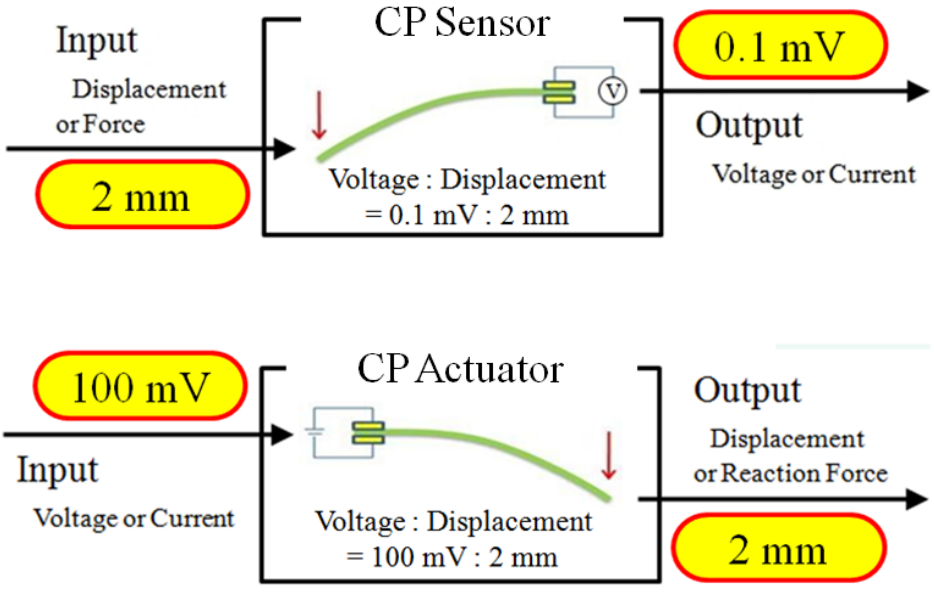

Fig. 3.1 Non-invertible input-output relation in mechanical sensor and actuator

The present study newly attempts the numerical simulation of the mechanical sensors using conducting polymers which generate electricity in the transient response to mechanical stimulation. In addition, the present study reports the simulation results of the important physical quantities over the microscale thickness that have not been obtained from the experiments (Alici et al., 2008). The other obtained results (Alici et al., 2008) are

also compared with our simulation results, and the transient behaviors of the mechanical sensors are explained, e.g. the non-invertible relation, relaxation and hysteresis.

The present simulation procedure modifies and integrates the existing theories (Alici et al., 2006, Nemat-Nasser and Zamani, 2006, Toi and Jung, 2007, Wu et al., 2007, Alici et al., 2008, Toi and Mochizuki, 2010), and it is efficiently simplified as possible as transient behaviors are expressed. Wu et al. (2007) showed that the mobile ion movement is dominant factor than chemical oxidation-reduction reaction in the voltage polarity of the sensor. Based on the hypothesis, the present study focuses on modeling of the fluid flow of pores which are induced by mechanical stresses and results in the sensitive electric potential. In addition, the present study employs Biot poroelasticity theory (Biot, 1941) in order to estimate the unknown pressure of porous conducting polymers. Wang et al. (2008) and Scherer et al. (2009) mentioned that Poisson effect causes significant inaccuracy as the width-to-thickness ratio of a beam is increased. In order to compensate the inaccuracy, the Biot poroelastic theory is modified as Poisson effect is considered as initial strain. The governing equations and fields are spatially simplified as one dimensional in thickness direction of the sensors, because their variations over thickness dominantly determine the behavior of the sensor, and the time cost of two or three dimensional analysis becomes enormous because the large gradients of the physical parameters on surfaces needs very small mesh sizes. Lastly, the procedure of numerical simulation and discretization of a beam element are introduced. The theoretical models are discretized and adopted into finite element method and finite difference method, and then fully coupled simulation is conducted to reproduce the transient behaviors of the sensors so that the mechanical deformation results in the electric potential. Lastly, the results of the simulation are illustrated, such as the histories of the deflection, reaction force, pore pressure, ion concentration and electric potential with respect to position and time. The simulation results are validated with the experimental results, and they are discussed and summarized.

The structure of the sensors using conducting polymers is identified as that of typical actuators. Alici et al. (2006 and 2008) introduced a type of the conducting polymer actuators and sensors as shown in Fig. 3.2. It is the composite of five layers. The material of the out- most layers is PPy (Polypyrrole), the middle layer is PVDF (Polyvinylidene fluoride). The PPy is an electro-active conducing polymer, and the PVDF is the reservoir

for electrolyte where the ion and solvent are stored for the actuation and sensation. Platinum is coated between the PPy and PVDF to improve conductivity. The thickness of the platinum is 10-100Å. The thickness is very much thin compared to the length, so the effects of a mechanical stiffener and an electrical conductor are negligible in the thickness direction.

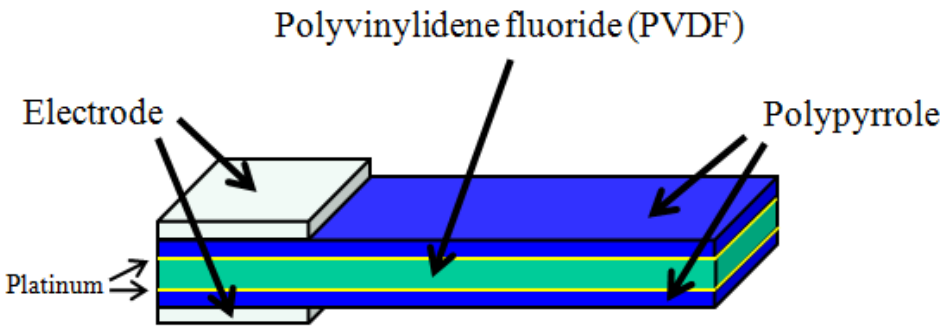

Fig. 3.2 Structure of mechanical sensor using Polypyrrole (Wu et al., 2007)

The transient behavior of the conducting polymer sensors is characterized that the reaction force and electric potential have the relaxations and hysteresis. The schematics are illustrated in Figs. 3.3 and 3.4 from the experimental results (Alici, G. et al., 2008). Responding to mechanical stimulation, the reaction force is immediately generated, and then gradually reduced even when the displacement remains constant as shown in Fig. 3.3. The relaxation is caused by the fluid transport through the pores of the solid matrix as the typical phenomenon of porous media. In addition, electrical potential, as shown in Fig. 3.4, is also changed with the mechanical reaction force and then gradually relaxed. It is due to the redistribution of charge density by the transport of mobile ions (Nemat-Nasser and Zamani, 2006, Wu et al., 2007, Alici et al., 2008). Wu et al. (2007) mentioned that the polarity of the electric potential depends on the type of counter-ions. That is, the transport of mobile ions is dominant factor rather than chemical oxidation-reduction reaction in the polarity of voltage. Provided that large ions are trapped and immobile, only small ions are moveable with fluid flow. Thus, the distribution of the mobile ions determines electric potential. Furthermore, the peak of electric potential is induced in the transient response to the mechanical stimulation, and has time lag behind the peak of reaction force as shown in Fig. 3.4.

The mechanism of the mechanical sensor using conducting polymers is shown in Fig. 3.5. When the conducting polymer sensor deforms as a bending of composite beams in solid mechanics, the expansion or contraction of volume takes place with respect to a position in the beam section. By resisting the deformation, the internal stresses of the solid matrix and the pressure of fluid filling the pores of the solid matrix are induced. The pressure causes the ions and solvent to be pushed out from the shrunk side and to be sucked into the dilate side. The movements of the pore fluid cause the gradual relaxation of reaction forces. Furthermore, the movement of mobile ions causes an instant unbalance of the distribution of charge density, and the gradient of charge density results in electric potential difference. Subsequently, the mobile ion concentration is diffused, and the electric potential is gradually decreased to the neutralization of the electric charges.

As the electro-active actuation of the conducting polymers are flexibly deformed when electric current flows. The actuation is also caused by the movements of the ion and solvent molecules. Therefore, the actuation and sensation can be fundamentally understood with the same transport phenomena. The problem is that the generated electric potential of the sensor is very much smaller, micro-volts as about one thousandth of the supplied electric potential of the actuator of the same structure with respect to the same displacement as shown in Fig. 3.1. To cope with the non-invertible input-output relation and to propose computational system for design, the present study newly attempts the numerical simulation for the transient behavior of mechanical sensor using the conducting polymers.

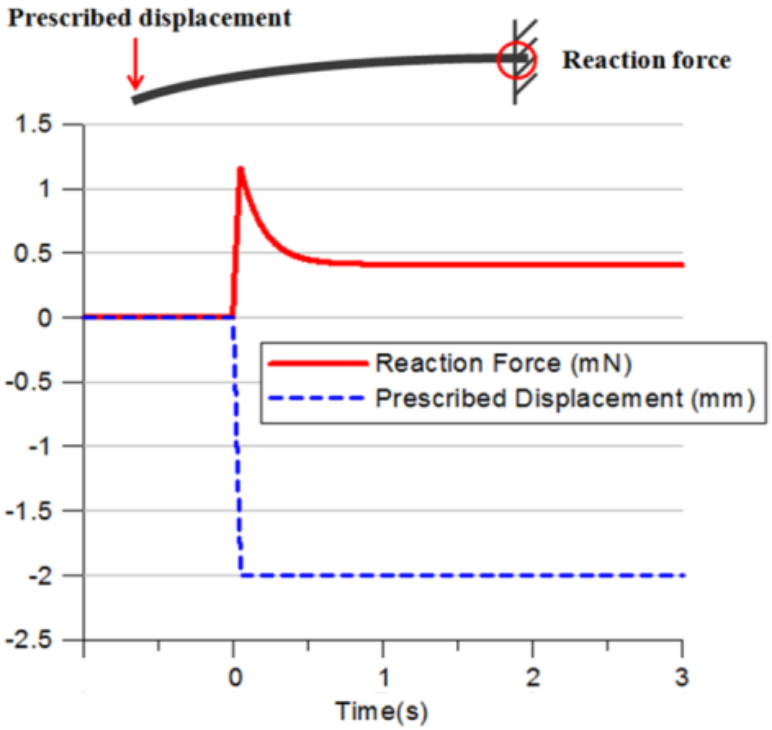

Fig. 3.3 Schematic of relaxation of reaction force

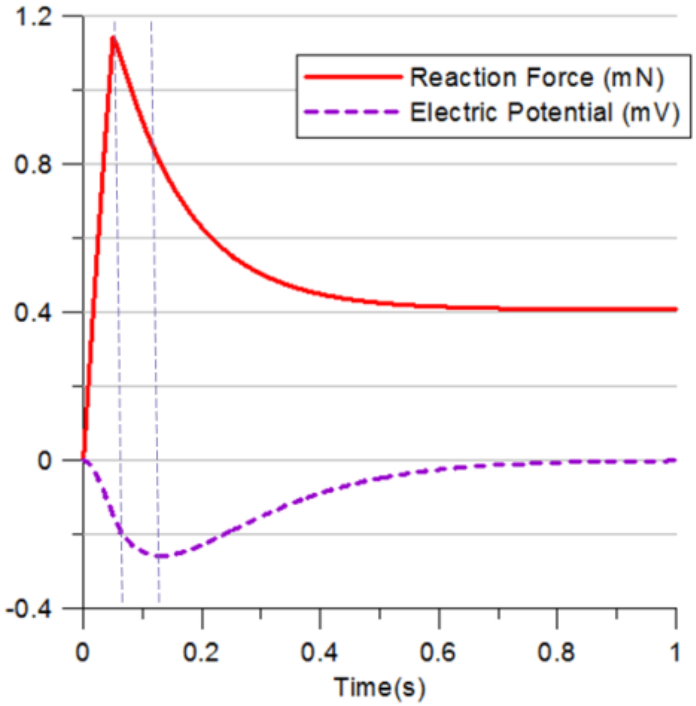

Fig. 3.4 Schematic of relaxation and hysteresis of reaction force and electric potential

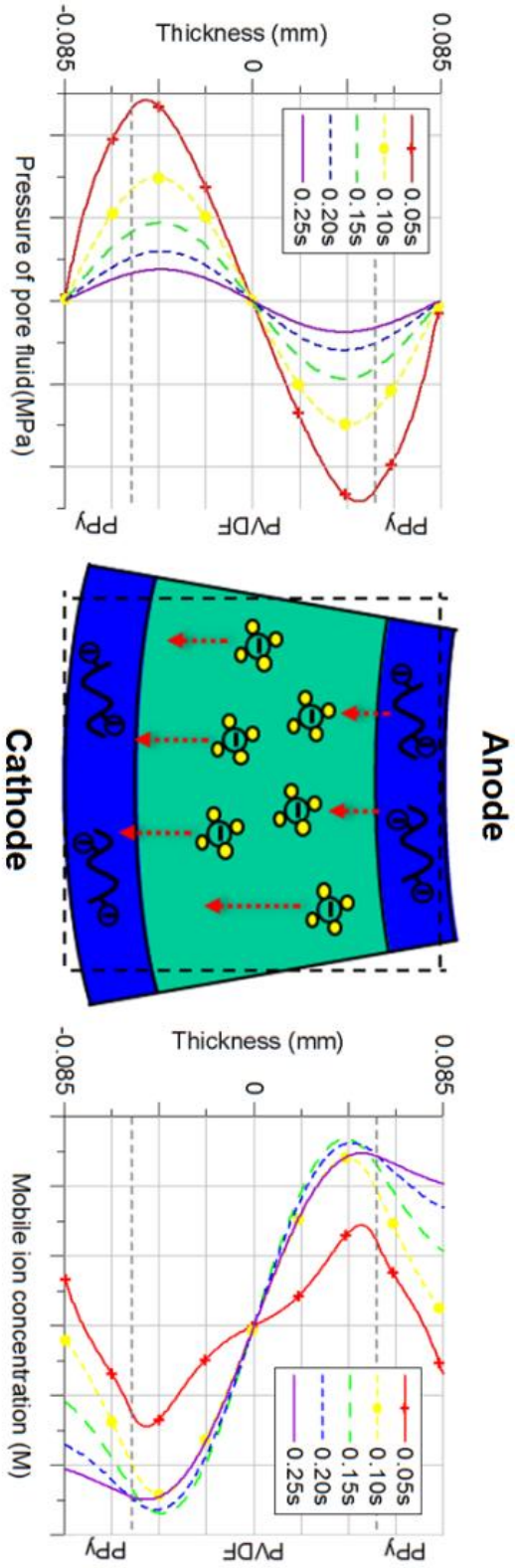

Fig. 3.5 Mechanism of mechanical sensor using conducting polymer (simulation)

3.2 Theoretical Models

3.2.1 Biot Poroelastic Theory

Conducting polymers consist of two phases, a polymer matrix and electrolyte. The polymer matrix is a porous solid, and the electrolyte is a fluid filling the pores of the polymer matrix. Resisting mechanical deformation, the internal stresses of solid matrix and the pressure of fluid filling the pores of the solid matrix are induced. The gradient of pore pressure drives the fluid flow in porous medium, and then the stresses of fluid and solid are relaxed until a stationary state. This transient behavior with the relaxation can be considered with poromechanics.

Assuming conducting polymers as a continuum and neglecting acceleration and body force from Cauchy's equations of motion, the basic governing equation is established with the below quasi-static equilibrium equation.

$$\frac{\partial \sigma_{ij}^{t}}{\partial x_j} = 0 \tag{3.1}$$

where, σ_{ij}^{t} is total stress component of a porous element.

Next, Biot constitutive equation (Biot, 1941) is employed into idealizing the mechanical behavior of the conducting polymers. Biot constitutive equation considers the compressibility of the solid matrix and pore fluid, assuming the solid matrix and pore fluid as elastic bodies. Biot constitutive equation is linear quasi-static elastic theory, defining the stress components as a linear combination of the strain tensor and the pore pressure with the independent coefficients of the stress-strain relations. In case of isotropic and homogeneous material, Rice and Cleary (1976) renewed Biot constitutive equation using conventional material parameters such as Skempton coefficient and undrained Poisson's ratio. Wang et al. also employed the renewed Biot constitutive equation with the conventional parameters. The renewed Biot constitutive equation with zero initial stress and fluid pressure is given as follows (Wang et al., 2008).

$$\sigma_{ij}^{t} = (K^{d} - \frac{2}{3}G^{d})e^{t}\delta_{ij} + 2G^{d}\varepsilon_{ij}^{t} - bp\delta_{ij} \tag{3.2}$$

$$e^{t} = \varepsilon_{kk}^{t} \tag{3.3}$$

$$b = 1 - \frac{K^{d}}{K^{s}} \tag{3.4}$$

where, σ_{ij}^{t} is the total stress components, p is the fluid pressure in pores, ε_{ij}^{t} is the total strain components, e^{t} is the total volumetric strain, G^{d} is the drained shear modulus, K^{d} is the drained bulk modulus, K^{s} is the non-porous bulk modulus, b is Biot coefficient, and δ_{ij} is Kronecker delta.

Alternatively, the above constitutive equation, Eq. (3.2), can be rewritten in terms of the total strain components as follows.

$$\varepsilon_{ij}^{t} = \frac{1+v^{d}}{E^{d}}(\sigma_{ij}^{t} + bp\delta_{ij}) - \frac{3v^{d}}{E}(\frac{\sigma_{kk}^{t}}{3} + bp)\delta_{ij} \tag{3.5}$$

where, v^{d} is the drained Poisson's ratio, E^{d} is the drained elastic modulus.

The continuity equation of the compressible fluid inside a saturated porous medium is given by

$$\frac{d(\phi\rho_{f})}{dt} = -\nabla\cdot(\rho_{f}\bar{f}) \tag{3.6}$$

where, ϕ is the Lagrangian porosity referring the ratio of pore space to the overall volume, ρ_{f} is the density of fluid, and $\bar{f}$ is the volume flux vector of fluid (Wang et al., 2008).

The Biot poroelastic theory employed the Darcy law to govern the flow of a fluid in pores. The general Darcy law is given as

$$\bar{f} = \frac{\kappa_{h}}{\eta}(\nabla p - \rho_{f}\bar{g}) \tag{3.7}$$

where, κ_h is hydraulic permeability, η is dynamic viscosity of fluid, ρ_f is density of fluid, and $\bar{g}$ is body force vector (Wang et al., 2008).

The stiffness of the porous bulk element is varied with the pressure of the fluid in the pores. In Eq. (3.2), the pressure of the pore fluid is unknown, so Biot (1941) employed additional relation of the pressure. In the original Biot poroelastic theory, the parameters in the additional relation had not been conventional. After Biot poroelastic theory, Rice and Cleary (1976) introduced the term of 'undrained condition' assuming that time scale is too short to allow the loss or gain of pore fluid in an element by diffusive transport to or from neighborhood element. The undrained condition is defined with the below.

$$\Delta(\phi\rho_f) = 0 \tag{3.8}$$

Using the undrained condition, Rice and Cleary introduced the following relations which were earlier proposed by Skempton as follows (Rice and Cleary, 1976).

$$\Delta p = -B\frac{\Delta\sigma_{kk}^{t}}{3} \tag{3.9}$$

$$B = \frac{\frac{1}{K^d} - \frac{1}{K^s}}{-\frac{1+\phi}{K^s} + \frac{\phi}{K^f} + \frac{1}{K^d}} \tag{3.10}$$

$$v^u = \frac{3v^d + B(1-2v^d)b}{3 - B(1-2v^d)b} \tag{3.11}$$

where, B is Skempton coefficient, K^f is bulk modulus of pore fluid, v^u is undrained Poisson's ratio, and the others are mentioned previously.

Provided that the material parameters on the undrained condition are isotropic and homogenous, only two parameters are needed to describe the elastic behavior of the porous material on the undrained condition. Beside the undrained Poisson's ratio in the Eq. (3.11), undrained bulk modulus can be obtained from the tensor contraction of the Eq. (3.2).

$$\sigma_{kk}^{t} = 3K^{d}e^{t} - 3bp = 3K^{u}e^{t} \tag{3.12}$$

where, K^{u} is undrained bulk modulus in the undrained condition

Using the above Eq. (3.12) and Skempton coefficient and Biot coefficient, the relation between the drained bulk modulus and the undrained bulk modulus is introduced as follows (Wang, 1993)

$$\frac{1}{K^{u}} = \frac{1}{K^{d}}(1-bB) \tag{3.13}$$

The undrained parameters estimates the total stresses on the undrained condition without the unknown pressure, and then the pressure of the pore fluid is estimated by Eq. (3.9) which is the relation between the hydrostatic stress of bulk element and the pressure of the pore fluid on the undrained condition. The pressure becomes the driving force in the transport of the mass flux of fluid in the porous medium. Coupling Biot constitutive equation, Eq. (3.2), the continuity equation, Eq. (3.6), and Darcy law, Eq. (3.7), the field equation of the pressure, neglecting body forces, is obtained as follows (Rice and Cleary, 1976).

$$D_{f}\nabla^{2}\left(\sigma_{kk}^{t} + \frac{3}{B}p\right) = \frac{\partial}{\partial t}\left(\sigma_{kk}^{t} + \frac{3}{B}p\right) \tag{3.14}$$

where, D_{f} is diffusivity coefficient, which was introduced by Rice and Cleary (1976).

$$D_{f} = \frac{\kappa_{h}}{\eta}\left[\frac{2G^{d}(1-\nu^{d})}{(1-2\nu^{d})}\right]\left[\frac{B^{2}(1+\nu^{u})^{2}(1-2\nu^{d})}{9(\nu^{u}-\nu^{d})(1-\nu^{u})}\right] \tag{3.15}$$

In addition, the coupling of solid stress and fluid pressure needs to satisfy Beltrami-Michell compatibility condition with the below (Wang et al., 2008).

$$\nabla^{2}\{(1+\nu)\sigma_{ij} - \nu\sigma_{kk}\delta_{ij}\} + \frac{\partial^{2}\sigma_{kk}}{\partial x_{i}\partial x_{i}} + b(1-2\nu)\left\{\nabla^{2}p\delta_{ij} + \frac{\partial^{2}p}{\partial x_{i}\partial x_{i}}\right\} = 0 \tag{3.16}$$

By tensor contraction, the following compatibility equation is obtained (Wang et al., 2008).

$$\nabla^2(\sigma_{kk} + \Lambda p) = 0 \tag{3.17}$$

$$\Lambda = \frac{2b(1-2\nu)}{1-\nu} = \frac{6(\nu_u - \nu)}{B(1-\nu_u)(1-\nu)} \tag{3.18}$$

The mechanical behavior of the porous conducting polymer and pore fluid can be analyzed by the aforementioned Biot poroelastic theory. The analysis of the transient behavior needs to be accurately simulated because the electric potential of the sensor is generated from the transient region of the mechanical response as shown in Fig. 3.4. In the sensation, the gradient of pressure drives the movement of mobile ions resulting in electric potential. In the actuation, the electric field dominantly causes the fluid transport in the porous medium. Hence, the pressure of the pore fluid interacts with mechanical stress and electric field in both of the actuation and sensation of the conducting polymers, and the pressure field has to be analyzed with the mechanical stress and electric potential fields. Coupling with the mechanical stress and electric potential fields, the field equation of the pressure, Eq. (3.14), is rewritten as follows.

$$\frac{\kappa_h}{\eta}\left(\nabla^2 p - \phi FC\nabla^2 V\right) = \frac{3(\nu^u - \nu^d)}{2G^d B(1+\nu^d)(1+\nu^u)} \frac{\partial}{\partial t}\left(\sigma_{kk}^t + \frac{3}{B} p\right) \tag{3.19}$$

where, V is electric potential, C is ion concentration, κ_h is hydraulic permeability, η is dynamic viscosity, and F is Faraday constant, and the others were mentioned previously.

Therefore, the pressure field of the pore fluid is calculated by the above Eq. (3.19). In the transient behavior of conducting polymers, the mechanical total stresses and reaction force are instantaneously increased by the pore pressure. Subsequently, the diffusion of pressure in the Eq. (3.19) relaxes the total stresses and reaction force as typically phenomena of porous media. As for typical mechanical sensors using conducting polymers, the governing equation, Eq. (3.1) can be reduced by idealizing deformation field as a bending of beams in solid mechanics.

3.2.2 Layered Timoshenko Beam Model

The mechanical deformation of actuators and sensors using conducting polymers is experimentally observed as the bending of a beam in solid mechanics (Alici et al., 2006, Nemat-Nasser and Zamani, 2006, Wu et al., 2007, Alici et al., 2008). In the present study, layered Timoshenko beam model is employed to express the deformation of the mechanical sensor to express the non-linear distribution of axial stresses as shown in Fig. 3.6. The Layered Timoshenko beam in solid mechanics is given as follows (Toi, 2008).

$$u(x,z) = -z\theta(x) \tag{3.20}$$

$$w(x,z) = w(x) \tag{3.21}$$

$$\varepsilon_x^t(x,z) = \frac{\partial u}{\partial x} = -z\frac{d\theta}{dx} \tag{3.22}$$

$$\gamma_{zx}^t(x) = \frac{\partial w}{\partial x} + \frac{\partial u}{\partial z} = \frac{dw(x)}{dx} - \theta(x) \tag{3.23}$$

where, u is axial displacement, z is distance from neutral axis, θ is rotation of the normal section, w is lateral displacement, ε_x^t is axial strain, γ_{zx}^t is transverse shear strain.

The constitutive equation from Hooke's law of elastic solids is simplified by the assumed displacement field of the layered Timoshenko beam model is as follows (Toi, 2008).

$$\sigma_x^t(x,z) = E^t(z)\varepsilon_x^t(x,z) \tag{3.24}$$

$$\tau_{zx}^t(x,z) = \alpha\, G^t(z)\gamma_{zx}^t(x) \tag{3.25}$$

where, E^t is elastic modulus, G^t is shear modulus, α is shear correction factor employed as 5/6 in case of rectangular section (Toi, 2008).

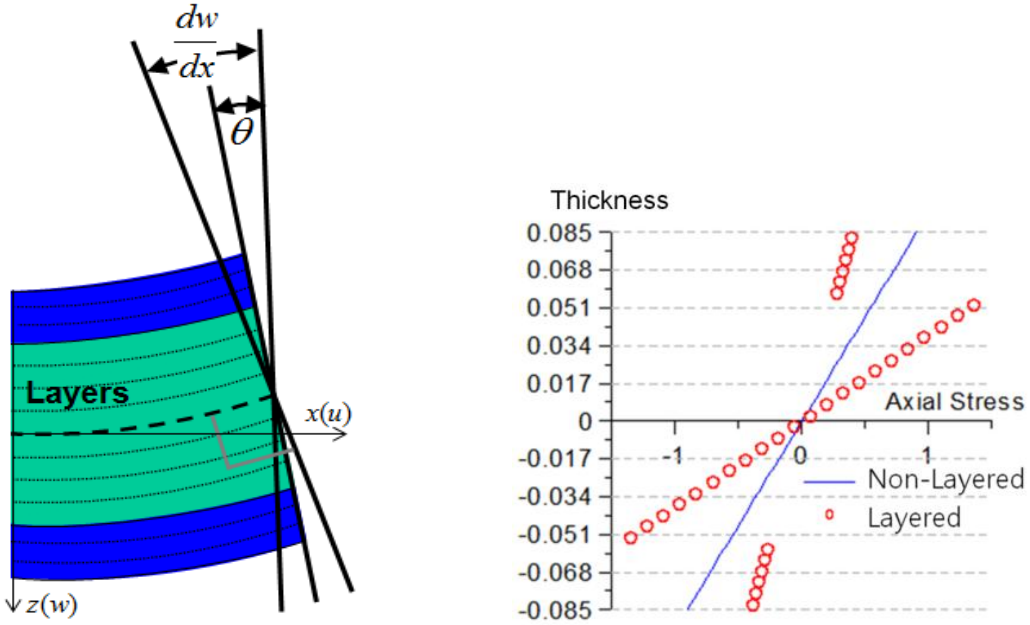

Fig. 3.6 Displacement field of layered Timoshenko beam model (L), and Comparison of axial stresses between non-layered beam and layered beam (R)

In the present study, the layered beam model is selected because the conducting polymer sensors have the non-linear distribution of the axial stresses over thickness. The beam section of the conducting polymer sensor has to be subdivided into several layers, each of which has different physical parameters. That is, each layer in a finite beam element corresponds to each grid of the fields of other physical parameters such as fluid pressure, ion concentration and electric potential.

The total stresses in transient behavior of porous beams are significantly affected by the pressure of the pore fluid as the typical drainage phenomenon in poromechanics. Regarding the bending of porous beams, Wang et al. (2008) showed the inconsistency between Eq. (3.16) and Eq. (3.17) on the assumption of the traction- free condition at the lateral surface. After that, Scherer et al. (2009) compared the approximated analytical solution for the pure bending behaviors of the porous beam with the numerical result from the three-dimensional finite element analysis, and demonstrated that the deficiency from the traction-free condition is negligible even on the transient response. However, the difference between theory and experiment can be observed in the mechanical sensors using conducting polymers. In the experiment of Alici et al. (2008), the peak of the reaction force of the conducting polymer sensor, as shown in Fig. 3.4, is three times larger

than the relaxed reaction force. The peak reaction force is dominantly caused by the pressure of pore fluid, because the electrical and chemical effects on that condition are negligible, e.g. the one thousandth of the actuation electric potential and the independency of polarity on chemical reactions. In addition, the transverse shear deformation and its rate are negligible because of the high ratio of length to thickness as shown in Fig. 3.7.

In spite of the large reaction force in the experiment, the elastic modulus of the porous beam on the undrained condition is about 1.2 times larger than the one on the drained condition. The deformation field of a bending of beams results in the uniaxial stress state but fluid cannot resist uniaxial stress. Thus, the uniaxial state cannot express the peak reaction force which is three times larger than the relaxed reaction force. If the pore fluid cannot freely flow on the undrained condition, the pressure of the pore fluid is not zero. Thus, the total hydrostatic stress with the pressure of the pore fluid, in Eq. (3.9), is not zero because Biot poroelastic theory is analogous to the thermal expansion model. Scherer et al. (2009) also mentioned that the pressure distribution over the width of a beam causes Poisson effect to the axial direction and that the Poisson effect causes significant inaccuracy of the analytical solution as the ratio of width to thickness.

Even though the Poisson effect is considered, the peak of the fluid pressure on the undrained condition, which is obtained from the undrained bulk modulus and Poisson's ratio of the Biot poroelastic theory, can be lower than the one to express the experimental reaction force. That means that three-dimensional finite element analyses also can result in lower undrained reaction forces. Wang et al. (2008) mentioned that the accuracy of the transient behavior of poroelastic beams is dependent on the Poisson's ratio and compressibility of the constituents. It is expected that the Poisson's ratio and Poisson effect of fluid-saturated porous beams on the undrained condition are varied with the dimensions of the mechanical sensor using conducting polymers.

The present study modifies the undrained Poisson's ratio obtained from Eq. (3.11) in the Biot poroelastic theory, and employed the Poisson effects of the pore pressure to the axial direction. Therefore, the constitutive equation of the beam model is proposed as follows:

$$\nu^B = \beta \nu^u \tag{3.26}$$

$$\sigma_y^u = \sigma_z^u = -bp \tag{3.27}$$

$$\sigma_x^u = E^d \varepsilon_x^t - (1 + 2\nu^B) bp \tag{3.28}$$

$$\tau_{zx}^u = \alpha\, G^d \gamma_{zx}^t \tag{3.29}$$

where, ν^B is beam undrained Poisson's ratio, β is correction factor of the Poisson effect, and G^d is drained shear modulus. The correction of the undrained Poisson's ratio makes the peak of the numerical reaction force reached at the peak of the experimental reaction force.

Using the undrained bulk modulus and beam undrained Poisson's ratio, the undrained hydrostatic stress is obtained and substituted into the field equation of the pressure, Eq. (3.19). In the numerical simulation, the effect of the pore pressure is implemented as a kind of external force in order to consider the Poisson effect and to remove additional constitutive relation, because the Biot poroelastic theory is analogous to the thermal expansion model.

3.2.3 Poisson-Nernst-Planck Equations

Alici et al. (2008) measured the reaction forces and electric potential generated from the conducting polymer sensor when a prescribed or stepwise deflection was applied, and proposed an experimental relation that the generated electric potential is proportional to the non-layered ordinary bending stress. Earlier black-box models have been proposed for simplicity, but the non-invertible relation between electric potential and bending stress results in different parameters between the actuation and sensation of the same conducting polymers. Furthermore, the electric potential is generated during the transient behaviors. Recently, the analysis of ion transport has been applied in many fields. Even though the analysis for the sensation of conducting polymers has not been reported, the electro-active actuation has been more accurately analyzed with the consideration of ion transport phenomena (Nemat-Nasser and Zamani, 2006, and Toi and Jung, 2007). Nemat-Nasser

and Zamani (2006) employed Poisson-Nernst-Planck equations for the analysis of ion transport and electric potential. The present sensor model employed Poisson-Nernst-Planck equations to analyze the ion distribution and electric potential as the actuator models do. Poisson-Nernst-Planck equations are the coupling of Nernst-Planck equation and Poisson equation. Nernst-Planck equation is the balance equation of the concentration of particles defined in continuum based on mass conservation principle. Poisson equation is well known as the field equation to analyze electric potential field from the distribution of charge density in electrostatics. In the present study, Poisson-Nernst-Planck equations are spatially simplified as one-dimensional in the thickness direction of the sensors, in order to correspond to the other fields of the physical quantities such as the mechanical solid stress and fluid pressure. The flux of $I-$species is obtained by Nernst-Planck equation as follows (Nemat-Nasser and Zamani, 2006)

$$J = -\frac{CD}{RT}\nabla\mu - Cf \tag{3.30}$$

where, J is mobile ion flux, C is ion concentration, D is diffusivity coefficient and μ is chemical potential of $I-$species, respectively. R is gas constant, T is absolute temperature, f is the volume flux of fluid. The chemical potential is defined by (Nemat-Nasser and Zamani, 2006)

$$\mu = \mu_0 - RT\ln(\gamma C) + zFV \tag{3.31}$$

where, μ_0 is reference chemical potential, γ is affinity, z is species charge, F is Faraday constant and V is electric potential.

Wu et al. (2007) observed that the polarity of voltage is dependent on the type of counter-ions. The observation leads that mobile ion movement is a dominant factor than chemical oxidation-reduction reaction. If conducting polymer molecules and large dopants are immobile, only mobile ions are redistributed by the fluid flux. Thus, it is assumed that the gradient of the concentration of mobile ions dominantly determines the distribution of charge density which results in electric potential. Reducing Eq. (3.30) for one type of

mobile ions, the transport equation of the mobile ion from Eq. (3.30) and Eq. (3.31) is rewritten as (Nemat-Nasser and Zamani, 2006)

$$J = -D\frac{\partial C}{\partial z} - zDC\frac{F}{RT}\frac{\partial V}{\partial z} + Cf \tag{3.32}$$

The continuity equation is also employed as

$$\frac{\partial C}{\partial t} = -\frac{\partial J}{\partial z} \tag{3.33}$$

The generated electric potential in the mechanical sensor using conducting polymers is micro-volts as about one thousandth of the supplied electric potential in the actuator with respect to the same displacement and structure. The very small amount of electricity from the initially neutral condition is caused by the gradient of mobile ion flux as the pore fluid flows by the gradient of the pore pressure. Embedding the effect of the pressure diffusion into Nernst-Planck equation, the redistribution of the mobile ion concentration is obtained as follows:

$$\frac{\partial C}{\partial t} = D\left\{\frac{\partial^2 C}{\partial z^2} - z\phi C\left(\frac{F}{RT}\right)\frac{\partial^2 V}{\partial z^2}\right\} - C\frac{\kappa_h}{\eta}\frac{\partial^2 p}{\partial z^2} \tag{3.34}$$

Next, the well known Poisson equation in electrostatics is employed as

$$\frac{\partial^2 V}{\partial z^2} = -z\frac{F}{k_e}(C - C^0) \tag{3.35}$$

where, k_e is electric permittivity, and C^0 is concentration of immobile ions.

According to Poisson-Nernst-Planck equations, Eq. (3.34) and Eq. (3.35), the mobile ion concentration is redistributed and its distribution causes electric potential as the output of the mechanical sensor. In the numerical simulation, Poisson-Nernst-Planck equations with the Biot poroelastic theory and layered Timoshenko beam model are implemented for the analysis of the transient behavior of the mechanical sensors using conducting polymers.

3.3 Numerical Formulations

In the numerical simulation for the transient behavior of the mechanical sensor using conducting polymers, the typical structure (Alici et al., 2006, Alici et al., 2008) is selected as shown in Fig. 3.2. The dimensions of the structure are illustrated in Fig. 3.7. The platinum membrane is negligible in the thickness direction because of its very thin thickness. As shown in Fig. 3.7, each beam element is subdivided into different layers, so the fields of fluid pressure, mechanical total stress, ion concentration and electric potential are spatially discretized as one-dimensional in the thickness direction of the sensor.

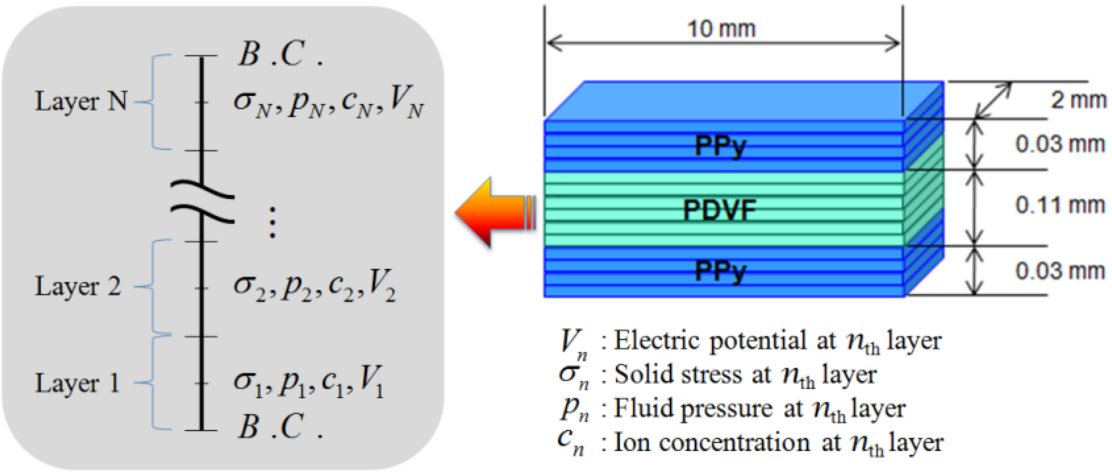

Fig. 3.7 Discretization in thickness direction

As illustrated in Fig. 3.8, the procedure of numerical simulation is the followings.

First, the Biot coefficient in Eq. (3.4), Skempton coefficient in Eq. (3.10), the undrained bulk modulus in Eq. (3.13) and beam undrained Poisson's ratio in Eqs. (3.11) and (3.26) are respectively determined with the material parameters.

Second, the undrained volumetric strains are, using the undrained bulk modulus and beam undrained Poisson's ratio, numerically obtained with the finite element method. The finite element method has well employed to the simulation of porous media and conducting polymers (Alici et al., 2006, Toi and Jung, 2007, Wang et al., 2008, Scherer et al., 2009). The finite element formulation is as follows (Toi, 2008,).

$$[S^u]\{\Delta u\} = \{\Delta f^{ext}\} \tag{3.36}$$

$$[S^u] = \int_V [B]^T [D^u][B] dV \tag{3.37}$$

$$\{\Delta \varepsilon^u\} = [B]\{\Delta u\} \tag{3.38}$$

where, $[S^u]$ is undrained stiffness matrix, $\{\Delta u\}$ is nodal displacement increment vector, $\{\Delta f^{ext}\}$ is external force increment vector, $[B]$ is strain-displacement matrix, $[D^u]$ is undrained stress-strain relation matrix, $\{\Delta \varepsilon^u\}$ is undrained strain increment vector, and n is number of each layer. The present study employs the layered Timoshenko model in section 3.2, and the undrained bulk modulus and beam undrained Poisson ratio are converted to elastic modulus and shear modulus. The element stiffness matrix is, $[S_e^t]$, preventing the shear locking by 1-point Gauss-Legendre integration, as follows (Toi, 2008).

$$[S_e^t] = \begin{bmatrix} \left(\frac{G^t A}{L}\right) & \left(\frac{G^t A}{2}\right) & \left(-\frac{G^t A}{L}\right) & \left(\frac{G^t A}{2}\right) \\ & \left(\frac{E^t I}{L} + \frac{G^t AL}{4}\right) & \left(-\frac{G^t A}{2}\right) & \left(-\frac{E^t I}{L} + \frac{G^t AL}{4}\right) \\ & & \left(\frac{G^t A}{L}\right) & \left(-\frac{G^t A}{2}\right) \\ sym. & & & \left(\frac{E^t I}{L} + \frac{G^t AL}{4}\right) \end{bmatrix}$$

$$E^t = 3K^t(1-2v^t)$$
$$G^t = 3K^t(1-2v^t)/2(1+v^t) \tag{3.39}$$

where, L is element length, A is element section area, and $K^t = K^u$, $v^t = v^B$ on the undrained condition. Solving Eq. (3.36), nodal displacements are obtained, and then the layered axial undrained strains, $\Delta \varepsilon_{x\,n}^u$, are obtained by Eq. (3.22).

Third, using the layered axial undrained strains, the pseudo pore pressure on the undrained condition, p_n^p, is obtained with the below.

$$p_n^p = p_n - BK_n^u \Delta e_n^u = p_n^p - BK_n^u (1-2\nu_n^B)\Delta\varepsilon_{xn}^t \tag{3.40}$$

Fourth, the field equation of the pore pressure, Eq. (3.19) is discretized as shown in Fig. 3.7, and the pore pressure is updated as follows.

$$p_n = p_n^p + \frac{\kappa_{hn}}{\eta}\frac{2G_n^d B_n^{\,2}(1+\nu_n^d)(1+\nu_n^B)}{9(\nu_n^B-\nu_n^d)}\left(\frac{p_{n-1}^p - 2p_n^p + p_{n+1}^p}{\Delta z^2} - z\phi_n C_n F\frac{V_{n-1}-2V_n+V_{n+1}}{\Delta z^2}\right)\Delta t \tag{3.41}$$

The increment of the undrained pressure, the last term in Eq. (3.41), is updated, and then the other terms are calculated.

Fifth, using the obtained pore pressure from Eq. (3.41), the total stresses with the pressure are calculated based on Eq. (3.2). The pore pressure is implemented as a kind of external force, because the Biot poroelastic theory is analogous to the thermal expansion model. In case of beam model, the Poisson effect of the pore pressure is additionally considered because undrained condition is not uniaxial stress state, so the Poisson effect is embedded into the axial total stress using Eq. (3.28). Therefore, the mechanical states with the pressure diffusion of the pore fluid are calculated, and the finite element stiffness equation is as follows.

$$[S^d]\{\Delta u\} = \{\Delta f^{ext}\} + \{\Delta f^{p}\} + \{\Delta f^{pp}\} \tag{3.42}$$

$$\{\Delta f^{p}\} = \int_V [B]^T \{b\Delta p\delta_{ij}\}dV \tag{3.43}$$

$$\{\Delta f^{pp}\} = \int_V [B]^T \{2\nu^B b\Delta p\delta_{ij}\}dV \tag{3.44}$$

$$[S^d] = \int_V [B]^T [D^d][B]dV \tag{3.45}$$

$$\{\Delta\varepsilon^t\} = [B]\{\Delta u\} \tag{3.46}$$

$$\{\Delta\sigma_n^t\} = [D_n^d(K_n^d, v_n^d)]\{\Delta\varepsilon_n^t\} \tag{3.47}$$

where, $[S^d]$ is drained stiffness matrix, $\{\Delta f^p\}$ is force increment vector of the fluid pressure in pores, $\{\Delta f^{pp}\}$ is force increment vector of the Poisson effect in the beam model, $[D^d]$ is drained stress-strain relation matrix, $\{\Delta\varepsilon^t\}$ is total strain increment vector, and $\{\Delta\sigma^t\}$ is total stress increment vector. Using the element stiffness matrix on the drained condition, $K^t = K^d$, $v^t = v^B$, the total displacements or reaction forces are calculated in Eq. (3.42).

Next, the fields of the mobile ion concentration and electric potential are obtained with Poisson-Nernst-Planck equations, Eqs. (3.34) and (3.35), using the finite difference method. The field equations of mobile ion concentration and electric potential are discretized as

$$\Delta C = \left(D_n \left(\frac{C_{n-1} - 2C_n + C_{n+1}}{\Delta z^2} - zC_n \left(\frac{F}{RT} \right) \frac{V_{n-1} - 2V_n + V_{n+1}}{\Delta z^2} \right) - C_n \frac{\kappa_{hn}}{\eta} \frac{p_{n-1} - 2p_n + p_{n+1}}{\Delta z^2} \right) \Delta t \tag{3.48}$$

$$\frac{V_{n-1} - 2V_n + V_{n+1}}{\Delta z^2} = -z\phi_n \frac{F}{k_{en}} \left(C_n - C_n^0 \right) \tag{3.49}$$

Finally, the electric potential is obtained from the above equations as the output of the sensor model, and the transient behavior of the mechanical sensor using conducting polymers are numerically analyzed.

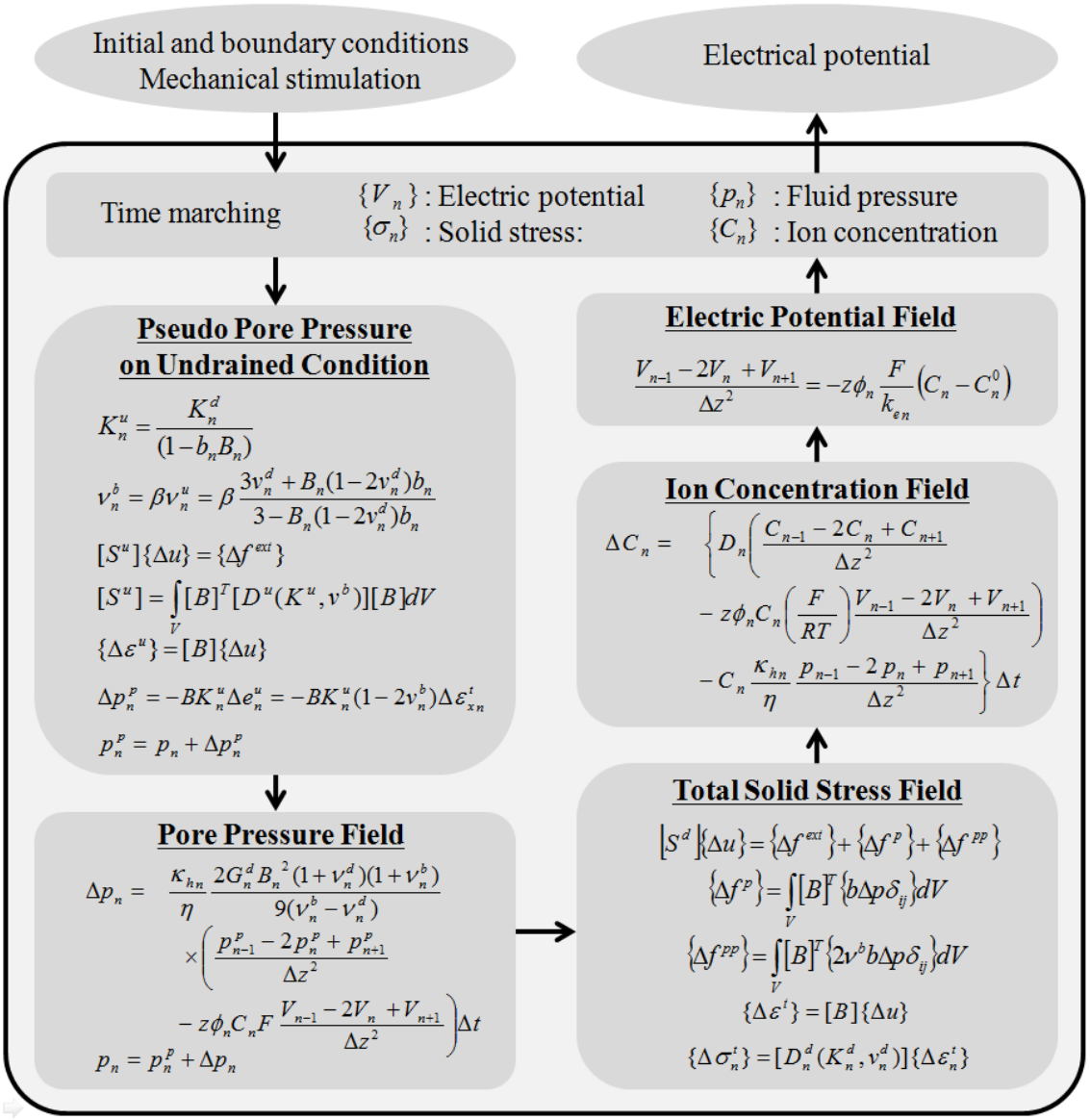

Fig. 3.8 Flowchart of numerical simulation

3.4 Simulation Results

The material parameters are determined by macroscale experiments. As for the sensor in Fig. 3.7, its physical parameters were determined from the references (Spinks et al., 2002, Alici et al., 2006, Wu et al., 2007, Alici et al., 2008) as shown in Table 1. Using the material parameters, the monotonic case at a prescribed displacement is simulated on the basis of the experiment (Alici et al., 2008). As the prescribed displacement at the beam tip is input as shown in Fig. 3.9, the results of the simulation are obtained as shown in Figs. 3.10~3.17.

Table 3.1 Material parameters for numerical simulation

Porosity, ϕ	PPy	0.20	PVDF	0.70
Elastic modulus of drained porous solid, E^d	PPy	80 MPa	PVDF	90 MPa
Elastic modulus of non-porous solid, E^s	PPy	160 MPa	PVDF	1360 MPa
Drained Poisson's ratio, v^d	PPy	0.365	PVDF	0.313
Shear correction factor, α	5/6			
Correction factor of Poisson effect, β	0.975			
Hydraulic permeability of pore fluid, κ_h	PPy	1.4×10^{-13} mm^2	PVDF	4.9×10^{-13} mm^2
Dynamic viscosity, η	0.00253 Pa · s			
Diffusivity of mobile ion, D	κ_{h_n}/η			
Absolute temperature, T	293 K			
Electric permittivity, k_e	PPy	3.0×10^{-1} F/m	PVDF	10.5×10^{-1} F/m
Concentration of immobile ions, C^0	0.050 M			
Species charge, z	-1			

As shown in Fig. 3.10, the reaction force gradually decreases with time even on the constant deflection. In addition, the peak of reaction force is more than two times of the relaxed reaction force. Such a large reaction force cannot be expressed by the pure bending of the Biot poroelasticity. The present study modified the undrained Poisson's ratio with the correction factor, so numerical reaction force could be agreed with the experimental reaction force. The black box models (Wu et al., 2007, Alici et al., 2008, Toi

and Mochizuki, 2010) between reaction force and voltage are available only for relaxed monotonic condition. The present study insists that the relation between reaction force and voltage depends on the internal conditions such as pore pressure and ion concentration.

As illustrated in Fig. 3.11 and 3.12, the pressure of the pore fluid was obtained with the interactions of the bending stress and electric field. The pore pressure over thickness is simultaneously increased along with the increase of the reaction force in Fig. 3.11. It shows that the reaction force is peaked by the pore pressure on the undrained condition. Subsequently, the pore pressure is decreased with the relaxation of the reaction force at the same time in Fig. 3.12. The relaxation of the reaction force is expressed by the pressure diffusion.

Alici et al (2006) assumed the distribution of volume expansion over thickness, but the present simulation result gives precise prediction with time. In the present result, the peak of the pore pressure is positioned near the interface but inside of the inert PVDF. The gradient of pressure means the direction of the pore fluid, so the flow of the pore fluid is disturbed by the peak. The present study proposes that the sudden change of permeability and porosity near the interface of the PPy and PVDF is a major factor on the design and control of the sensor. If the position of the pressure peak is controlled, the generated electricity increases and leakage decreases.

The distribution of the mobile ion concentration with respect to time is shown in Fig. 3.13 and 14. The distribution of the mobile ion concentration is following the distribution of the pore pressure a little bit later. The movements of the mobile ions are caused by the mass flux of the pore fluid with the pressure diffusion in Fig. 3.13. The mobile ion concentration is peaked even when the pressure of pore fluid is being decreased, and then the mobile ion concentration is, after time lag, decreased. It is understood that the movements of the mobile ions are not from instantaneous stresses but from the diffusion of pore pressure, so the time lag between reaction force and electric potential occurs.

The pore pressure and ion concentration over the microscopic thickness is difficult to be measured, so these numerical results would be helpful for other indirect prediction from macroscopic observation. If the distribution of the ion concentration is controlled by the material parameters such as porosity and permeability in Table 1, the performance of the sensor would be enhanced.

Finally, the electric potential is obtained from the mobile ion concentration as shown in Figs. 3.15 and 3.16. The mobile ion concentration determines the distribution of charge density, and then the distribution of the charge density results in the electric potential. Therefore, the difference of the electric potentials on the top and bottom is obtained as the output of the transient response of the mechanical conducting polymer sensor. The time history of the electric potential generated in the sensor is shown in Fig. 3.17.

In summary, the present numerical simulation well expressed the transient behavior of the mechanical sensor. The numerical simulation quantitatively expressed the transient behavior, and its results gave good understanding for the mechanism and features of the transient behavior. The mechanical deformation of the sensor induces the pressure of the pore fluid in polymer matrix, which results in the peak of mechanical reaction forces, and then the gradient of the pore pressure drives the mass flux of the pore fluid with the relaxation of the pore pressure and reaction force. The fluid flow also causes the movements of ions, but only mobile ions are movable so that the distribution of charge density is changed. The distribution of charge density finally causes electric potential as the output of the mechanical sensor which is very small amount than the electric potential of the actuator on the same structure and deflection. From the simulation results, it is concluded that the relaxation and hysteresis are dominantly induced by the pressure diffusion of the pore fluid as transient behaviors. In addition, the transport phenomena are very important in the transient behaviors of the mechanical sensor using conducting polymers, so the properties related to the transport are key factors for design and control.

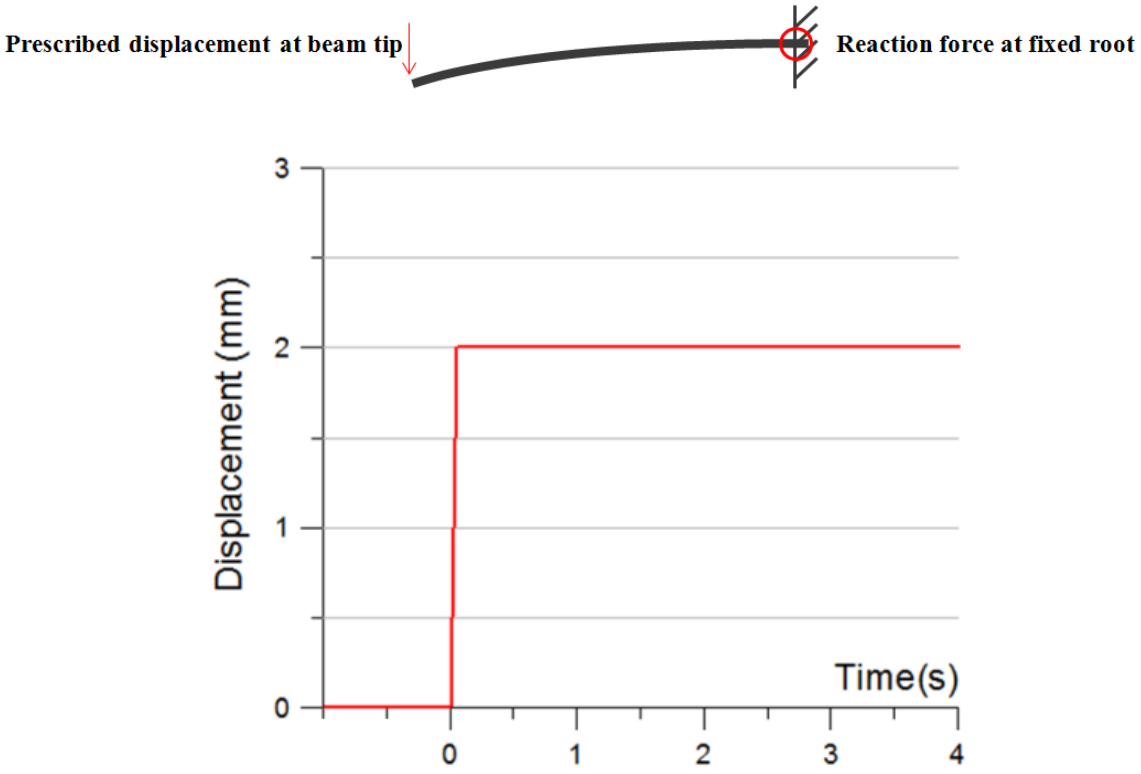

Fig. 3.9 Time history of prescribed deflection (simulation and experiment)

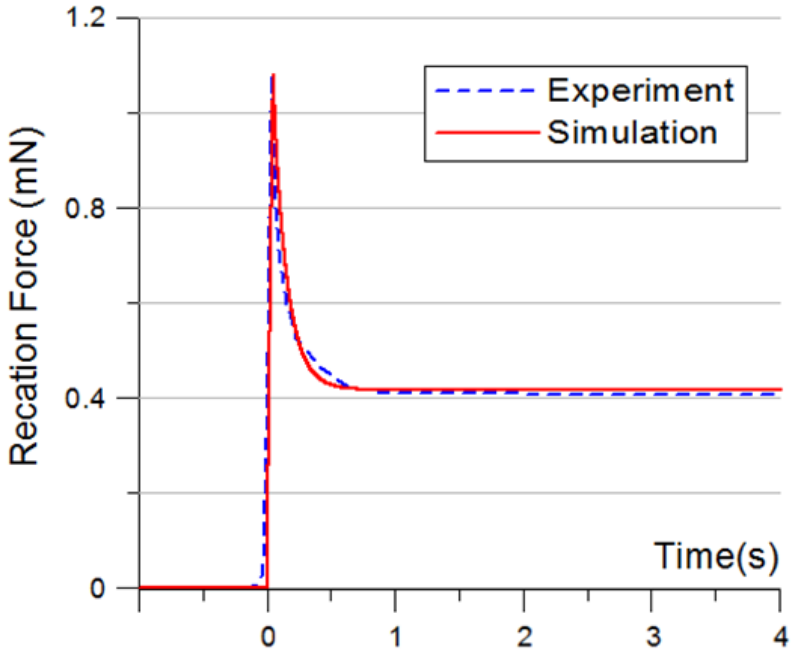

Fig. 3.10 Time history of reaction force (simulation and experiment)

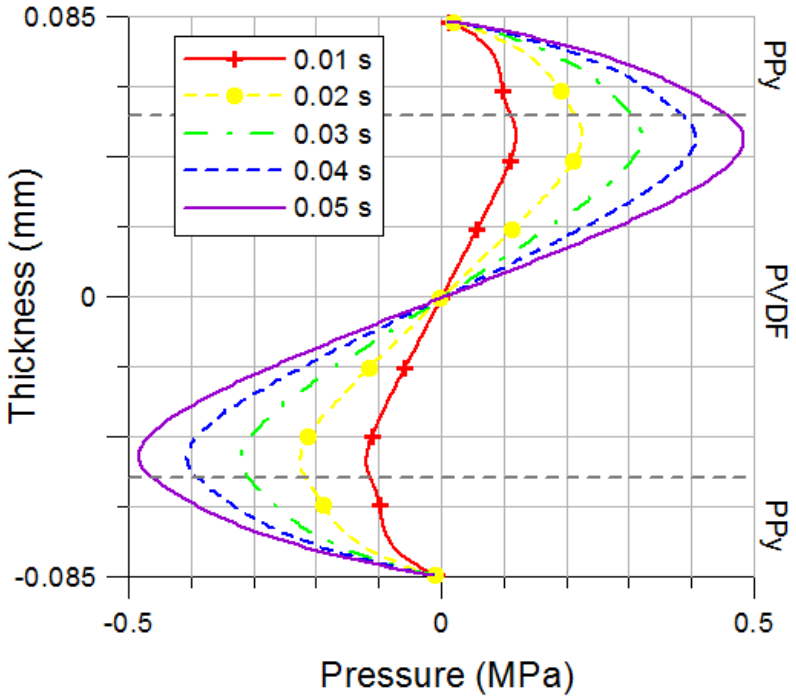

Fig. 3.11 Pressure distribution at beam root until peak (simulation)

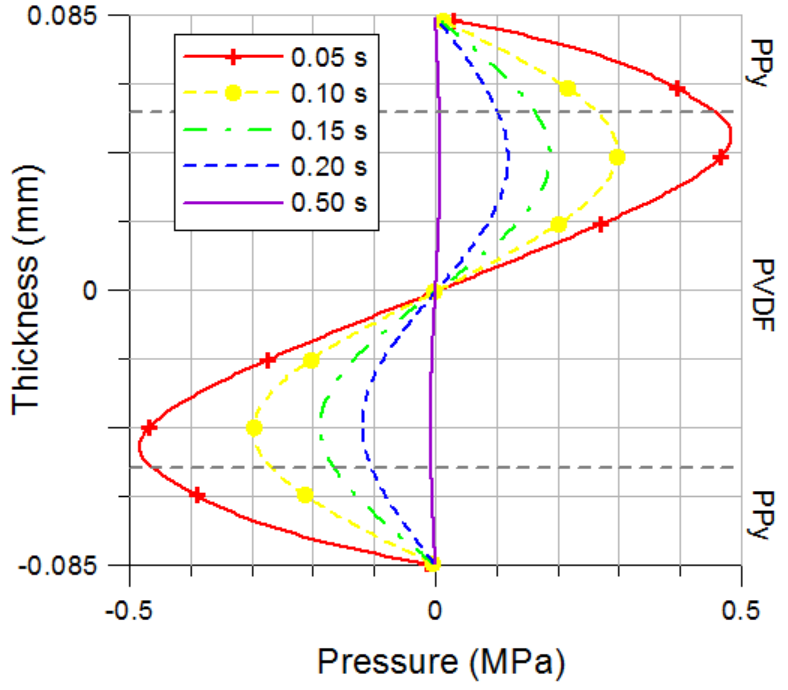

Fig. 3.12 Pressure distribution at beam root during relaxation (simulation)

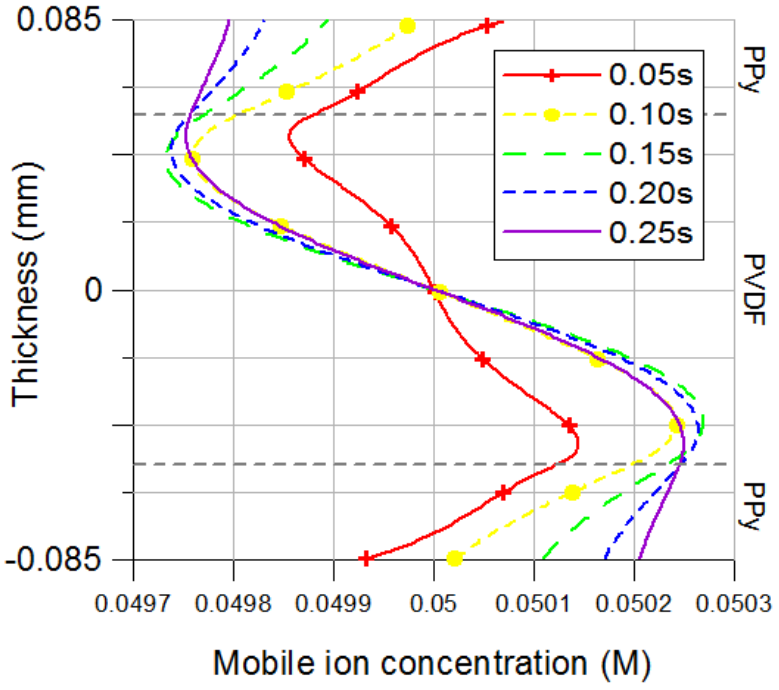

Fig. 3.13 Mobile ion concentration at beam root until peak (simulation)

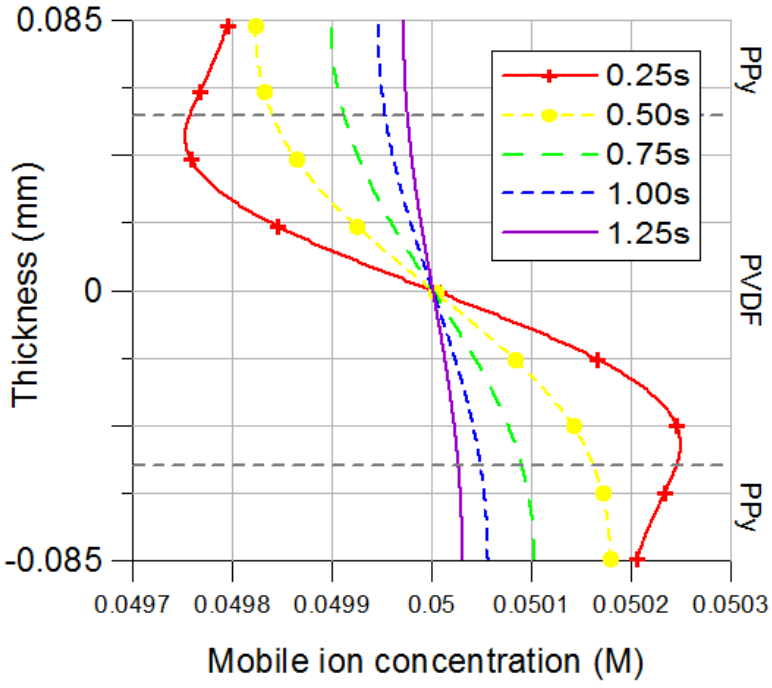

Fig. 3.14 Mobile ion concentration at beam root during relaxation (simulation)

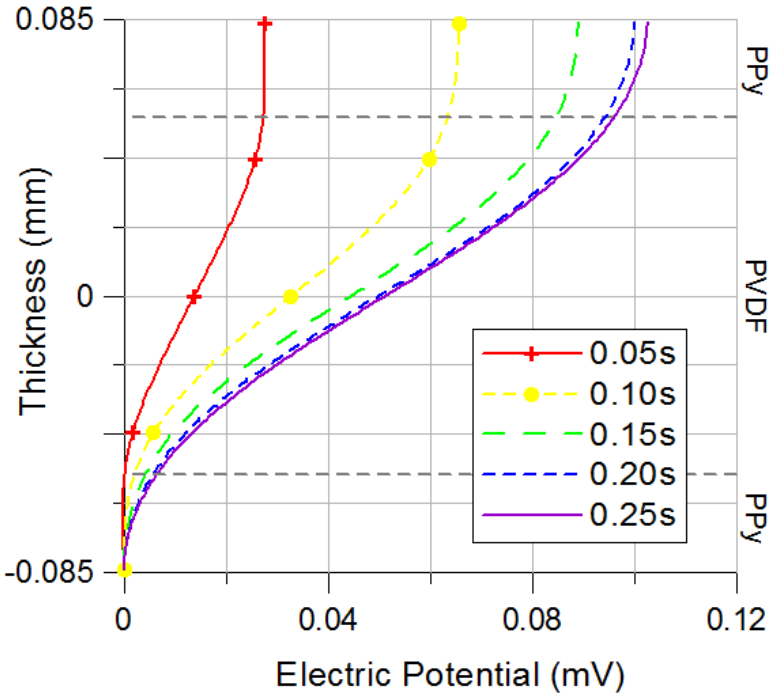

Fig. 3.15 Electric potential at beam root until peak (simulation)

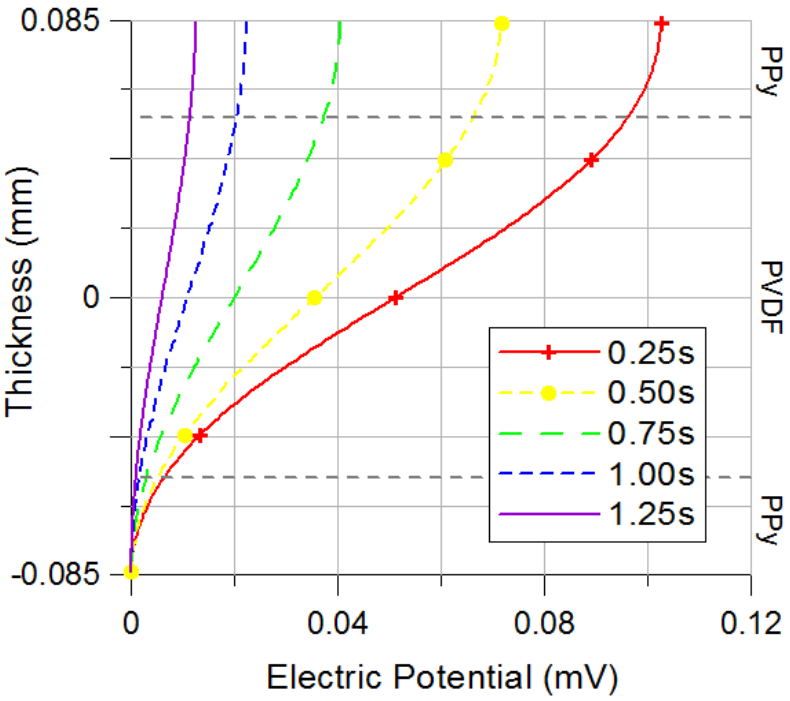

Fig. 3.16 Electric potential at beam root during relaxation (simulation)

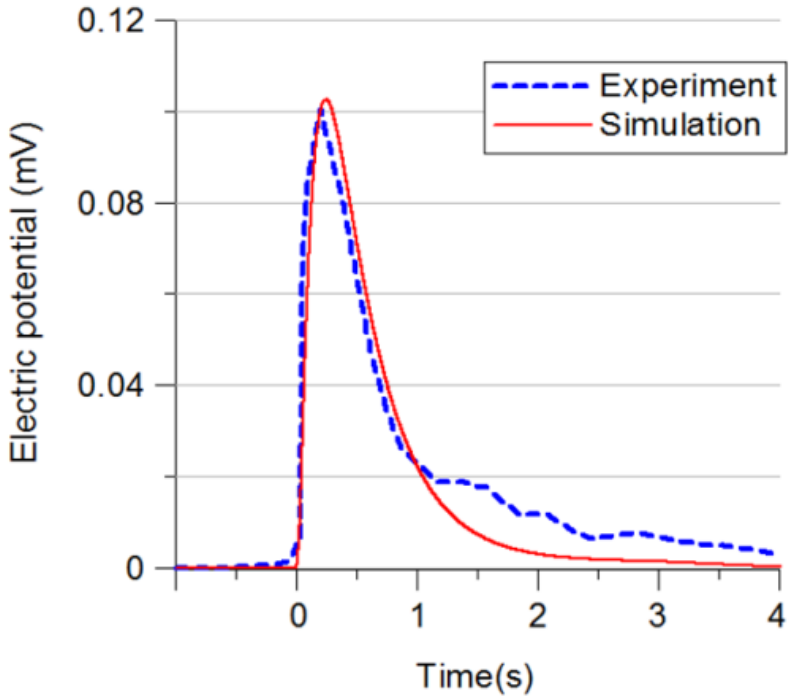

Fig. 3.17 Electric potential with respect to time (simulation and experiment)

Additionally, the reaction force and electrical potential with different correction factors of the Poisson effect, β, on the same prescribed deflection are illustrated in Figs. 3.18 and 3.19. The results show that the transient behavior of the sensor is significantly sensitive to the Poisson effect. The sensitivity is magnified by the bulk modulus of the pore fluid which is much stronger than the bulk modulus of the solid matrix. The Poisson's ratio is related to the volumetric strain of beams, so has a significant effect on the undrained pore pressure which is from the uniform stresses of the undrained stiffness even when three dimensional analysis. The undrained reaction force from the beam of the Biot poroelasticity, $\beta=1.0$, is lower than the experimental result as shown in Figs. 3.18 and 3.19, so the previous results in Figs. 3.10~3.17 employs the one parameter of the correction factors of Poisson effect, $\beta=0.975$.

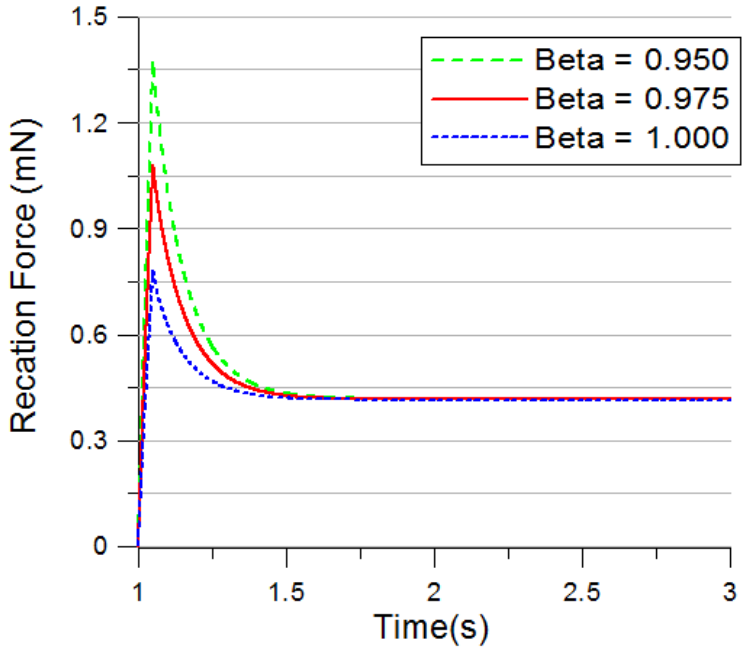

Fig. 3.18 Reaction force with different correction factors of Poisson effect, β, on the same prescribed deflection in Fig. 3.9

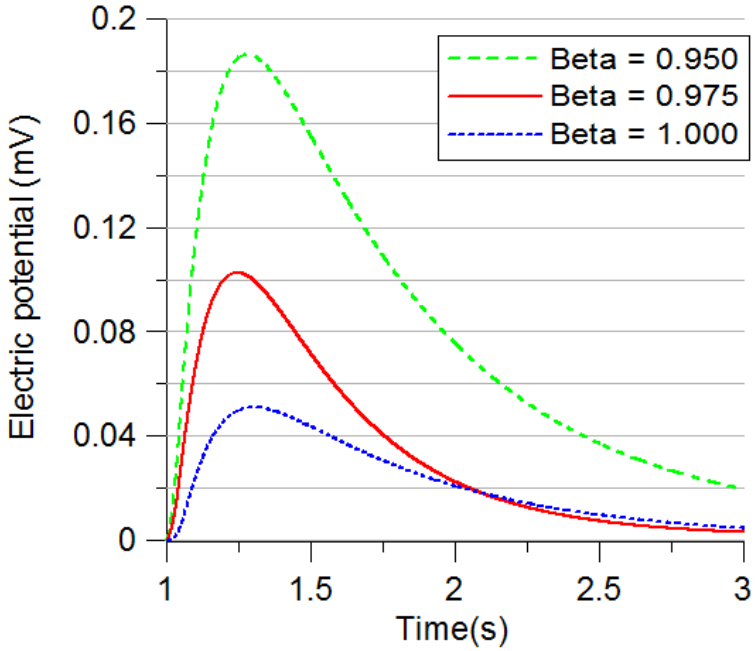

Fig. 3.19 Electric potential with different correction factors of Poisson effect, β, on the same prescribed deflection in Fig. 3.9

Lastly, an example for the transient behaviors of the mechanical sensors is introduced. As shown in Fig. 3.20, the rapid loading and unloading deflections, which is instantaneously increased and rapidly came back to initial position before relaxation, are prescribed. As a result, the reaction force and electric potential are obtained as shown in Fig. 3.21 and 3.22. As shown in Fig. 3.21, the reaction forces become positive and negative even when deflections are positive all the time. In Fig. 3.22, electric potentials has time lag, so the stepwise deflections during the time lag cannot be estimated from electric potential. From the simulation results, the hysteresis of reaction force and electric potential can be observed. It is shown that the transient behavior of the mechanical sensors is different from monotonic or static behaviors. In this case, empirical relations between mechanical deformation and electric potential are not reasonable any more. This simulation shows the insufficiency of black box models.

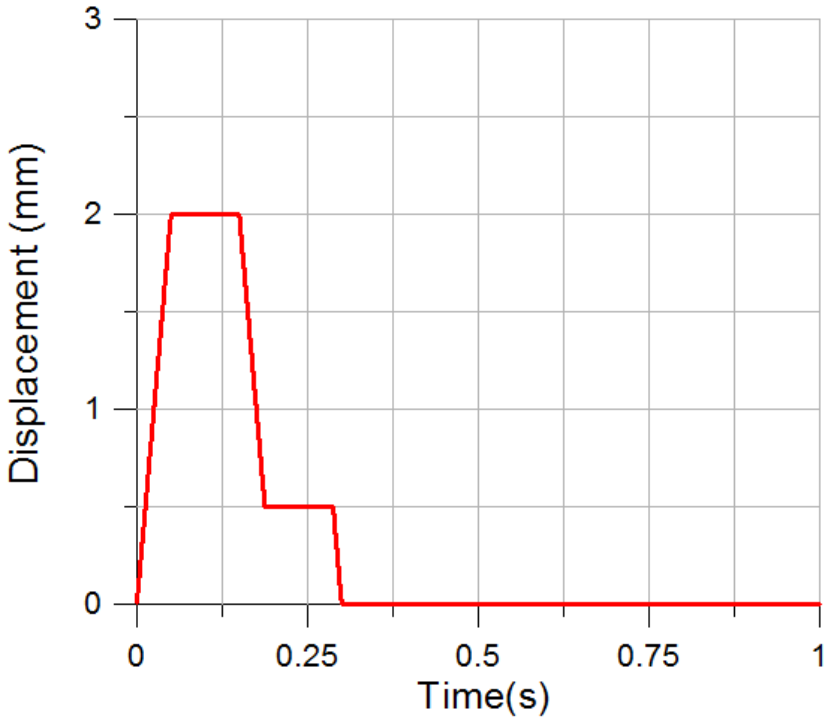

Fig. 3.20 Time history of prescribed stepwise deflection (simulation)

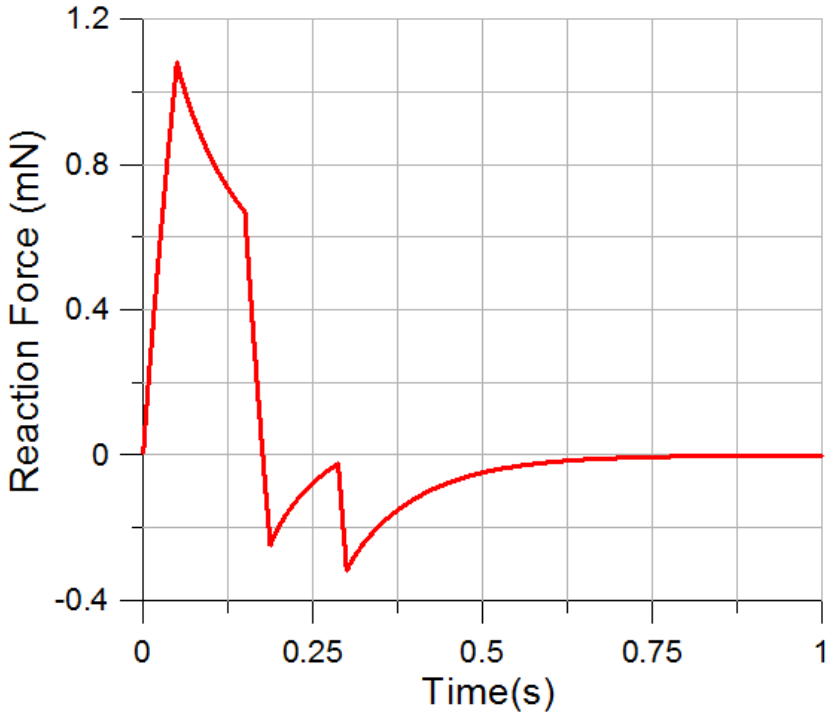

Fig. 3.21 Time history of reaction force (simulation)

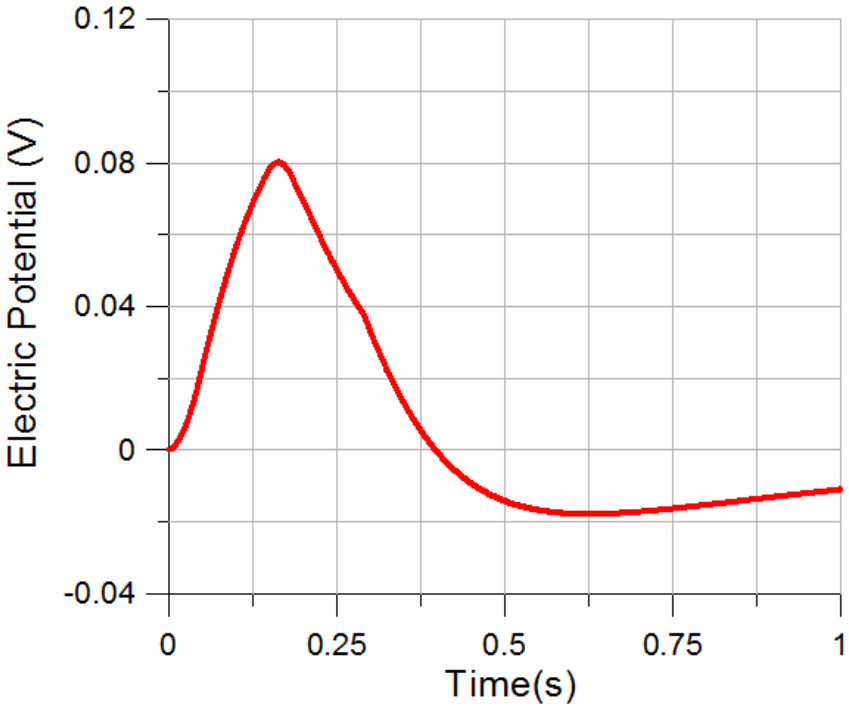

Fig. 3.22 Electric potential with respect to time (simulation)

3.5 Conclusion

The computational system for the mechanical sensors using conducting polymers has been scarce and insufficient in contrast with many simulations for the actuators. The experimental relations between the mechanical stress and electric potential are very much different in the actuation and sensation for the same conducting polymer, and the peaks of the mechanical stress and electric potential are generated in the transient response with relaxation and hysteresis. In the present study, the computational system for the transient behavior of the mechanical sensors was newly introduced. As a result, the transient behavior of the conducing polymer sensors was well expressed by the numerical simulation compared with the experimental results. It is concluded that the transport phenomenon of pore fluid is very important in the transient behaviors of the mechanical sensors, so mechanical properties related with the transport of the pore fluid such as porosity and permeability are key factors for design and control of the mechanical sensors. In addition, the relaxation and hysteresis of the mechanical reaction force and electric potential are explained by the pressure diffusion as the typical phenomena in fluid-saturated porous media.

In the computational system for the mechanical sensor, the Biot poroelastic theory, layered Timoshenko beam model and Poisson-Nernst-Planck equations are mainly employed, which are also applicable to the actuators. Embedding driving forces into the theoretical models with physical variables such as solid stress, fluid pressure, ion transport and electric potential, the governing equations consider the interactions between porous solid, pore fluid and mobile ions, and express the transient response of the mechanical sensors. The governing equations are employed into the fully coupled simulation with the time-marching, using finite element and finite difference methods.

The variations of physical variables over the thickness of the mechanical sensors dominantly determine the behavior of the mechanical sensors. The present study is simplified to one-dimensional analysis in the thickness direction. The transient behavior of porous beams is significantly sensitive to the Poisson effect, so the Poisson effect is added into the present beam model on the basis of the analogy between the Biot poroelastic

theory and thermal expansion model. The experimental reaction force can be larger than the analytical or numerical reaction force, so the undrained Poisson's ratio of the Biot poroelastic theory is modified using the correction factor in this study. Further research is more detailed consideration, such as three-dimensional analysis, multi-phase ion transport, energy loss and so on.

3.6 References

Alici, G. et al., 2006, A methodology towards geometry optimization of high performance polypyrrole (PPy) actuators, Smart Materials and Structures, Vol. 15, No. 2, pp. 243-252

Alici, G. et al., 2008, Response characterization of electroactive polymers as mechanical sensors, IEEE/ASME Transactions on Mechatronics, Vol. 13, pp. 187-196

Biot M. A., 1941, General theory of three-dimensional consolidation, Journal of Applied Physics, Vol. 12, pp. 155 -164

Rice J. R., Cleary MP, 1976, Some basic stress diffusion solution for fluid-saturated elastic porous media with compressible constituents, Reviews of Geophysics and Space Physics, Vol. 14, pp. 227–241

Scherer G.W et al., 2009, bending of a poroelastic beam with lateral diffusion, International Journal of solid and structure, Vol. 46, pp. 3451-3462

Spinks, G. M. et al., 2002, Strain response from polypyrrole actuators under load, Advanced Functional Materials, Vol. 12, pp. 437–440

Nemat-Nasser, S. and Zamani, S., 2006, Modeling of electro-chemo-mechanical response of ionic polymer-metal composites with various solvents, Journal of Applied Physics, Vol. 100, pp. 64310-64318

Toi, Y. and Jung W.S., 2007, Finite element modeling of electro-chemical-poroelastic behaviors of conducting polymers, Computers and Structures, Vol. 85, pp. 1453-1460

Toi, Y., 2008, A Course on Computational Solid Mechanics (Modeling and Simulation of Materials and Structures), Corona Publishing Company, pp.50-52, pp.144-156

Toi, Y. and Mochizuki, K, 2010, Computational modeling of sensor using conducting polymer [in Japanese], Seisan Kenkyu, Vol. 62, No. 5, pp. 553-556

Wang H.F., 1993, Quasi-static poroelastic parameters in rock and their geophysical applications, Pure and Applied Geophysics, Vol. 141, No. 2, pp. 269-286

Wang Z.H. et al., 2008, Bending of fluid-saturated linear poroelastic beams with compressible constituents, International Journal for Numerical and Analytical Methods in Geomechanics, Vol. 33, pp. 425-447

Wu, Y. et al., 2007, Soft mechanical sensors through reverse actuation in Polypyrrole, Advanced Functional Materials, Vol. 17, pp. 3216-3222

Chapter 4

Numerical Simulation of Mechanical Sensors Using Hydrated IPMCs

4.1. Introduction

IPMCs (ionic polymer-metal composites) have been known as intelligent materials having actuating and sensing functions, e.g. from electricity to deformation and from electricity to deformation. Owing to versatile characteristics such as low voltage, lightweight, easy access and flexibility, IPMCs have attracted attention as prospective applicants for artificial muscles, robotics, MEMS and so on (Jung et al., 2010). For example, Wang et al. (2009) introduced bio-inspired tactile sensors based on Flemion. Such applications are based on actuating and sensing functions with mechanical and electrical measures. In order to investigate the actuating and sensing functions, some papers (Nemat-Nasser and Zamani, 2006 and Jung et al., 2010) have attempted to establish the simulation model of IPMCs, but the simulation of the mechanical sensing behaviors of IPMCs has not been reported except for black box models. Hence, the present study newly attempts the numerical simulation of the mechanical sensors using the IPMCs.

IPMCs have both of actuating and mechanical sensing functions, but the functions are not compatible with each other. Wang et al. (2009) investigated Flemion-based IPMCs with the generated voltage of mechanical sensing mode and the supplied voltage of actuating mode. The generated voltage of sensing mode is very much smaller than the supplied voltage of actuating mode with respect to the same displacement and structure. The non-invertible response of the mechanical sensors is shown in Fig. 4.1.

The typical structure of IPMCs is illustrated in Fig. 4.2. It consists of an ionic polymer and metal deposits. The ionic polymer is a membrane that play roles electrolyte in the transport of ions and solvent, and the metal deposits function as electrodes. In the membrane, ionomers are composed of hydrophobic backbone polymers and the covalently attached anions which are hydrophilic. Through the backbone polymer, mobile cations and water molecules move with mechanical and elector-chemical forces (Nemat-Nasser and Wu, 2003).

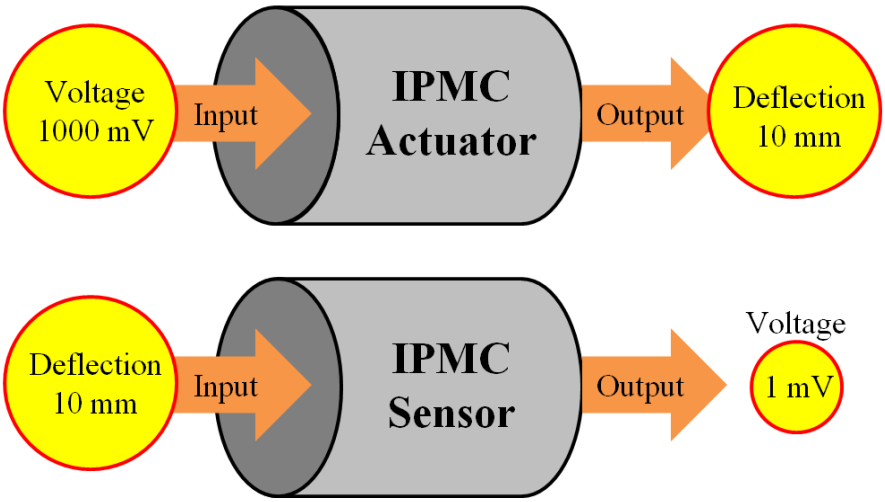

Fig. 4.1 Non-invertible black box of mechanical sensor and actuator using the same IPMC

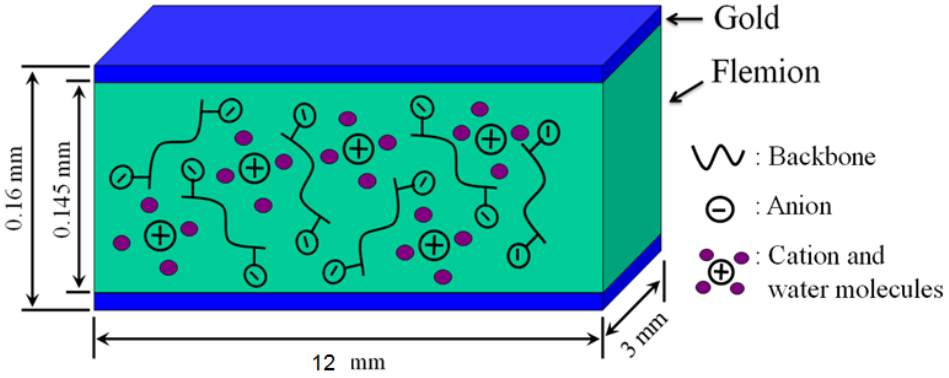

Fig. 4.2 Typical structure of IPMCs

The very small electric potential of mechanical sensors using IPMCs is explained with the following mechanism. When a porous IPMC is mechanically deformed, the pressure of pore fluid is changed by mechanical interaction between solid matrix and pore fluid. Subsequently, non-uniform pressure causes water and ions to be pushed out from shrunk side and to be sucked into dilate side as shown in Fig. 4.3. The movement of the ions causes the instant unbalance of charge density distribution, and the gradient of charge density results in electric potential. Therefore, electricity is generated corresponding to the magnitude of the mechanical stimulation (Wang et al., 2009).

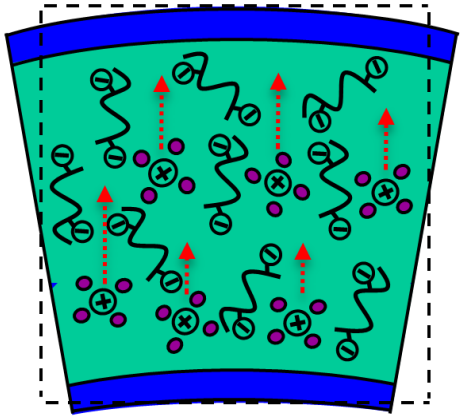

Fig. 4.3 Ion transport of IPMCs

Upon the above mechanism, the distributions of interesting parameters in the microscale thickness of IPMCs are very important, but the distributions are not easy to be obtained experimentally. Here, numerical simulation can be added to the quantitative estimation and design of mechanical sensors using IPMCs. Until now, the distributions of the interesting parameters in the mechanical sensing response have not been reported in spite of those in the actuating response. The detailed models of IPMC actuators (Nemat-Nasser and Zamani, 2006 and Jung et al., 2010) have been proposed, but the existing models of the actuators cannot be inversely applied to the mechanical sensors. Therefore, the present study proposes the simulation model of mechanical sensors using IPMCs and reports the simulation results with the distributions of interesting parameters in the thickness direction of IPMCs.

We previously attempted the numerical simulation of mechanical sensors using conducting polymers such as PPy-PVDF-PPy composite (Yoo and Toi, 2013). Differently from the conducting polymers, the ionic polymers of IPMCs, e.g. Flemion and Nafion, have significant hydration effects on volume and mechanical stiffness. Zhao et al. (2011) experimentally showed the volume swelling of Nafion with water absorption. Nemat-Nasser and Wu (2003) measured the volume and mechanical stiffness of Flemion and Nafion with respect to water uptake. The ionic polymers have the significant changes of volume and mechanical stiffness as water is absorbed due to hydration.

The above hydration effect is modeled with the followings. The total strains of ionic polymers are decomposed as stress-induced and hydration-induced parts, and the hydration-induced strain is considered as eigen-strain. The hydration-induced strain covers the eigen-strain due to applied electric force in actuating mode. Nemat-Nasser and Zamani (2006) and Jung et al. (2010) expressed the actuating deformation of IPMCs with eigen-strain. They identified the parameter of 'hydration' as water uptake which is defined as the volume fraction of water to polymer, and the hydration parameter leads to eigen-strain in structural analysis. In the present study, the pressure of water in a hydrated IPMC is divided into stress-induced and hydration-induced parts. The stress-induced pressure accounts for the instantaneous increase and subsequent relaxation of pore pressure when mechanical forces are externally applied. The hydration-induced pressure accounts for the contribution of water migration due to hydration. Next, the stress-induced strain and stress-induced pressure are embedded into the constitutive equations of Biot poroelasticity (Biot, 1941). The coefficients of the constitutive equations, which mean mechanical stiffness, are expressed by empirical relations with water uptake from conventional mechanical tests.

The sensing response of IPMCs shows the relaxation and time lag of reaction force and electric potential. In the experiment of Wang et al. (2009), Flemion-based IPMCs show that reaction force is sharply increased and quickly relaxed but electrical potential is gradually increased and slowly decreased. The transient response is resultant from the interactions between polymer matrix, water, mobile ion and electric potential. Modeling the interaction terms, Yoo and Toi (2013) integrated basic equations, e.g. layered Timoshenko beam model, Biot poroelastic model, Darcy-flow model and Poisson-Nernst-Plank model, and they numerically expressed the relaxation and time lag of reaction force and electric potential. The present study employs and modifies those models with the followings. The layered Timoshenko beam model simplifies the deformation of the mechanical sensors to reduce the time cost of calculation (Yoo and Toi, 2013). The Biot poroelastic model (Biot, 1941) considers the mechanical interaction between polymer matrix and water. The Biot poroelastic model was introduced with undrained parameters (Rice and Cleary, 1976). The undrained parameters are also employed into the modeling the instantaneous peak of reaction force. In the bending of a poroelastic beam, axial stress is affected by the lateral distribution of pore pressure

(Scherer et al., 2009). The Poisson effect is modeled with modified undrained Poisson's ratio (Yoo and Toi, 2013). In Darcy-flow model, water migration due to hydration is modeled by embedding hydration potential. The hydration potential is modeled with the empirical chemical potential in the free-swelling of IPMCs. Zhao et al. (2011) obtained the water activity of Nafion with respect to water uptake at free swelling equilibrium. Poisson-Nernst-Plank model analyzes ion transport and electric potential (Nemat-Nasser and Zamani, 2006). With the existence of porous polymer, the total concentration of ion to bulk IPMCs is used, and the convention and diffusion terms are embedded into the Poisson-Nernst-Plank model. As a result, the distributions of mechanical stress, pore pressure, ion concentration and electric potential are estimated with time.

Next, the procedure of numerical simulation is introduced that the multi-fields of layered finite beam elements are discretized and the basic equations are numerically formulated. Lastly, the transient behaviors of a mechanical sensor using a Flemion are numerically simulated with different deflections, and the numerical results are compared with experimental results.

4.2 Theoretical Models

4.2.1 Constitutive Equations

IPMCs consist of an ionic polymer and metal deposits as shown in Fig. 4.2. The ionic polymer is considered as a mixture of solid and fluid components. For example, the total volume of the mixture is decomposed into each volume of polymer matrix and water. On the conventional framework, the present study introduces two parameters, water uptake and porosity.

Water uptake is employed as a parameter to account for the hydration level of ionic polymers. Dry ionic polymers absorb a significant amount of water and their volume is spontaneously swollen. The phenomenon is known as hydration. Furthermore, mechanical stiffness is significantly changed with the water absorption. Nemat-Nasser and Wu (2003) identified the parameter of 'hydration' as water uptake, and they measured the volume and stiffness of ionic polymers with water uptake. The water uptake is actually estimated by the mass fraction of absorbed water to dry polymer. The present study would define the water uptake as

$$w = \frac{m^f}{m^s} = \frac{m^t - m^{dry}}{m^{dry}} \tag{4.1}$$

where w is water uptake, m^f is the mass of absorbed water, m^s is the mass of polymer matrix, m^t is the total mass of a hydrated ionic polymer, and m^{dry} is the mass of the ionic polymer on dry condition.

Porosity is a very common parameter in poromechanics, and is defined as the volume fraction of pores to bulk materials (Biot, 1976). If water is saturated in pores, porosity is equal to the volume fraction of fluid to bulk materials. The porosity is, referring to initial volume, introduced as

$$\phi = \frac{V^f}{V_0^t} \tag{4.2}$$

where, ϕ is porosity, V^f is the volume of fluid component, and V_0^t is the total volume of a hydrated ionic polymer on initial condition ($t=0$).

Assuming that polymer matrix and water are incompressible (but total volume is changed with pore volume), the water uptake in Eq. (4.1) becomes $w = V^f / V^s$. Thus, the following relation between water uptake, porosity and volumetric strain is derived as

$$e^t = \varepsilon_{kk}^t = \Delta\phi = \frac{\Delta w}{1+w_0} \tag{4.3}$$

where, e^t is the total volumetric strain of bulk material, ε_{kk}^t is the total strains of bulk material and w_0 is initial water uptake.

The volume of ionic polymers is significantly changed with the humidity of surroundings. In case of actuating mode, ionic polymers are deformed when electricity is externally applied. On stress-free condition, ionic polymers can be deformed as electrochemical state is changed. In order to consider the electrochemically induced deformation, the present study decomposes the total strains of ionic polymers into stress-induced strains and hydration-induced strains as follows.

$$\varepsilon_{ij}^t = \varepsilon_{ij}^s + \frac{e^h}{3}\delta_{ij} \tag{4.4}$$

Where, ε_{ij}^s is stress-induced strains, e^h is hydration-induced strain and δ_{ij} is Kronecker delta. The stress-induced strains are observed when mechanical forces are applied, and the hydration-induced strain is observed when water is migrated by electrochemical forces. The hydration-induced strain is considered as eigen-strain in structural analysis. Nemat-Nasser and Zamani (2006) modeled the actuating deformation of IPMCs with eigen-strain. The eigen-strain due to electric force is also included in the hydration-induced strain.

In the sensing mode of IPMCs, pore pressure is instantaneously changed and relaxed like reaction force (Yoo and Toi, 2013). On stress-free condition, the pore pressure of a hydrated ionic polymer is initially different from the pressure of surroundings like

osmosis. The present study decomposes the pore pressure as stress-induced and hydration-induced parts.

$$p^t = p^s + p^h \tag{4.5}$$

where, p^t is pore pressure, p^s is stress-induced pressure and p^h is hydration-induced pressure. The stress-induced pressure accounts for the transient part of pore pressure with relaxation when mechanical forces are externally applied. The hydration-induced pressure accounts for the contribution of water migration due to hydration. The hydration-induced pressure becomes the total pore pressure on free swelling condition including the actuation due to electricity. Nemat-Nasser and Wu (2006) introduced the pressure of clusters assuming one spherical inclusion problem. Jung et al. (2010) modeled fluid pressure to lead to the volumetric strain of Flemion-based actuators. Those pressures in other actuator models are included in the hydration-induced pressure.

Yoo and Toi (2013) employed Biot poroelastic constitutive equations to consider the transient response of mechanical sensors using conducting polymers. Upon the decompositions of strain and pore pressure, the stress-induced strain and stress-induced pressure are embedded into the Biot poroelastic constitutive equations. The thickness of IPMCs is very thin compared to the length, so the bending deformation can be considered within elastic range. The constitutive equations of a hydrated ionic polymer are proposed as

$$\varepsilon_{ij}^t - \frac{e^h}{3}\delta_{ij} = \frac{1+\nu}{E}(\sigma_{ij} + b(p^t - p^h)\delta_{ij}) - \frac{3\nu}{E}(\frac{\sigma_{kk}}{3} + b(p^t - p^h))\delta_{ij}$$

$$= \varepsilon_{ij}^s = \frac{1+\nu}{E}(\sigma_{ij} + bp^s\delta_{ij}) - \frac{3\nu}{E}(\frac{\sigma_{kk}}{3} + bp^s)\delta_{ij} \tag{4.6}$$

where, σ_{ij} is total stress, E is elastic modulus, ν is Poisson's ratio and b is Biot coefficient. As mentioned before, the mechanical stiffness of ionic polymers are changed as water is absorbed. Nemat-Nasser and Wu (2003) obtained the elastic modulus of Nafion and Flemion with respect to water uptake. They observed that elastic modulus exponentially decreases with water uptake. The coefficients in constitutive equations are

conventionally obtained from static tensile experiments. On the conventional framework, the coefficients of a hydrated ionic polymer are expressed with empirical relations with water uptake. For example, the elastic modulus and bulk modulus of a hydrated ionic polymer can be expressed as exponential functions of water uptake.

$$E = E_{dry} \exp(-Qw_0) \tag{4.7}$$

$$K = K_{dry} \exp(-Rw_0) \tag{4.8}$$

where, E_{dry} is elastic modulus on dry condition, K is the bulk modulus of a hydrated ionic polymer, K_{dry} is bulk modulus on dry condition, Q and R are empirical coefficients.

The Biot coefficient in Eq. (4.6) is introduced as (Scherer et al., 2009).

$$b = 1 - \frac{K}{K^s} \tag{4.9}$$

where, K^s is the bulk modulus of solid matrix.

The sensing response of IPMCs shows the instantaneous peak of reaction force higher than static reaction force (Wang et al., 2009). The instantaneous peak is explained with the instant contribution of absorbed water to the mechanical stiffness of total bulk. If fluid in pores has not enough time to flow, then the pore fluid instantly resists deformation. The instantaneous behaviors are modeled with pore pressure on undrained condition as $\Delta(\phi\rho_f) = 0$, where ρ_f is the density of fluid. On the undrained condition, the relation between the stress-induced pressure and the undrained stress is introduced as (Rice, J.R. and Cleary, M.P., 1976)

$$\Delta p^s = -B\frac{\Delta\sigma_{kk}}{3} \tag{4.10}$$

$$B = \frac{\frac{1}{K} - \frac{1}{K^s}}{-\frac{1+\phi}{K^s} + \frac{\phi}{K^f} + \frac{1}{K}} \tag{4.11}$$

where, B is Skempton coefficient, K^f is the bulk modulus of fluid in pores, and the others are mentioned previously.

On the undrained condition, the mechanical stiffness of a hydrated IPMC will be increased, so the undrained stiffness is additionally estimated. The undrained bulk modulus and Poisson's ratio are introduced as (Rice, J.R. and Cleary, M.P., 1976)

$$K^u = \frac{K}{1-bB} \tag{4.12}$$

$$v^u = \frac{3v + B(1-2v)b}{3 - B(1-2v)b} \tag{4.13}$$

where, K^u is undrained bulk modulus and v^u is undrained Poisson's ratio.

4.2.2 Basic Equations

The solid stresses of IPMCs can be obtained by the quasi-static equilibrium equation as

$$\frac{\partial \sigma_{ij}}{\partial x_j} = 0 \tag{4.14}$$

The deformation field of IPMCs can be idealized as a bending motion, thereby their constitutive equations are reduced (Nemat-Nasser and Wu, 2006). Yoo and Toi (2013) mentioned that pore pressure is non-linearly and significantly varied in micro-thickness of IPMCs and dominantly affects on the sensitivity of IPMCs. The present study employs layered approach into a beam model to obtain interesting parameters in thickness direction as shown in Fig. 4.4. The layered Timoshenko beam model (Toi, 2008) is introduced as follows.

$$u_1 = -x_2\theta \tag{4.15}$$

$$\varepsilon_{11}^t = \frac{\partial u_1}{\partial x_1} = -x_2 \frac{d\theta}{dx_1} \tag{4.16}$$

$$\gamma_{21}^{t} = \frac{\partial u_2}{\partial x_1} + \frac{\partial u_1}{\partial x_2} = \frac{\partial u_2}{\partial x_1} - \theta \tag{4.17}$$

where, u_1 is axial displacement, u_2 is lateral displacement, x_2 is distance from neutral axis, θ is rotation of normal section, ε_{11}^{t} is axial strain, γ_{21}^{t} is transverse shear strain.

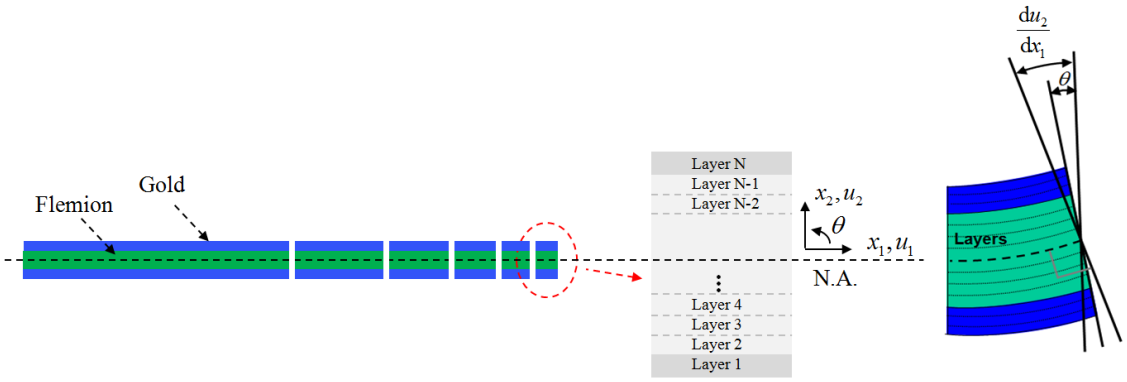

Fig. 4.4 Layered Timoshenko beam element

Scherer et al. (2009) mentioned Poisson effect that the uniaxial stress of a beam in transient behaviors is affected by the distribution of pore pressure. Yoo and Toi (2013) simply added the Poisson effect into axial stress of beam with modified undrained Poisson's ratio. Employing the Poisson effect, the constitutive equations of Eq. (4.6) are reduced in layered Timoshenko beam model as follows.

$$\sigma_{11} = E(\varepsilon_{11}^{t} - \frac{e^{h}}{3}) - bp^{s} - 2v^{B}bp^{s} \tag{4.18}$$

$$\tau_{21} = \alpha\, G\, \gamma_{21}^{t} \tag{4.19}$$

$$v^{B} = \beta\, v^{u} \tag{4.20}$$

where, G is total shear modulus, α is shear correction factor, v^{B} is beam undrained Poisson's ratio, and β is the correction factor of Poisson effect.

Next, water transport in a hydrated ionic polymer is introduced. From Biot poroelastic theory (Biot, 1941, and Rice and Cleary 1976), water transport in a porous material is modeled as

$$\frac{\partial \phi}{\partial t} - \nabla \cdot f_w = \frac{\partial e^t}{\partial t} - \nabla \cdot f_w = 0 \tag{4.21}$$

where, f_w is the volume flux of water in pores.

Rice and Cleary (1976) introduced undrained volume change with undrained parameters from Biot poroelastic theory. The present study models the volumetric strain rate with stress-induced and hydration-induced pressures.

$$\frac{\partial e^t}{\partial t} = \frac{9(v^B - v)}{B^2 E(1+v^B)} \frac{\partial}{\partial t}\left(B\frac{\sigma_{kk}^u}{3} + p^s + p^h \right) \tag{4.22}$$

The volume flux in Eq. (4.21) can be described with Darcy law (Biot, 1941). The present study models water migration due to hydration with hydration potential, then the volume flux of water in a hydrated ionic polymer becomes

$$f_w = -\frac{\kappa_h}{\eta_w} \nabla(p^s + p^h + H\Phi + z_{cation} c_{cation} F\psi) \tag{4.23}$$

where, κ_h is hydraulic permeability, η_w is dynamic viscosity, H is hydration coefficient, Φ is hydration potential, z_{cation} is cation valence, c_{cation} is cation concentration, F is Faraday constant and ψ is electric potential.

Next, the modeling of hydration-induced strain is introduced with water migration due to hydration. Zhao et al. (2011) estimated the water activity of Nafion with respect to water uptake. From such experiments, the water activity of a hydrated ionic polymer without any external force can be expressed as an empirical relation with water uptake. For example, the water activity in a certain range can be simply assumed as an exponential function with water uptake.

$$a_w(w) = 1 - \exp(-Aw) \tag{4.24}$$

where, a_w is the water activity of a hydrated ionic polymers without any external force and A is an empirical coefficient.

The hydration potential in Eq. (4.23) is modeled as an empirical chemical potential which is obtained from free swelling equilibrium without any external force. If the empirical chemical potential is expressed with the above water activity, then hydration potential is expressed as a function of water uptake.

$$\Phi_w = \mu_{w0} + RT \ln a_w(w) \tag{4.25}$$

where, μ_{w0} is the chemical potential of pure water, R is gas constant, and T is absolute temperature.

The hydration-induced pressure is resultant from electrochemically induced phenomena, but it is hydraulic pressure. On free swelling condition, the change of hydration potential accompanies the change of pore pressure with the balance of the mechanical interaction of fluid and solid. Therefore, the hydration coefficient in Eq. (4.23) is modeled as

$$H(w) = \frac{\partial p^h}{\partial \Phi} \tag{4.26}$$

Differentiating the hydration potential in Eq. (4.25) with water uptake leads to

$$\frac{\partial \Phi}{\partial w} = \frac{RT}{a_w}\frac{\mathrm{d}a_w}{\mathrm{d}w} = \frac{RTA\exp(-Aw)}{1-\exp(-Aw)} \tag{4.27}$$

From Eq. (4.3) and Eq. (4.22), the variation of hydration-induced pressure with water uptake is

$$\frac{\partial p^h}{\partial w} = \frac{B^2 E(1+\nu^B)}{9(\nu^B-\nu)}\frac{1}{1+w_0} \tag{4.28}$$

From Eq. (4.27) and Eq. (4.28), the hydration coefficient in Eq. (4.23) is obtained as

$$H(w) = \frac{B^2 E(1+v^B)}{9(v^B - v)(1+w_0)} \frac{1-\exp(-Aw)}{RTA\exp(-Aw)} \tag{4.29}$$

From Eq. (4.23) and the related parameters, hydration-induced strain in the transient behaviors of IPMCs is obtained as

$$\frac{\partial e^h}{\partial t} = -\frac{\kappa_h}{\eta_w}\nabla^2\left(p^h + HRT\ln a_w + z_{cation}c_{cation}F\psi\right) \tag{4.30}$$

Next, the transport phenomena of ions in IPMCs are analyzed with Poisson-Nernst-Plank model. The molar concentration of ions is obtained by Nernst-Planck equation, and electric potential is obtained by Poisson equation with the molar concentration of ions. In ionic polymers of IPMCs, covalently attached anions are assumed as uniformly distributed and fixed, then mobile cations are only considered in the Poisson-Nernst-Plank model (Nemat-Nasser and Zamani, 2006). In the present study, the total concentration of mobile cation in ionic polymers refers to the amount of ion to the total volume of bulk material, $C_I = \phi c_I$, where c_I is molar concentration referring to the amount of ion to the volume of absorbed water. In the present study, the convection with water flow is added in order to express the generation of electric potential in sensing mode. In addition, the interaction between ions and polymer is added with the fraction of ions to the volume of polymer matrix, $c_I V^f / V^s = c_I w$. The Poisson-Nernst-Plank equations are modified as follows.

$$\frac{\mathrm{d}C_I}{\mathrm{d}t} = D_{Iw}\left(\nabla\cdot(\phi\nabla c_I) + \frac{z_I F}{RT}\nabla\cdot(\phi c_I\nabla\psi)\right) + D_{Ip}\nabla^2(c_I w) - \nabla\cdot(c_I f_w) \tag{4.31}$$

$$\nabla^2\psi = z_I\frac{F}{k_e}(C_I - C_I^0) \tag{4.32}$$

where, D_{Iw} is ion-water diffusivity, z_I is valence, D_{Ip} is ion-polymer diffusivity, k_e is electric permittivity, and C_I^0 is concentration of immobile ions. As a result, water flow in pores results in the redistribution of ion concentration, then electric potential is

generated. The aforementioned Poisson-Nernst-Plank equations, Biot poroelastic theory and layered Timoshenko beam model express the hydration and transient behaviors of mechanical sensors using IPMCs.

4.3 Numerical Formulations

Finite element method is employed into the numerical analysis of mechanical sensors using IPMCs. The sensor is subdivided by layered Timoshenko beam elements. The beam elements are also discretized in the thickness direction on the fields of interesting parameters such as axial stress, pore pressure, ion concentration and electric potential as shown in Fig. 4.5. Based on the discretization, basic equations are numerically formulated with the followings.

First, the instantaneous response of IPMCs, when mechanical force is applied, is obtained by considering the undrained condition. Using the undrained stiffness from Eq. (4.12) and (4.13), the incremental formulation of finite element stiffness equation is as follows.

$$\left[S^u\right]\left\{\Delta u^u\right\} = \left\{\Delta f^{ext}\right\} \tag{4.33}$$

$$[S^u] = \int_V [B]^T [D^u][B] dV \tag{4.34}$$

$$\{\Delta \varepsilon^u\} = [B]\{\Delta u^u\} \tag{4.35}$$

where $[S^u]$ is undrained stiffness matrix, $\{\Delta u^u\}$ is undrained nodal displacement increment vector, $\{\Delta f^{ext}\}$ is external force increment vector, $[B]$ is strain-displacement matrix, $[D^u]$ is undrained stress-strain relation matrix, $\{\Delta \varepsilon^u\}$ is undrained strain increment vector. The coefficients in the undrained stress-strain relation matrix are determined by undrained parameters. Yoo and Toi (2013) introduced the components in the above stiffness matrix. The undrained behavior accompanies the instantaneous pore pressure on water in pores.

Second, the obtained increment if the undrained strains in Eq. (4.35) are used for the estimation of the instantaneous change of pore pressure with Eq. (4.10). The change of

pore pressure on the undrained condition is added into stress-induced pressure. The stress-induced pressure of n-th layer, p_n^s, is updated as follows.

$$p_n^s = p_n^s - B\frac{\Delta\sigma_{kk}^u}{3} = p_n^s - BK_n^u\Delta e_n^u = p_n^s - BK_n^u(1-2v_n^B)\Delta\varepsilon_{x\,n}^u \tag{4.36}$$

Third, the above stress-induced pressure becomes non-uniformly distributed, so water in pores starts to flow. The amount of migrated water is estimated by the gradient of the non-uniform stress-induced pressure. At the same time, the stress-induced pressure is also relaxed as water is migrated. The phenomenon is modeled from Eq. (4.23), then the increment of stress-induced pressure is obtained with the followings.

$$(f^{w1})_{n+1} = -\frac{\kappa_h}{\eta_w}\frac{p_{n+1}^s - p_n^s}{\Delta x_2}, \qquad (f^{w1})_n = -\frac{\kappa_h}{\eta_w}\frac{p_n^s - p_{n-1}^s}{\Delta x_2},$$

$$\Delta e_n^s = -\frac{\Delta t}{\Delta x_2}\left\{(f^{w1})_{n+1} - (f^{w1})_n\right\}\Delta t \tag{4.37}$$

$$\Delta p_n^s = \frac{B^2E(1+v^B)}{9(v^B - v)}\Delta e_n^s \tag{4.38}$$

where, f^{w1} is volume flux with stress-induced pressure and x_2 is local coordinate in the thickness of a beam element as shown in Fig. 4.4.

Fourth, hydration-induced strain is calculated with Eq. (4.30). The increment of the hydration-induced strain is as follows.

$$(f^{w2})_{n+1} = -\frac{\kappa_h}{\eta_w}\frac{p_{n+1}^h - p_n^h}{\Delta x_2}, \qquad (f^{w2})_n = -\frac{\kappa_h}{\eta_w}\frac{p_n^h - p_{n-1}^h}{\Delta x_2},$$

$$(f^{w3})_{n+1} = -\frac{\kappa_h}{\eta_w}\frac{H_{n+1}\Phi_{n+1} - H_n\Phi_n}{\Delta x_2}, \qquad (f^{w3})_n = -\frac{\kappa_h}{\eta_w}\frac{H_n\Phi_n - H_{n-1}\Phi_{n-1}}{\Delta x_2},$$

$$(f^{w4})_{n+1} = \frac{\kappa_h}{\eta_w}z_{cation}c_{cation}FE_{n+1}, \qquad (f^{w4})_n = \frac{\kappa_h}{\eta_w}z_{cation}c_{cation}FE_n,$$

$$\Delta e^h = -\frac{\Delta t}{\Delta x_2}\left\{ \left((f^{w2})_{n+1} + (f^{w3})_{n+1} + (f^{w4})_{n+1}\right) - \left((f^{w2})_n + (f^{w3})_n + (f^{w4})_n\right) \right\} \quad (4.39)$$

where, f^{w2} is volume flux with hydration-induced pressure, f^{w3} is volume flux with hydration potential and f^{w4} is volume flux with electric potential,

Fifth, total pressure, porosity and water uptake are also updated from Eq. (4.3) and Eq. (4.21).

$$\Delta p_n^h = \frac{B^2 E(1+v^B)}{9(v^B - v)} \Delta e^h \quad (4.40)$$

$$p_n^t = p_n^t + \Delta p_n^s + \Delta p_n^h \quad (4.41)$$

$$\phi_n = \phi_n + \Delta\phi_n = \phi_n + \Delta e_n^s + \Delta e_n^h \quad (4.42)$$

$$w_n = w_n + \Delta w_n = w_n + \left(1 + w_n^0\right)\Delta\phi_n \quad (4.43)$$

Using the stress-induced pressure in Eq. (4.38) and the hydration-induced strain in Eq. (4.39), the structural analysis of mechanical IPMC sensors is conducted with Biot poroelastic constitutive equation. The stress-induced pressure, beam Poisson effect and hydration-induced strain are implemented as external forces into finite element formulation. The finite element stiffness equation with initial strain method is as follows.

$$[S]\{\Delta u\} = \{\Delta f^{ext}\} + \{\Delta f^s\} + \{\Delta f^h\} + \{\Delta f^B\} \quad (4.44)$$

$$\{\Delta f^s\} = \int_V [L]^T \{b\Delta p^s \delta_{ij}\} dV \quad (4.45)$$

$$\{\Delta f^h\} = \int_V [L]^T [D]\{\frac{\Delta e^h}{3}\delta_{ij}\} dV \quad (4.46)$$

$$\{\Delta f^{beam}\} = \int_V [L]^T \{2bv^B \Delta p^s \delta_{ij}\} dV \quad (4.47)$$

where, $[S]$ is stiffness matrix, $\{\Delta f^s\}$ is the force increment vector of stress-induced pressure, $\{\Delta f^h\}$ is the force increment vector of hydration effect, $[D]$ is stress-strain

relation matrix with water uptake. $\{\Delta f^B\}$ is the force increment vector of the Poisson effect only for beam models. Since the pore pressure acts on the lateral direction of uniaxial stress condition, the Poisson effect of the pore pressure is added. In order to match with the peak of reaction forces in experiments, the undrained Poisson's ratio is modified by the correction factor from the Eq. (4.20). Solving the Eq. (4.44), the mechanical states with the relaxation are numerically analyzed.

Lastly, the fields of mobile ion concentration and electric potential are obtained with Poisson-Nernst-Plank equations, Eq. (4.31) and Eq. (4.32). The field equations of mobile ion concentration and electric potential are obtained as follows.

$$(f^{c1})_{n+1} = -D_{Iw}\frac{\phi_n + \phi_{n+1}}{2}\frac{c_{n+1} - c_n}{\Delta x_2}, \quad (f^{c1})_n = -D_{Iw}\frac{\phi_n + \phi_{n-1}}{2}\frac{c_n - c_{n-1}}{\Delta x_2},$$

$$(f^{c2})_{n+1} = D_{Iw}\frac{zF}{RT}\frac{C_{n+1} + C_n}{2}E_{n+1}, \quad (f^{c2})_n = D_{Iw}\frac{zF}{RT}\frac{C_n + C_{n-1}}{2}E_n,$$

$$(f^{c3})_{n+1} = -D_{Ip}\frac{c_{n+1}w_{n+1} - c_n w_n}{\Delta x_2}, \quad (f^{c3})_n = -D_{Ip}\frac{c_n w_n - c_{n-1}w_{n-1}}{\Delta x_2},$$

$$(f_w)_{n+1} = (f^{w1})_{n+1} + (f^{w2})_{n+1} + (f^{w3})_{n+1} + (f^{w4})_{n+1},$$

$$(f_w)_n = (f^{w1})_n + (f^{w2})_n + (f^{w3})_n + (f^{w4})_n,$$

$$\Delta C = -\frac{\Delta t}{\Delta x_2}\left((f^{c1})_{n+1} - (f^{c1})_n + (f^{c2})_{n+1} - (f^{c2})_n + (f^{c3})_{n+1} - (f^{c3})_n + \frac{c_{n+1} + c_n}{2}(f_w)_{n+1} - \frac{c_n + c_{n-1}}{2}(f_w)_n\right) \tag{4.48}$$

$$n = 2,\ 3,\ 4,\ \cdots,\ (N+1), \quad E_1 = 0, \quad E_n = E_{n-1} - z\frac{F}{k_e}\left(C_n - C_n^0\right)\Delta x_2 \tag{4.49}$$

$$n = 3,\ 5,\ 7,\ \cdots,(N+1), \quad \psi_1 = 0, \quad \psi_n = \psi_{n-2} - \frac{E_n + 4E_{n-1} + E_{n-2}}{3}\Delta x_2 \tag{4.50}$$

From the above equations, the electric potential is obtained as the output of the sensor model. Through the aforementioned procedure, the transient behaviors of mechanical sensors using IPMC are numerically analyzed with the fields of the stresses and strains of IPMCs, pore pressure, ion concentration and electric potential of each layer in Fig. 4.5.

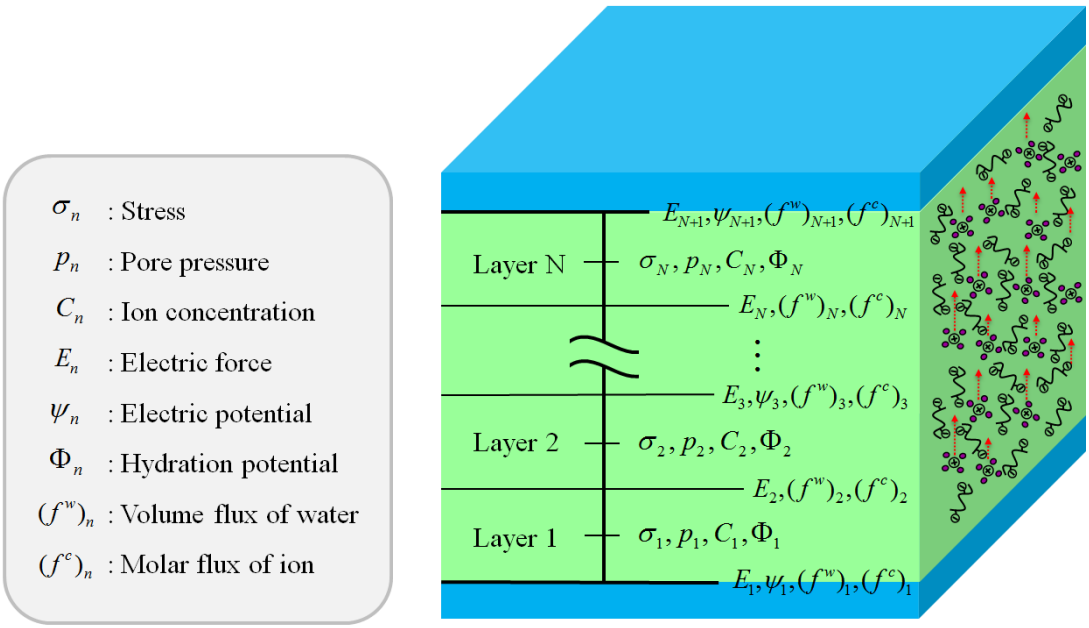

Fig. 4.5 Discretization of IPMCs

4.4 Simulation Results

The numerical formulation in the previous chapter is adopted into the in-house code of finite element program, and the transient response of a mechanical sensor using Flemion in the experiment of Wang et al. (2009) is numerically simulated. The experiment measured electric potentials from the different deflections with time. The geometry of the mechanical sensor is illustrated in Fig. 4.2. Regarding the mechanical sensor, the physical parameters for the present simulation are determined as shown in Table 1. The material parameters can be determined by macroscale experiments.

As shown in Fig. 4.5, the region of ionic polymer is only discretized, and the outer surfaces of the polymer are assumed that water cannot be leaked. As the boundary condition of the structural analysis, the root of the mechanical sensors is fixed and the free tip is prescribed with different deflections as shown in Fig. 4.6. In details, 4, 5, 6 and 10mm deflections are prescribed for 1 sec, the deflections are kept for 9 sec, and return to initial positions for a second. As a results, reaction force, pore pressure, water uptake, ion concentration and electrical potential are obtained with respect to time and thickness direction as shown in Figs. 4.6-4.13.

As shown in Fig. 4.7, reaction forces are obtained as different deflections are input. Responding to loads by the prescribed deflections, the reaction forces are instantaneously increased with small amounts of peaks. And then, the peaks are quickly relaxed and the reaction force becomes steady on constant deflections. The magnitudes of the peaks and steady reaction forces are almost proportional to the magnitudes of prescribed deflections. At 10 sec, the deflections are prescribed to initial position. The unloading behaviors apparently show the same peaks and relaxation with the loading behaviors, and return to zero reaction force.

From Fig. 4.8, the numerical results are shown only for 4mm deflection case, in order to show the time histories of interesting parameters. The other cases of 5, 6 and 10 mm deflections have the same patterns in the distributions of interesting parameters. The distributions of pore pressure over the thickness at fixed root are shown in Fig. 4.8 and 4.9. As shown in Fig. 4.8, the stress-induced pressure is spontaneously increased with the

deflection and reaction force for a second, and then the stress-induced pressure is relaxed to zero. The stress-induced pressure is induced on the undrained condition resulting in the transient reaction force, and shows the typical distributions of Biot poroelasticity. In Fig. 4.9, the change of total pore pressure from initial pore pressure is shown with respect to time and thickness. At 1 sec, the pore pressure peaks and then relaxed due to the contribution of the stress-induced pressure, but the pore pressure does not return to initial pore pressure even when static state is reached. The remained pore pressure means the change of hydration-induced pressure. After unloading, the hydration-induced pressure returns to initial pore pressure.

Water uptake is also shown in Fig. 4.10. The distribution of water uptake in thickness direction with time shows water migration in pores. During loading, water in pores is rapidly migrated due to the stress-induced pressure, and then slowly flows even when deflection is fixed. The peak of water uptake is delayed than the peak of pore pressure. That is, water migration is derived by the gradient of pore pressure. However, the driving force due to hydraulic pore pressure balances with driving force due to hydration and electric potential resulting in the constant gradient of water uptake and pore pressure from 2sec to 10sec in Fig 4.9 and 4.10. On unloading, water in pores is rapidly migrated and the volume flux is gradually decreased until uniform distribution. The transport of water solution in ionic polymers also has an effect to the distribution of ion concentration that water flow delivers mobile ions. The distribution of total concentration of cation is illustrated in Fig. 4.11. Following the water transport in Fig. 4.10, the cations are redistributed, and spontaneously result in the redistribution of charge density. The redistribution of charge density determines electric potential. The time history of distributions of electric potentials is illustrated with thickness and time in Fig. 4.12. With the molar flux of cation, the electric potential is spontaneously changed, but the redistribution of cation is slower than the response of pore pressure. Related to the transports of water and ions, the electric potential shows relatively-smooth peaks and gradual relaxations with time. As the output of mechanical sensors using IPMCs, the time histories of electric potentials are obtained with different deflections, as shown in Fig. 4.13. The obtained electric potentials from the present simulation are well agreed with the electric potentials of the experiments of Wang et al. (2009).

Therefore, the non-invertible black box between actuating and mechanical sensing modes is explained with interesting parameters from the numerical results, and the very small electric potential in mechanical sensing response is numerically expressed. Furthermore, the transient behavior, e.g. relaxation and time lag, are modeled and the time dependency of the mechanical sensing behaviors of IPMCs is shown. The hydration effect on the mechanical sensors is also estimated in the present study.

Table 4.1 Material parameters for the present simulation

Input parameters	
Initial water uptake	$w_0 = 0.3470$
Initial porosity	$\phi_0 = w_0/(1+w_0) = 0.2576$
Elastic modulus on dry condition	$E_{dry} = 2461.2\ MPa$
Empirical coefficient of Elastic modulus	$Q = 7.2409$
Elastic modulus	$E = E_{dry}\exp(-Qw_0) = 199.5MPa$
Bulk modulus on dry condition	$K_{dry} = 10255\ MPa$
Empirical coefficient of Bulk modulus	$R = Q$
Bulk modulus	$K = K_{dry}\exp(-Rw_0) = 665MPa$
Bulk modulus of polymer matrix	$K^s = K_{dry}$
Hydration coefficient	$A = Q$
Initial concentration of cation to water	$c_{I0} = 0.01M$
Initial total concentration of cation	$C_{I0} = \phi_0 c_{I0} = 0.002576M$
Valence of cation	$z_I = +1$
Hydraulic permeability	$\kappa_h = 1.0\times10^{-14}mm^2$
Dynamic viscosity	$\eta_w = 0.862\times10^{-9}MPa\cdot s$
Ion-water diffusivity	$D_{Iw} = 1.186\times10^{-15}mm^2$
Ion-polymer diffusivity	$D_{Ip} = 1.186\times10^{-15}mm^2$
Electric permittivity	$k_e = 7.5\times10^{-6}F/mm$
Absolute temperature	$T = 293K$
Correction factor of shear stiffness	$\alpha = 5/6$
Correction factor of Poisson's ratio	$\beta = 1.0$
Elastic modulus of gold	$E = 1946MPa$
Poisson's ratio of gold	$v = 0.42$

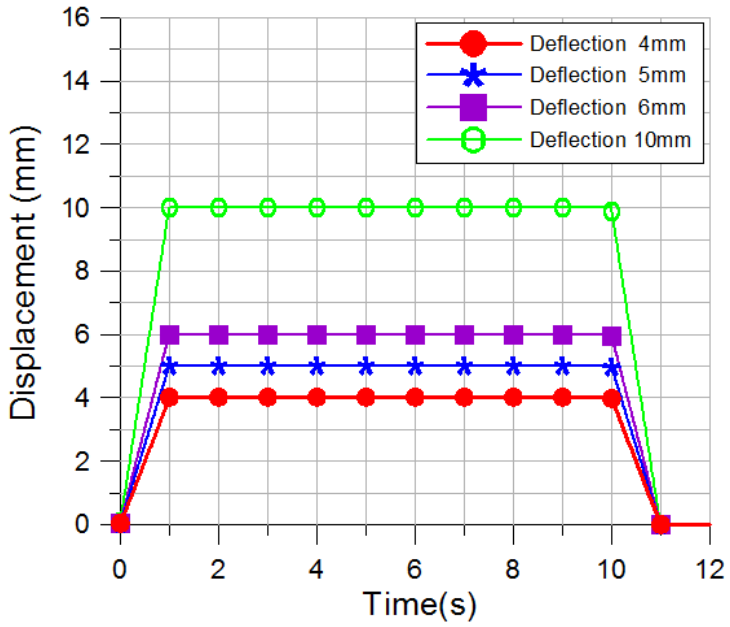

Fig. 4.6 Prescribed tip deflection with time (simulation and experiment)

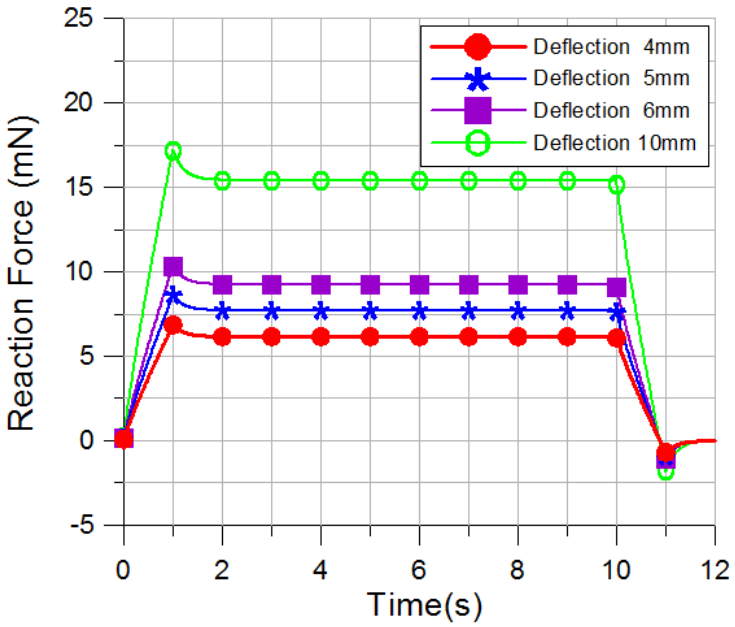

Fig. 4.7 Reaction force with time (simulation)

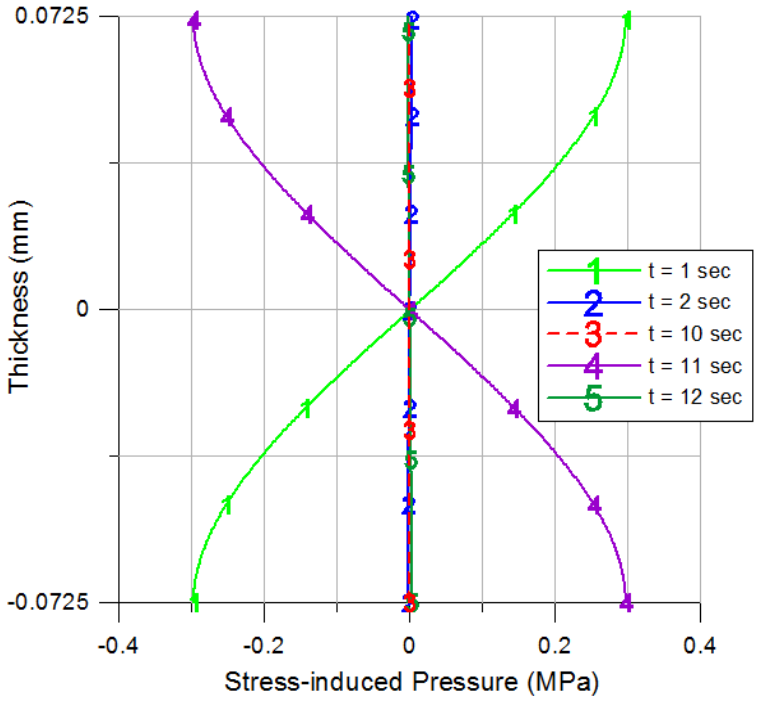

Fig. 4.8 Stress-induced pressure over thickness with time in case of 4mm deflection (simulation)

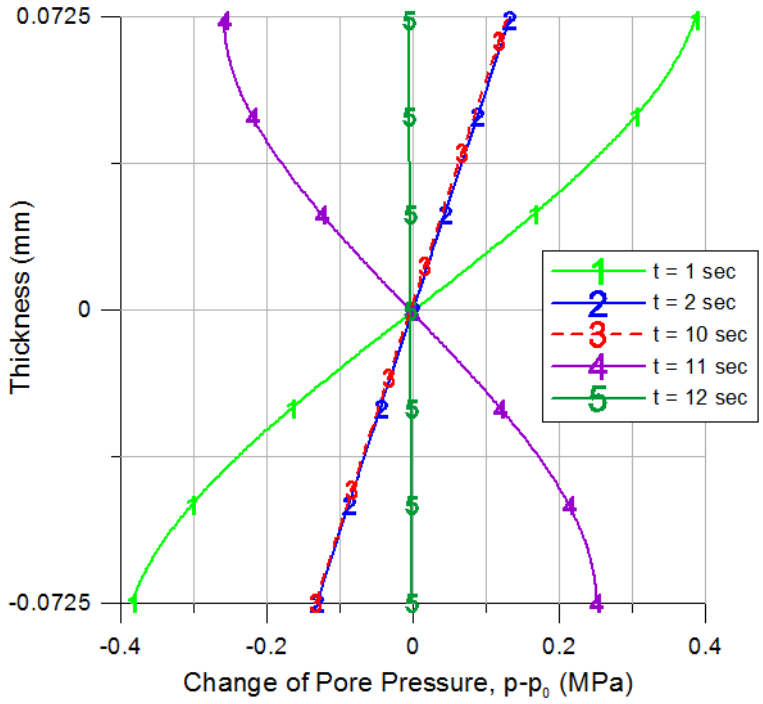

Fig. 4.9 Total pore pressure over thickness with time in case of 4mm deflection (simulation)

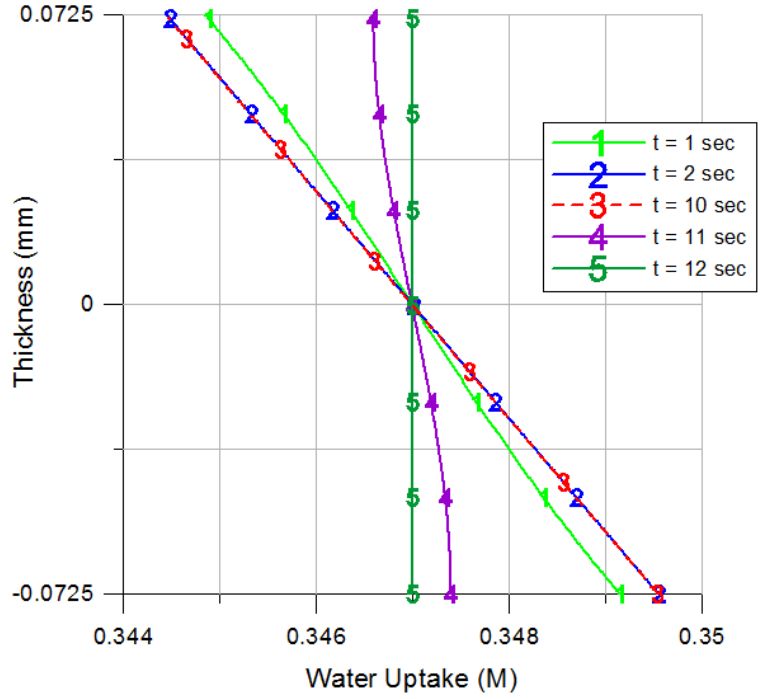

Fig. 4.10 Water uptake over thickness with time in case of 4mm deflection (simulation)

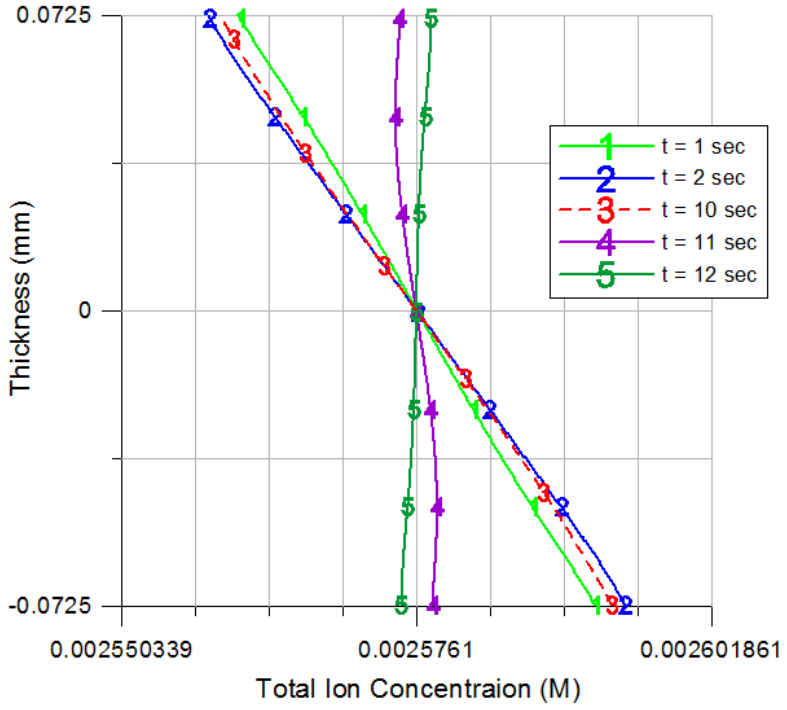

Fig. 4.11 Ion concentration over thickness with time in case of 4mm deflection (simulation)

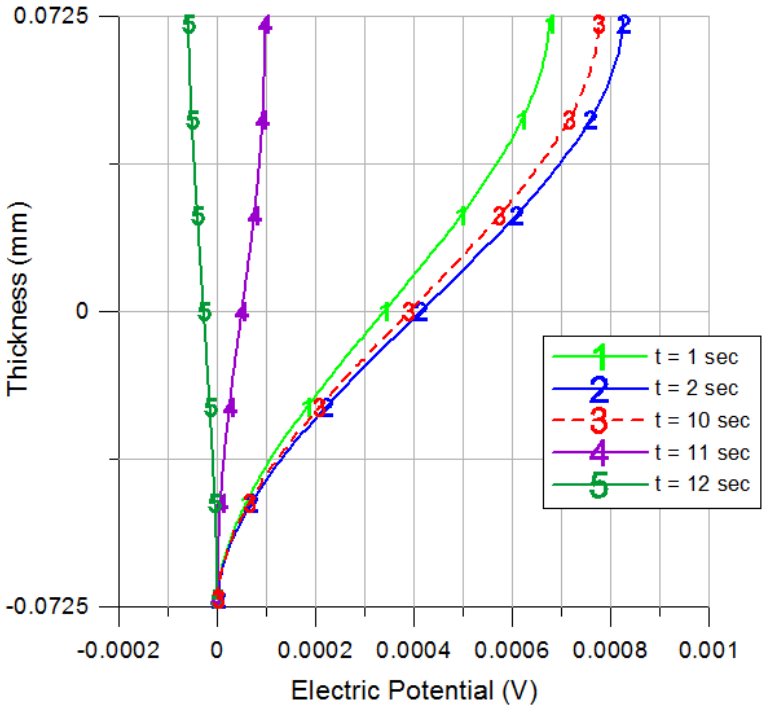

Fig. 4.12 Electrical potential over thickness with time in case of 4mm deflection (simulation)

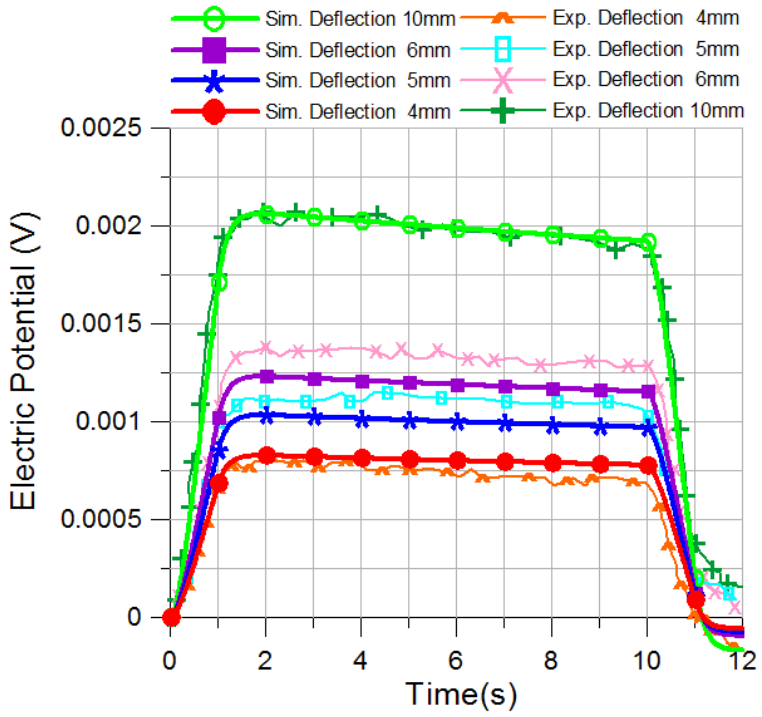

Fig. 4.13 Time history of voltage with different deflections (simulation and experiment)

4.5 Conclusion

The present study has attempted the numerical modeling of mechanical sensors using IPMCs and introduced its simulation procedure and results. The model of mechanical sensors using conducting polymers in the previous work (Yoo and Toi, 2013) was modified, and the hydration effects of IPMCs were newly considered with the followings.

First, the hydration effects on volume and stiffness has been considered. The present study decomposed the total strains of IPMCs as stress-induced strain and hydration-induced strain. The hydration-induced strain covered the electrochemically induced strains including actuating deformation, and the hydration-induced strain was handled as eigen-strain. Furthermore, pore pressure was decomposed into stress-induced pressure and hydration-induced pressure, and the stress-induced strain and stress-induced pressure were embedded into Biot constitutive equation. The volume swelling due to hydration was modeled with water migration due to electrochemically induced driving forces. The driving force was expressed with hydration potential employing an empirical chemical potential at free swelling equilibrium. The hydration potential was embedded into Darcy flow model with the modeling of hydration coefficient. As a result, the water migration due to hydration and electric potential was estimated and the hydration- induced strain was estimated with Biot poroelastic theory. The hydration-induced strain was added into the structural analysis of the mechanical sensing responses.

Second, the transient response with relaxation and time lag of reaction force and electric potential has been numerically simulated. The simulation of mechanical sensors using IPMCs was employed Timoshenko beam model, Biot poroelastic model and Poisson-Nernst-Plank model. The instantaneous pore pressure in the transient behaviors was estimated on the undrained condition, water migration due to the pore pressure was expressed and the ion transport following the water migration was modeled to induce electricity. In Timoshenko beam model, Poisson effect due to pore pressure was considered for the transient response of a porous beam. In Biot poroelastic model, hydration-induced strain and pressure were embedded, and undrained beam Poisson's ratio was employed. In Poisson-Nernst-Plank equations, ion transport with water flow and

interaction between ions and polymer were considered, and charge density to the total volume of bulk material was obtained. Next, the related models were numerically formulated, and they were employed into one-dimensional finite element program because the variations of physical quantities over microscale thickness are dominant.

Third, interesting parameters, which are significantly important in the mechanism of the mechanical sensors, were obtained with respect to time and thickness of IPMCs, and the non-invertible relation between deformation and electric potential in actuating and mechanical sensing modes were investigated. That is, the qualitative explanation for the very small output of electric potential was quantitatively estimated. From the simulation results, the distributions of solid stress, fluid pressure, water uptake, ion concentration and electric potential would be helpful for understanding the mechanism of IPMCs. The water transport in IPMCs is a key factor for design and control of mechanical IPMC sensors.

4.6 References

Biot, M.A., 1941, General theory of three-dimensional consolidation, Journal of Applied Physics, vol. 12, pp. 155-164

Jung, W.S. et al, 2010, Computational modeling of electrochemical- mechanical behaviors of Flemion-based actuators considering the effects of electro-osmosis and electrolysis, Computers and Structures, Vol. 88, pp. 938–948

Nemat-Nasser, S. and Wu, Y., 2003, Comparative experimental study of ionic polymer-metal composites with different backbone ionomers and in various cation forms, Journal of Applied Physics, Vol.93, No.9, pp.5255-5267

Nemat-Nasser, S. and Zamani, S., 2006, Modeling of electro-chemo-mechanical response of ionic polymer-metal composites with various solvents, Journal of Applied Physics, Vol.100, No.6, pp.4310-4318

Rice, J.R. and Cleary, M.P., 1976, Some basic stress diffusion solution for fluid-saturated elastic porous media with compressible constituents, Reviews of Geophysics and Space Physics, Vol. 14, pp. 227–241

Scherer, G.W. et al., 2009, Bending of a poroelastic beam with lateral diffusion, International Journal of solid and structure, Vol. 46, pp. 3451-3462

Toi, Y., 2008, A Course on computational solid mechanics (in Japanese), Corona Publishing Company, pp. 50-52, pp. 144-156

Wang, J. et al., 2009, Bio-inspired design of tactile sensors based on Flemion, Journal of Applied Physics, Vol.105, No.8, pp.3515

Yoo, S. and Toi, Y., 2013, Numerical Simulation of Mechanical Sensors Using Conducting Polymers, Journal of Solid Mechanics and Materials Engineering, Vol. 7, No.6, pp. 585-600

Zhao, Q. et al., 2011, Diffusion and interfacial transport of water in Nafion, The Journal of Physical Chemistry B, Vol.115, No. 12, pp 2717–2727

Chapter 5

Final Conclusion

5.1 Final Conclusion

The present study has newly attempted to simulate mechanical sensors using ionic electroactive polymers, conducting polymers or IPMCs (ionic polymer metal composites).

Conducting polymers and IPMCs have attracted attentions as electroactive materials since the late 1980s. They have a strong advantage of low voltage requirement, 1~3V. Such a low voltage range is harmless for human body, so conducting polymers and IPMCs have been received amplified attentions in the fields of robotics, MEMS, artificial muscle and medical engineering. Massive reports for the electroactive properties of conducting polymers and IPMCs have so far been accumulated, but the reports of numerical simulation are almost for actuators not for mechanical sensors. Conducting polymers and IPMCs show both of actuating and mechanical sensing behaviors, e.g. mechanical deformation is induced by electric potential, and electric potential is generated by mechanical deformation. The mechanical sensing behaviors have given an expectation for the integration of actuating and mechanical sensing functions like human muscles. Recently, the mechanical sensors have been investigated and bio-inspired sensors have been invented with the mechanical sensors. Numerical simulation can be added to the investigation and design of the mechanical sensors.

In order to simulate the mechanical sensors, the present study has developed computational systems. In chapter 2, simple computational system has been introduced with black box model. In chapter 3 and 4, more complicated model with Biot poroelastic theory and Poisson-Nernst-Planck equations has been introduced.

The performances of the actuators and mechanical sensors are directly related to mechanical properties and behaviors. In order to predict the performance of the mechanical sensors more precisely, structural analysis is needed to be accurate. Therefore, the present study has employed layered Timoshenko beam theory, and introduced finite element analysis.

For the estimation of mechanical sensors, black box model has been conventionally employed. The black box model means an empirical relation between the input and output of the mechanical sensors. However, the empirical relation is non-invertible, because the generated electric potential of mechanical sensing mode is very much smaller than the electric potential of actuating mode with respect to the same displacement. The black box model cannot explain the non-invertible relation. Therefore, the mechanism of the mechanical sensors have been modeled in detail, and the internal process of the mechanical sensing behaviors has been quantitatively explained with the numerical results of reaction force, pore pressure, water uptake, ion concentration and electric potential .

Furthermore, mechanical sensors using conducting polymers or IPMCs show transient responses with relaxation and time lag of reaction force and electric potential. That is, the performances of the mechanical sensors are time dependent. Therefore, the transient responses are modeled and numerically reproduced.

In addition, IPMCs shows hydration effect that mechanical stiffness and volume are significantly changed as water uptake is absorbed. The hydration effect was modeled in chapter 4. Total strain was decomposed as hydration-induced strain and stress-induced strain, and pore pressure was also decomposed as hydration-induced pressure and stress-induced pressure. Here, the stress-induced strain and stress-induced pressure were embedded into Biot poroelastic constitutive equations. Nest, water migration due to hydration was modeled with hydration potential and hydration coefficient. From the present simulation results, we would emphasize that fluid transport in the pores is a key factor for design and control of mechanical sensors.

The applications of the present study can be thought as follows. As mentioned before, mechanical sensors using ionic electroactive polymers such as conducting polymers or IPMCs show dependencies on time, initial condition, water uptake and so on. In order to analyze the behaviors of the mechanical sensors more precisely, the present computational system could be helpful. Until now, a lot of researches have been conducted based on black box model using linear relations between mechanical stress and electric voltage, but the present study attempted to overcome the black box model. Furthermore, the present study tried to analyze the continuous measurements of the mechanical sensors using the time history of electric potential. If the measured history of electric potential is reproduced by the present model, we can estimates the history of mechanical stimulation or verify the

measurement. For fabrication or design of the mechanical sensors, more complicated model can give understanding and prediction, not only time-dependent response but also the distributions of important parameters over thickness, which are difficult to be measured, and their contributions on performance. For users, the data for time dependant responses has to be provided because of the relaxation and time lag and hydration effects on the performance of the mechanical sensors. The fundamental phenomena in the present study can be found in other materials and applications, e.g. transient responses, hydration and ion transport of porous materials.

List of Figures

Chapter1 Introduction

Chapter 2 Black Box Model of Mechanical Sensors Using Conducting Polymers

Chapter 3 Numerical Simulation of Mechanical Sensors Using Conducting Polymers

Chapter 4 Numerical Simulation of Mechanical Sensors Using Hydrated IPMCs

Chapter 5 Final Conclusion

List of Tables

Acknowledgments

First of all, I would appreciate the supervision, favor and kindness of my advisor, Professor, Yutaka TOI. His guidance and advice have attributed my study and research. I would never have been able to finish my doctoral thesis without his guidance and advice. Moreover, His support and encouragement have helped me to finish my doctoral course. In addition, I thank for giving me a chance to work part time in his lab. As far as I remember, I have been the beneficiary of his kindness. Once again, I would like to express my deepest gratitude to my advisor.

I would acknowledge my committee members, Professor Katsuyuki Suzuki, Professor Fumitoshi Sato, Professor Yoji Okabe, Professor Daisuke Kitazawa. They accepted to be the members of the committee for my doctoral thesis. Their insightful criticisms and constructive suggestions have improved my doctoral thesis.

Many thanks go in particular to my lab mates, Doctor Woosang Jung, Doctor Masanori Oka, Doctor He Jie, Researcher Yanfei Xian for their encouragement and practical advice in my research, study and life in Japan.

My doctorial course was financially supported by the Grant from the Korean scholarship foundation in Japan and the Grant for the Promotion of Doctorate Researchers from the University of Tokyo. In addition, the part job in Toi lab in the Institute of Industrial Science, the University of Tokyo has removed financial instability. I would appreciate their financial supports.

Lastly I warmly thank my friends and family who have believed in and supported me. I wish all of them a happy and safe.

Seongwon Yoo

November 2014